UMINHO I 2022

Fábio Emanuel da Silva Gonçalves

Development of Smart Hydrogels for Biomedical Applications

Universidade do Minho
Escola de Engenharia

Fábio Emanuel da Silva Gonçalves

Development of Smart Hydrogels for Biomedical Applications

outubro de 2022

Universidade do Minho
Escola de Engenharia

Fábio Emanuel da Silva Gonçalves

Development of Smart Hydrogels for Biomedical Applications

Dissertação de Mestrado
Mestrado Integrado em Engenharia Biomédica
Ramo de Eletrónica Médica

Trabalho efetuado sob a orientação de
Doutora Vanessa Fernandes Cardoso
e da
Professora Doutora Natália Maria Araújo Alves

outubro de 2022

DECLARAÇÃO

Nome: Fábio Emanuel da Silva Gonçalves

Endereço Eletrónico: a84663@alunos.uminho.pt

Título da Dissertação: Development of Smart Hydrogels for Biomedical Applications

Orientador: Doutora Vanessa Fernandes Cardoso

Coorientador: Professora Doutora Natália Maria Araújo Alves

Orientador de Empresa: Professora Doutora Susana Neves Rocha

Ano de Conclusão: 2022

Área de Especialização: Eletrónica Médica

DIREITOS DE AUTOR E CONDIÇÕES DE UTILIZAÇÃO DO TRABALHO POR TERCEIROS

ACKNOWLEDGMENTS

To my parents, brothers, and family, I will be forever grateful for your unwavering support, assurance, and care. Your motivation and strength inspired me to persevere. In particular, to my mother and father, there are no words to thank the opportunities given and the trust placed on me.

To Professor Doctor Vanessa Fernandes Cardoso, from the Centre for Microelectromechanical Systems of the University of Minho, I deeply appreciate the steady supervision provided in the practical work and the remarkable orientation in the elaboration of this dissertation. Your support was essential for the outline and fulfilment of this project. You always had the right word, for which I will be forever thankful.

To Professor Doctor Natália Maria Araújo Alves, from the 3B's Research Group, I profoundly appreciate the opportunity to pursue the research project that I always dreamed of. For all the support, flexibility, optimism, and steady sympathy, thank you. Moreover, to Doctor Daniela Alexandra Silva Peixoto and Doctoral Student Cátia Correia, I'm in full gratitude for everything that you taught me and for the daily guidance provided along all the work developed at the 3B's Research Group. Moreover, credit is due to Doctor Maria Conceição Jesus Rego Paiva and her students for the development of pristine graphene and amine-functionalized graphene, essential to fulfil some of the project fundamental aims. To my colleagues at the 3B's Research Group, I am thankful for the support and the friendly work environment.

To Professor Doctor Susana Rocha, from KU Leuven, I sincerely appreciate the opportunity to perform the research in your lab, which has an unmatched friendly environment that was my support basis during this period abroad. To you and Doctoral Student Johannes Vandaele, I am forever thankful for the orientation provided and knowledge shared. Also, I must thank Doctoral Students Maria Bravo and Sametlefou Aytekin for the personal friendship that we developed. It is the worthiest asset I brought from Belgium.

To my friends, you were, whenever I needed, my refuge, my fun, and my peace. I am lucky enough to have many to thank to, but I particularly thank Diana Lopes, Paulo Lima, João Rodrigues, Marina Passos, Carla Rodrigues, Ana Pinheiro e Joana Figueiredo.

Finally, to everyone that directly or indirectly contributed to the fulfilment of this project, I sincerely thank you.

STATEMENT OF INTEGRITY

I hereby declare having conducted this academic work with integrity. I confirm that I have not used plagiarism or any form of undue use of information or falsification of results along the process leading to its elaboration.

I further declare that I have fully acknowledged the Code of Ethical Conduct of the University of Minho.

RESUMO

Hidrogéis inteligentes são redes poliméricas responsivas que sofrem alterações nas suas propriedades quando estímulos, como temperatura, pH e campos elétricos ou magnéticos, são aplicados. Nas últimas décadas, os hidrogéis inteligentes tornaram-se uma próspera fronteira de pesquisa no campo da engenharia biomédica, inclusive em eletrónica médica, onde se mostram eficazes como biossensores, bioelétrodos, válvulas inteligentes e em aplicações de microfluídica.

No âmbito deste projeto, hidrogéis de ácido hialurónico modificado com dopamina e anticorpos do recetor Nogo foram desenvolvidos com potencial aplicação no tratamento de lesões no sistema nervoso central e, em particular, na espinal medula. Estas lesões são uma das principais causas de incapacidade a longo prazo e não existe tratamento atualmente. Sendo assim, torna-se urgente desenvolver novas estratégias capazes de induzir neuroregeneração e promover uma recuperação funcional do paciente. O ácido hialurónico foi quimicamente modificado com grupos catecol que reticulam quimicamente, permitindo a formação do hidrogel. A introdução de grafeno funcionalizado no hidrogel aumenta substancialmente a sua condutividade elétrica e o cultivo de células neuronais demonstrou que hidrogéis modificados com grafeno são biologicamente mais viáveis do que aqueles sem grafeno. De uma forma geral, os hidrogéis produzidos, inspirados na natureza, providenciam uma matriz tridimensional estável e biocompatível, com uma condutividade elétrica reforçada, revelando assim potencial como uma plataforma inteligente para o tratamento de lesões na espinal medula.

Ademais, hidrogéis termossensíveis baseados em poli(isocyano)péptidos foram utilizados para o estudo do efeito de sais na microestrutura destas redes tridimensionais. A influência de sais nas propriedades mecânicas e térmicas de hidrogéis já terá sido anteriormente provada e descrita. No entanto, o seu efeito na microestrutura destas redes era até agora pouco conhecido. Os resultados obtidos mostram que os três sais, iodeto, cloreto e perclorato de sódio, têm uma influência significativa no diâmetro e conectividade dos poros e na porosidade do hidrogel. Em particular, cloreto de sódio mostrou uma influência notável nestes parâmetros estruturais. Desta forma, conclui-se que a adição de sais a hidrogéis físicos fibrosos pode ser utilizada como técnica para manipular a sua microestrutura.

Assim, esta dissertação aborda duas classes diferentes de hidrogéis sob duas finalidades distintas. Todavia, ambos os sistemas apresentam um potencial promissor como materiais inteligentes em resposta a estímulos elétricos ou mecânicos/térmicos que deve ser futuramente escrutinado.

Palavras-Chave: Ácido Hialurónico, Efeito Hofmeister, Grafeno, Hidrogéis, Poli(isocyano)péptidos.

ABSTRACT

Smart hydrogels are stimuli-responsive polymeric networks able to undergo changes in their properties upon the application of triggers, such as temperature, pH and electric or magnetic fields. Since the last few decades, smart hydrogels became a thriving research frontier in the biomedical engineering field, including in medical electronics, where they were proved effective as biosensors, bioelectrodes, smart valves, and in microfluidic applications.

Herein, dopamine-modified hyaluronic acid (HA)-based hydrogels with nogo receptor (NgR) antibodies were developed to treat the central nervous system (CNS) and, in particular, spinal cord injuries (SCIs). These conditions are one of the leading causes of long-term disability across the world and there is no current treatment. Thus, it is urgent to develop novel strategies that induce neuroregeneration and promote functional recovery. Our chemically modified HA formed a hydrogel under alkaline pH by the chemical crosslinking of catechol groups. The introduction of functionalized graphene (FG) increased substantially the electrical conductivity of the hydrogels and upon the seeding of neuronal cells the hydrogel with graphene showed higher viability than the unmodified network. Overall, our bioinspired hydrogel provides a stable and biologically compatible three-dimensional (3D) matrix with a reinforced electrical conductivity and a promising potential as a smart scaffold-based therapy for SCIs.

In addition, thermosensitive and mechanoresponsive polyisocyanopeptide (PIC)-based hydrogels were used as a model system to study the effect of added salts on the microstructure of these 3D networks. Indeed, the influence of salts on hydrogels mechanical and thermal properties has already been proved and described. However, their effect on the microstructure of these networks was until now vastly unknown. The results obtained show that the three different salts, sodium iodide (NaI), sodium chloride (NaCl) and sodium perchlorate ($NaClO_4$), have a significant influence on the diameter and connectivity of the network pores, as well as on the overall porosity of the hydrogel. In particular, NaCl showed a remarkable influence on these structural parameters. Thus, it is concluded that the addition of salts to fibrous physical hydrogels may be used as a technique to tailor their microstructure.

Therefore, this dissertation is focused on two different types of hydrogels with two different aims. Both systems, however, present a promising potential as smart materials in response to electrical or mechanical/thermal stimuli that must be further scrutinized as future work.

Keywords: Graphene, Hofmeister Effect, Hyaluronic Acid, Hydrogels, Polyisocyanopeptides.

CONTENTS

LIST OF FIGURES

CHAPTER 2

The State of the Art

CHAPTER 3

Functionalized Hyaluronic Acid-based Hydrogels with Controllable Electrical Conductivity

CHAPTER 4

Thermosensitive Polyisocyanopeptide-based Hydrogels with Controllable Microstructure

CHAPTER 5

Conclusions and Future Perspectives

SUPPLEMENTARY INFORMATION

LIST OF TABLES

CHAPTER 4

Thermosensitive Polyisocyanopeptide-based Hydrogels with Controllable Microstructure

---

SUPPLEMENTARY INFORMATION

LIST OF ACRONYMS

Acronym	Designation
3D	Three-Dimensional
ADH	Adipic Dihydrazide
ATP	Adenosine Triphosphate
BM	Basement Membrane
CNS	Central Nervous System
CNTs	Carbon Nanotubes
CSPG	Chondroitin Sulphate Proteoglycan
DHA	Dopamine-Conjugated Hyaluronic Acid
DMEM	Dulbecco's Modified Minimum Essential Medium
DOPA	3,4-dihydroxyphenylalanine
DPBS	Dulbecco's Phosphate Buffered Saline
ECM	Extracellular Matrix
EDC	1-Ethyl-3-(3-dimethylaminopropyl) Carbodiimide
EGFR	Epidermal Growth Factor Receptor
EU	European Union
FG	Functionalized Graphene
FBS	Fetal Bovine Serum
GAG	Glycosaminoglycan
HA	Hyaluronic Acid
HGF	Hepatocyte Growth Factor
HSPG	Heparan Sulphate Proteoglycan

Acronym	Designation
IS	Interstitial Space
LCST	Lower Critical Solution Temperature
MAG	Myelin-associated Glycoprotein
MAP	Mussel Adhesive Protein
MMPs	Matrix Metalloproteinases
MSC	Mesenchymal Stem Cell
NaCl	Sodium Chloride
$NaClO_4$	Sodium Perchlorate
NaI	Sodium Iodide
$NaIO_4$	Sodium Periodate
NgR	Nogo Receptor
NgR2	Nogo Receptor 2
NHS	N-Hydroxysuccinimide
NPSC	Neural Progenitor/Stem Cell
NSC	Neural Stem Cell
OMGP	Oligodendrocyte Myelin Glycoprotein
OPC	Oligodendrocyte Precursor Cell
PBS	Phosphate Buffer Saline
PG	Pristine Graphene
PI	Propidium Iodide
PIC	Polyisocyanopeptide

Acronym	**Designation**
PLL	Poly-L-Lysine
PNN	Perineuronal Net
PNS	Peripheral Nervous System
PPy	Polypyrrole
RDHA	Reduced Dopamine-Conjugated Hyaluronic Acid
RGD	Arginylglycylaspartic Acid
RHOA	Ras Homolog A
S1PR2	Sphingosine 1-Phosphate Receptor 2
SCI	Spinal Cord Injury
SD	Standard Deviation
SEM	Scanning Electron Microscopy
TAMRA	Carboxy Tetramethyl-Rhodamine
TCPS	Tissue Culture Polystyrene Surface
UV	Ultraviolet Radiation

LIST OF SYMBOLS

Symbol	Description	Unit Symbol	Unit Name
T	Temperature	°C	Degree Celsius
G'	Storage Modulus	Pa	Pascal
σ	Stress	Pa	Pascal
γ	Strain		
K'	Differential Modulus	Pa	Pascal
G''	Loss Modulus	Pa	Pascal
c	Concentration	Kg L^{-1}	Kilogram per Litre
V	Electrical Potential	V	Volt
I	Electrical Current	A	Ampere
σ	Electrical Conductivity	S m^{-1}	Siemen per Meter
l	Length	m	Meter
A	Cross-sectional Area	m^2	Square Meter
Q	Swelling Ratio	%	Percentage
w	Weight	Kg	Kilogram

1. INTRODUCTION

In the first chapter, the motivation behind the project is presented, as well as its aims and the structure of the dissertation.

1.1 | Motivation

Hydrogels are crosslinked polymer networks with high hydrophilic behaviour [1]. These networks are called smart when their properties undergo changes upon the application of stimuli. Since the last few decades, hydrogels and in particular smart hydrogels became a thriving research frontier in the biomedical engineering field, including in medical electronics, where they were proved effective for instance as biosensors [2], bioelectrodes [3], smart valves [4], in microfluidic applications [5] and three-dimensional (3D) printing [6].

This dissertation approaches two different hydrogels for two different purposes. At the 3B's Research Group, under supervision of Doctor Vanessa Cardoso and Professor Doctor Natália Alves, a hyaluronic acid (HA)-based hydrogel with reinforced electrical conductivity was formulated and is described for the treatment of spinal cord injuries (SCIs). On the other hand, as a model system for the study of the effect of added salts on the microstructure of 3D networks, polyisocyanopeptide (PIC)-based hydrogels were used. This study was developed at KU Leuven, under an Erasmus+ scholarship, with supervision of Doctor Vanessa Cardoso and Professor Doctor Susana Rocha. While the first hydrogel is a chemically crosslinked and natural system potentially sensitive to electrical stimuli, the latter is a synthetic physical network responsive to thermal triggers.

1.1.1 | Spinal Cord Injuries: Prevalence, Social Impact, and the Importance of Novel Treatments

Central nervous system (CNS) injuries such as traumatic brain injuries and SCIs are one of the leading causes of long-term disability and death across the world [7]. In 2011, Crips *et al.* reported the global prevalence of SCI to be between 236 and 1009 per million [8]. More recently, Singh and co-workers, through extensive research across several databases, concluded that the prevalence of SCI around the world can vary from 250 to 906 per million. Indeed, several circumstances, such as the absence of a standardized method of assessment across regions, have prevented more accurate and precise estimates. Traffic accidents are typically the most common cause of SCI, followed by falls in the elderly population [9]. In addition to its high prevalence, SCIs are life-disrupting and life-threatening conditions. For instance, Chhabra *et al.* documented an in-hospital mortality rate of 10% in acute traumatic spinal cord injuries [10].

At the European level, according to the Commission and its statistical office, the Eurostat, every year there are about 10 thousand new SCIs in the European Union (EU), with more than 200 thousand EU citizens living with the disease [11].

The impact on the individual quality of life and the social costs of these conditions are enormous. Indeed, damage to the CNS usually results in severe neurological impairments which may cause limitations such as paralysis, limited mobility, and sensory loss. Moreover, unlike peripheral nervous system (PNS), completely functional restoration in damaged CNS is not yet possible in most clinical cases [12]. The traditional approach to the postinjury period is to limit the extension of the neurological damage through the augmentation of mean arterial pressure, early decompression, and through the intravenous administration of methylprednisolone, a corticosteroid anti-inflammatory agent. Afterwards, the treatments are palliative, focusing on the symptoms rather than the repairment of tissue [13].

As CNS injuries affect millions worldwide, cover the entire age spectrum, may be life-disrupting and even life-threatening with patient recovery being still very limited, there is an urgency in the European Union and across the globe to investigate and develop innovative and effective treatments for these conditions [14].

Recently, ambitious therapies have been developed or are under clinical trials. Some, such as the administration of hepatocyte growth factor (HGF) or granulocyte colony-stimulating factors, focus on neuroprotection. Others, however, focus on neuroregeneration, such as the administration of oligodendrocyte precursor cells (OPCs) or anti-Nogo antibodies and spinal cord stimulation. In addition, biomaterials have been increasingly investigated as they constitute a biodegradable and cytocompatible tool able to fill cavitation defects and reproduce the complex structural architecture of the extracellular matrix (ECM), while delivering treatments in a controlled and non-invasive manner. For instance, InVivo Therapeutics (Cambridge, Massachusetts) is currently assessing through a 20-patient clinical study the potential benefit of their developed Neuro-Spinal Scaffold, which has already shown the ability to promote tissue remodelling and neuronal growth [13].

Nevertheless, the unique microenvironment in the CNS after an injury occurs is extremely challenging to its treatment. Physical and chemical barriers, such as inflammation and scar formation, built after lesion harden the treatment of these conditions and despite recent progress the impetus is now to formulate new, effective, and minimally invasive treatments [15]. Herein, a HA-based hydrogel with enhanced adhesive and electrical properties is proposed as a vehicle for the delivery of Nogo Receptor (NgR) antibodies to promote neuroregeneration and functional recovery after the occurrence of a SCI.

1.1.2 | The Effect of Added Salts on the Microstructure of Polyisocyanopeptide-based Hydrogels

It is well known that living cells interact physically with their 3D microenvironment through mechanisms of mechanobiology [16]. As so, manipulating the physical properties of the surrounding environment impact cell behaviour and this has inspired strategies for tissue engineering applications [17]. As the importance of the scaffold physical properties becomes increasingly recognized, several techniques have surged in the past decades to allow for their tunability. For instance, the pore size and/or the porosity of hydrogels can be tailored by different approaches, such as cryogelation or through electrospinning. These methods, however, influence other properties of the hydrogel and require specific advanced equipment to be performed [18]. Therefore, novel, easily applicable and readily available strategies are required.

The addition of salts to physical hydrogels have been proved effective on the tunability of their mechanical, thermal, and swelling properties [19][20]. It may be hypothesized that such an effect on the overall properties of these 3D networks must also have an influence on their microstructure. To confirm this, this project proposes to study the effect of added salts on the microstructure of physical fibrous hydrogels. As a model system, PIC-based hydrogels will be used. These are mechanosensitive hydrogels that only form after the polymeric solution is under a certain critical temperature or above that temperature. When cooled down below their critical temperature, the hydrogel turns into a polymeric solution. Thus, they are thermoresponsive and thermoreversible smart networks [21]. Jaspers *et al.* already demonstrated the strong effect of salts on the critical temperature and mechanical properties of PIC hydrogels. Herein, the influence of salts on their microstructure was assessed.

1.2 | Project Aims

As previously stated, this project is subdivided in two major subprojects, one developed at the 3B's Research Group and the other worked at KU Leuven, through the Erasmus+ programme. Consequently, the dissertation is focused on two different yet related aims.

Firstly, there is undoubtably an urgency to develop efficient treatments for CNS injuries that focus on the regeneration of tissue. Biomaterials scaffolds constitute an opportunity to deliver those treatments and to build a permissive environment for neuroregeneration [13]. Therefore, this work aimed to study, develop, and assess HA-based hydrogels with functionalized graphene (FG) and NgR antibodies to induce axonal development and neuronal growth in the inhibitive environment of the CNS and, in particular, to promote recovery after a SCI.

Secondly, under the work developed at KU Leuven, the aim was to investigate how three different salts influence the microstructure of thermosensitive PIC hydrogels. Indeed, hydrogels are a versatile tool that can be tuned through several techniques to meet specific requirements of each application. Several studies already proved that the addition of salts to physical hydrogels is a successful method to tune some properties of these 3D hydrophilic networks [19][20]. However, structural properties, such as pore diameter, connectivity and the overall porosity of the hydrogels have been neglected in their analysis. Herein, the aim was to qualitatively analyse and quantify how three different salts, sodium iodide (NaI), sodium chloride (NaCl), and sodium perchlorate ($NaClO_4$), influence the three mentioned parameters related to the pore microstructure of PIC hydrogels.

1.3 | Dissertation Structure

The dissertation is divided in five chapters summarized below. These chapters approach the different studies and research work done to meet the project aims.

Chapter 1. Introduction. The introduction, as the name suggests, introduces to the audience the motivation behind the dissertation, as well as its aims and structure.

Chapter 2. The State of the Art. The second chapter of the dissertation presents to the audience the state of the art of current treatments in clinical evaluation for SCIs, focusing in particular on scaffold-based therapies. Afterwards, a brief review of HA-based scaffolds developed for the treatment of CNS injuries is described and the incorporation of graphene and NgR antibodies into these networks is discussed. Furthermore, PICs are introduced, and its smart properties and potential applications are presented. Finally, the Hofmeister effect of added salts on the PIC hydrogel properties is also discussed.

Chapter 3. Functionalized Hyaluronic Acid-based Hydrogels with Controllable Electrical Conductivity. In this chapter, the CNS composition is presented and the mechanisms involving the NgR are described. Dopamine-modified HA-based hydrogels with graphene and NgR antibodies are then introduced. The methods applied to evaluate its performance are described and the results obtained are discussed. Conclusions are also withdrawn.

Chapter 4. Thermosensitive Polyisocyanopeptide-based Hydrogels with Controllable Microstructure. The fourth chapter of the dissertation introduces the importance of scaffolds physical properties as guiders of cell behaviour. Furthermore, in this chapter, the methods applied to evaluate the influence of added salts on the microstructure of PIC hydrogels are presented, as well as the experimental results obtained and their respective conclusions.

Chapter 5. Conclusions and Future Work. In this fifth and final chapter, some conclusions and final considerations are presented about the work developed. In addition, perspectives about future work are considered and briefly outlined to pave the way for future developments and novel applications.

2. THE STATE OF THE ART

This chapter focuses on the state of the art of scaffold-based solutions for CNS injuries, especially composed of HA. In addition, it also provides an overview of PIC hydrogels and their overall properties.

2.1 | Introduction

Hydrogels are crosslinked polymer networks with high hydrophilic behaviour. When in contact with water a hydrogel absorbs large quantities of it and swells [1]. Since water is the greatest constituent of the human body, a hydrogel is deemed to have huge potential when applied for biomedical purposes [22]. In addition, they provide stable, insoluble, and flexible wet matrices with adequate porosity for diffusion of nutrients and cellular waste. Therefore, hydrogels can deliver structural and biochemical support for *in vivo* applications [1].

The hydrogel swelling reaches an equilibrium when a balance occurs between osmotic driving forces, which promote the entrance of water and other biological fluids into the hydrophilic matrix, and the cohesive forces exerted by the polymer network. The hydrogel swelling is therefore restricted by these cohesive forces, the extent of which depends mainly on the hydrogel crosslinking density. Hence, the gel swelling will be higher as more hydrophilic the hydrogel is and will be lower as the crosslinking extent is higher [23].

Hydrogels are called reversible or physical when their polymer chains are bounded by molecular entanglements and/or secondary forces such as ionic, H-bonding, or hydrophobic forces [24]. These hydrogels usually show poor mechanical properties and are less stable against degradation because of the reversible behaviour of their interactions [25]. On the other side, when the hydrogel consists of covalently crosslinked networks it is called a chemical hydrogel. These chemically crosslinked networks are more stable against degradation and their mechanical properties are usually higher in comparison to their physical counterparts [24][25].

The chains comprising the hydrogel network may be based on natural, synthetic, or hybrid combinations of both natural and synthetic polymers. Naturally derived hydrogels are widely thought to have an edge over synthetic materials where biocompatibility and biodegradability are concerned since natural hydrogels may provide better chemical, biological and morphological cues to cells than their synthetic counterparts [26]. As many natural polymers used in hydrogels are present in the ECM, these natural scaffolds can better mimic ECM environment for cell-based devices. Although synthetic hydrogels do not have any inherent bioactivity, synthetic polymers are reproducible and possess tuneable biochemical and physical behaviour. Thus, they can be designed to yield specific properties that may be difficult to obtain with natural hydrogels [6].

2.1.1 | Hydrogels Applications

The appearance of hydrogels dates back more than sixty years, when Wichterle *et al.* [27] studied and developed a hydrogel for contact lens. Since then, the investigation and uses of hydrogels have extended to cover a wide range of biomedical applications, such as microfluidics [5], biosensors [2][28], drug delivery systems [29][30], and tissue engineering strategies [31][32]. They may also be used as an ink for 3D bioprinting [6].

For instance, Erfkamp *et al.* developed a pH sensitive hydrogel to be used as a biosensor for the detection of urea. Herein, the enzyme urease was immobilized onto the hydrogel backbone. Urea reacts with urease, producing basic by-products that increase the pH. By increasing the pH, carboxylic groups present in the hydrogel backbone become charged, which leads to higher swelling due to charge repulsion. Thus, a higher concentration of urea means higher swellings. The swelling of the hydrogel is transduced into a quantifiable signal by a piezoresistive pressure sensor (Figure 2.1) [6].

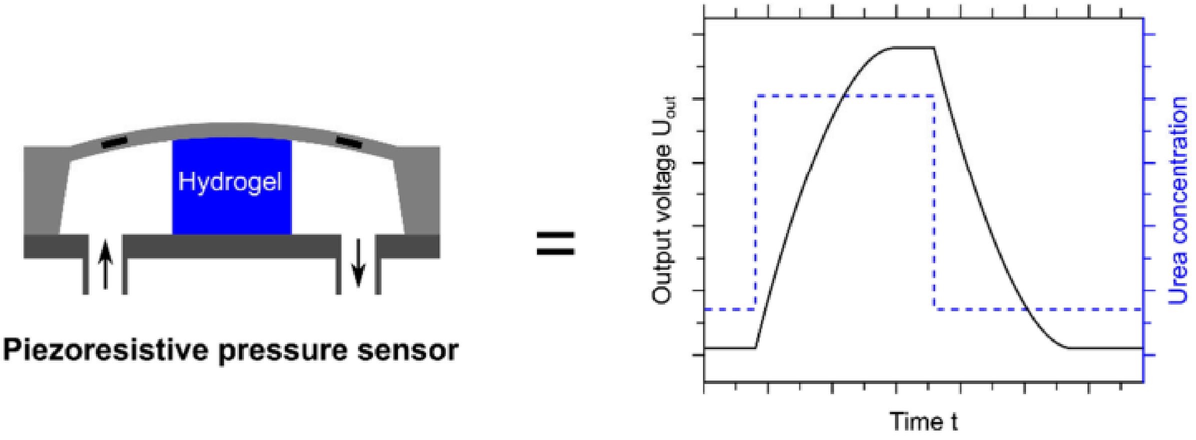

FIGURE 2.1

Measuring principle of a hydrogel-based urea biosensor. Urease is included in a pH-responsive hydrogel and the enzymatic hydrolysis of urea leads to a higher pH and consequently to the swelling of the hydrogel. The resulting swelling pressure is transformed into an output voltage through a piezoresistive transducer. Adapted from [2].

In addition to pH, hydrogels can be sensitive to several other stimulus, such as temperature, pressure, or electrical signals [6]. For instance, Gargava *et al.* developed smart hydrogel-based valves that open or close in response to a certain critical temperature [4].

Moreover, smart electrically conductive hydrogels have been increasingly applied across the biomedical field and, specifically, in bioelectronics. Conductive hydrogels can be used to detect physical signals of the human body, and collect biochemical information, namely glucose, enzymes, and other biomolecules, as well as electrophysiological signals, such as electrocardiograms, electroencephalography, and electromyograms [33]. For instance, Han *et al.* designed a conductive and adhesive hydrogel that was used as an electrode to detect electromyography and electrocardiogram signals. These hydrogels exhibited a better performance when compared to some commercial electrodes [3]. Furthermore, Zeng and co-workers produced a conductive hydrogel that was successfully used as a wearable sensor to monitor the large motions of the human body, namely finger bending, as well as wrist pulse and vocal vibration, with great accuracy and reliability [34].

Considering their high versatility and stimuli responsiveness, this project aims to design and develop a hydrogel-based treatment for SCIs. In addition, a different type of hydrogel was used as a model to study the effect of salts on the microstructure of these networks. As so, this chapter presents a state of the art about the polymer-based hydrogels used. Also, a brief overview of some promising current treatments in evaluation for SCIs is firstly presented.

2.2 | Therapeutic Strategies in the Central Nervous System

Currently, the treatments clinically used for CNS injuries are focused on neuroprotection and consist mainly of early decompression, blood pressure augmentation and intravenous methylprednisolone [13]. The latter one, however, has seen in recent years its clinical application extensively debated. Recently, Zhou *et al.* confirmed that methylprednisolone decreases microglia activation, suppress astrocytes activation, and promote functional recovery [13]. However, others argue that methylprednisolone risks outweigh its benefits. In addition to their controversies, these current treatments are not as successful on neuroregeneration, which is imperative to improve functional outcomes and the overall life quality of patients [35].

Therefore, several other neuroprotective and neuroregenerative strategies have emerged in preclinical research. These therapeutic strategies can be broadly divided into three different groups: pharmacological therapies, cell therapies and scaffold-based therapies [13].

HGFs, for instance, are very promising as a drug neuroprotective therapy. In animal SCI models, HGF increases neuron survival, promotes angiogenesis, and decreases oligodendrocyte apoptosis [36][37][38]. More recently, a phase I/II clinical trial (n = 48; NCT02193334) of the HGF KP-100IT (Kringle Pharma Inc., Osaka, Japan) has been finished [39], where motor improvements were registered, and the subjects did not show any serious adverse events caused by the drug [40]. A phase III trial (n = 25; NCT04475224) is now underway with results expected in 2023 [39].

On the other hand, Nogo antibodies have been increasingly evaluated as a potential neuroregenerative therapy. Indeed, recovery of motor function has been consistently demonstrated in rats as well as primates upon the administration of Nogo antibodies [41], which led to the initiation of clinical trials. ATI-355 (Novartis, Basel, Switzerland), for instance, is a monoclonal antibody against Nogo-A, a major inhibitor component in the CNS, which has successfully completed a phase I trial (n = 52; NCT00406016) [39], where it was well tolerated in humans and some functional improvements were verified [42]. A European group is now leading a phase II clinical trial (n = 114; NCT03935321) with results expected in 2023 [39].

A cell-based regenerative strategy to specifically target postinjury demyelination is the transplant of OPCs which preferentially differentiate to functional oligodendrocytes after transplantation [13]. Asterias Biotherapeutics Inc. (Fremont, California) has conducted a phase I/II dose-escalation trial (n = 25; NCT02302157) of their LCTOPC1 cell line [39], where it was concluded that LCTOPC1 can be safely administered to participants in the subacute period after cervical SCI. However, further studies need to be performed to assure the efficacy of LCTOPC1 in the treatment of SCI [43].

Biomaterials and scaffold-based therapies are another neuroregenerative solution increasingly investigated. Regeneration of the spinal cord tissue is often hindered by the presence of a substantial postinjury cystic cavity, which is a poor substrate that do not support cell migration and axon growth. Biomaterials have emerged as an exciting strategy to fill these cavities and to build a permissive environment for neuronal development [13]. InVivo Therapeutics (Cambridge, Massachusetts) has developed a porous bioresorbable polymer scaffold comprised of a synthetic biomaterial, poly(lactic-co-glycolic acid)-b-poly(L-lysine). In animal models, treatment with the Neuro-Spinal Scaffold has encouraged tissue remodeling and neuronal growth [44]. Two clinical trials (n = 20; NCT02138110) (n = 20; NCT03762655) are now underway with final results expected in 2024 and 2028, respectively [39]. The first trial, however, has already published some primary results which support the safety and potential benefit of the scaffold implantation and encourage the continuance of the clinical investigation [45].

For the treatment of SCIs, the aim was to develop a biomaterial-based hydrogel of HA. This is a polysaccharide, present in the CNS, highly scrutinized in research, whose properties will be described below.

2.2.1 | Hyaluronic Acid-Based Scaffolds

HA, or hyaluronan, is an anionic naturally occurring linear polysaccharide comprised of repeating disaccharide units of D-glucuronic acid and N-acetyl-D-glucosamine [46]. As a natural component of the ECM and the CNS in particular, HA is highly biocompatible and biodegradable. In addition, HA is engaged in several and complex cellular signalling events, such as migration and proliferation [47][48]. When in physiological conditions, HA is degraded through enzymatic hydrolysis by naturally occurring hyaluronidase [46]. In the bloodstream, the half-life of HA molecules is 3 to 5 min [49].

Lower molecular weight HA has been shown to promote angiogenesis, which is a key interest for wound healing and tissue regeneration applications [50], whereas high molecular weight HA (> 500 kDa) is potently anti-angiogenic [50]. In the CNS, application of HA to the injury site have been confirmed as effective in reducing the glial scar formation following CNS damage [51] and in reducing the deposition of CSGPs [52][53]. HA (110 kDa) hydrogel has also been found to have neuroprotective effects by relieving secondary injury after SCI [54]. In addition, crosslinked HA (400 kDa) scaffolds have been shown to promote neurite outgrowth [55].

Injury to the spinal cord results in the degradation of native high molecular weight HA ($\approx$ 2 MDa) into its low molecular weight forms (< 100 kDa), which leads to proliferation and activation of astrocytes. Thereby, the HA applied to the CNS should not have lower molecular weight as it might increase inflammation [52].

In addition to the polymer molecular weight, other properties must be considered upon the projection of a scaffold-based treatment, namely the ability of the structure to promote cell adhesion. To that purpose, the biological performance of HA scaffolds can be improved by its chemical conjugation with other components, such as peptides, antibodies, and growth factors [56].

Laminin, for instance, has a long-recognised role in the promotion of neurite outgrowth [57][58]. HA hydrogels modified with laminin have been shown to promote more neurite extension than those without laminin [59] and to provide the appropriate cues to promote migration of neural progenitor/stem cells (NPSCs) [60]. In addition, special domains of laminin such as arginylglycylaspartic acid (RGD), which is a short peptide sequence of arginine-glycine-aspartic acid, when included in HA hydrogels was shown to favour axonal ingrowth into the hydrogel scaffolds [56].

Collagen is another component of the ECM matrix highly applied in neural tissue engineering. Geissler *et al.* demonstrated that HA hydrogels with collagen type I and laminin, two main components of the ECM, can directly increase oligodendrocyte marker expression compared to other hydrogel compositions [61]. Another study has concluded that a hydrogel composed of HA and collagen promotes neurite sprouting, axon elongation and the expression of neurogenic proteins.

Moreover, the influence of the mechanical properties of the scaffold is at least as important as its biological properties. Saha *et al.* have shown that softer hydrogels (elastic moduli of 100-500 Pa) favoured the differentiation of neural stem cells (NSCs) into neurons, whereas harder hydrogels (approximately 1-10 kPa) promoted glial cultures [62]. In addition, *in vitro* spinal cord neurons show increased branching on softer substrates, while on stiffer substrates glial cell activation and inflammation are enhanced [63]. Georges *et al.* proved that astrocytes do not spread on soft hydrogels (shear modulus of 250 Pa), while neurons do and extend long neurites [64]. In addition, another study has concluded that between three hydrogel systems with Young's modulus of 0.68, 1.23 and 2.03 kPa, the softest hydrogel resulted in more robust cell proliferation and neuronal differentiation than the stiffer ones [65]. The body of evidence for an involvement of mechanical signals in controlling neuronal growth and possibly regeneration is continuously growing [63]. Furthermore, Kolewe *et al.* have shown that fewer bacteria adhere to softer hydrogels [66].

When projecting HA-based hydrogels, in addition to the properties previously mentioned, it is important to consider that native HA does not have the ability to crosslink and therefore to form a hydrogel. Chemical modifications must be introduced to allow for the crosslink of the HA chains. To that purpose, there are several chemical groups that can be considered, namely mussel-inspired catechol groups. Below, these strategies are further discussed.

2.2.2 | Dopamine-Modified Hyaluronic Acid Hydrogels

To produce a 3D hydrogel, HA chains must be crosslinked, either chemically or physically. In particular, chemically crosslinked HA hydrogels have been prepared by incorporation of thiol [67], aldehyde [67], dihydrazide [67], and methacrylate [68] moieties. Yet, these crosslinking mechanisms have some shortcomings. For instance, HA-methacrylate can form a hydrogel via conventional photopolymerization. However, this method generates free radicals that may damage cells and photopolymerized hydrogels often cause negative effects on the viability and proliferation of cells [69]. In addition, one of the main limitations of the crosslinking moieties previously mentioned is its deficiency of adhesiveness to biological tissues. High adhesive properties allow the hydrogel system to better interact with the physiological fluids and with the biological tissue, while staying immobilized at the injury site [70].

Biomimetic strategies based on mussel-inspired chemistry may provide alternative crosslinking methods that can overcome the shortcomings of current HA hydrogels. Mussel adhesive proteins (MAPs) have a unique ability to firmly adhere to different surfaces in aqueous environments through a special amino acid named 3,4-dihydroxyphenylalanine (DOPA). The presence of catechol groups in DOPA is responsible for the remarkable adhesive properties of these materials, even in the harsh conditions of the sea, that are impossible to mimic by human efforts until now [71].

Therefore, catechol groups can be incorporated in the HA backbone to improve its adhesion properties. Generally, catechol-modified HA is obtained by carbodiimide chemistry, where an amide bond is formed between the carboxylic group of HA and the primary amine of dopamine (Figure 2.2) [72].

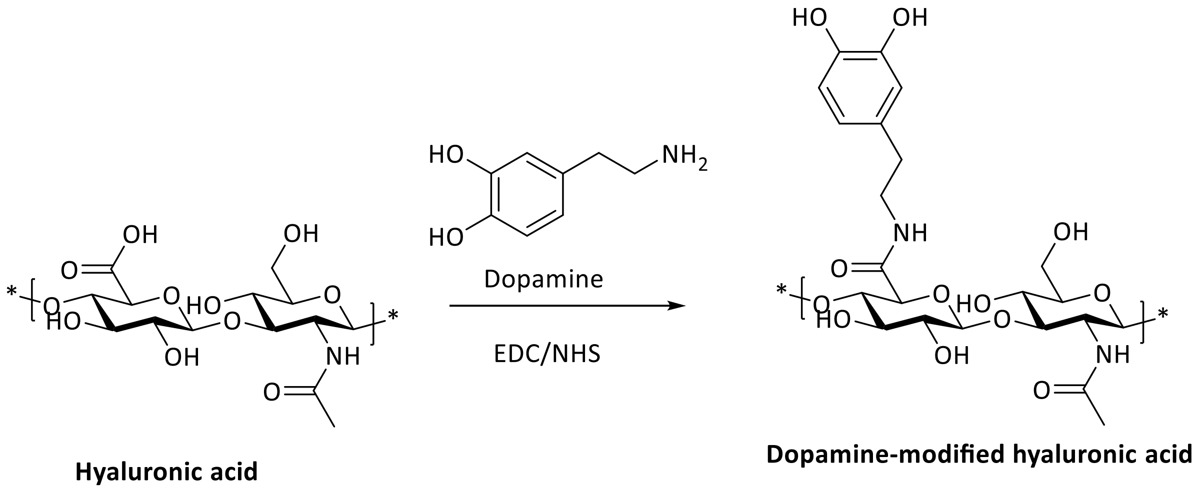

FIGURE 2.2

Synthesis of catechol-modified hyaluronic acid through carbodiimide chemistry, where 1-ethyl-3-(3-dimethylaminopropyl) carbodiimide (EDC), and N-hydroxysuccinimide (NHS) act as intermediaries.

Zhou *et al.* proposed a different approach to prepare HA-catechol (Figure 2.3) [47]. Here, HA is firstly oxidized using sodium periodate ($NaIO_4$), originating dialdehyde-functionalized HA. The formation of the Schiff base is then achieved by the reaction between dialdehyde groups in oxidized HA and the primary amine groups in dopamine. This method allows to achieve a higher degree of substitution of catechol groups than that obtained using the carbodiimide coupling reaction [47][71]. In addition, Zhou and co-workers have proved great adherence capacity to several organ tissues of rabbits, namely the heart, the liver, and the kidney [47].

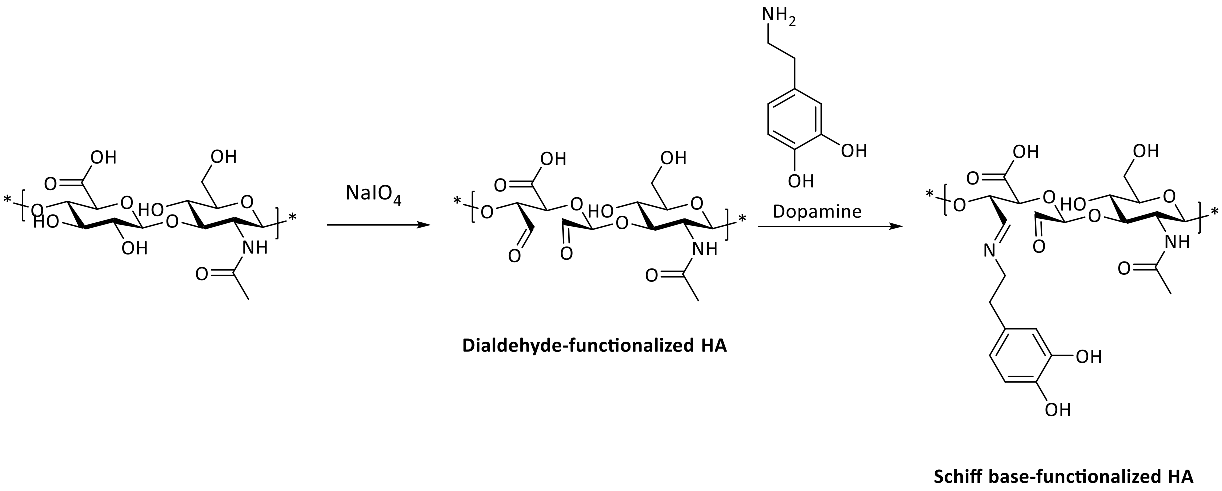

FIGURE 2.3

Synthesis route to obtain Schiff base-functionalized HA.

The catechol groups are oxidized at alkaline pH and are converted into catechol quinones, which easily react with several functional groups and specifically with other catechols, resulting in chemical crosslinking between HA chains through the formation of catechol-catechol adducts. By this mechanism, the chemically crosslinked catechol-modified HA hydrogel is formed (Figure 2.4) [70].

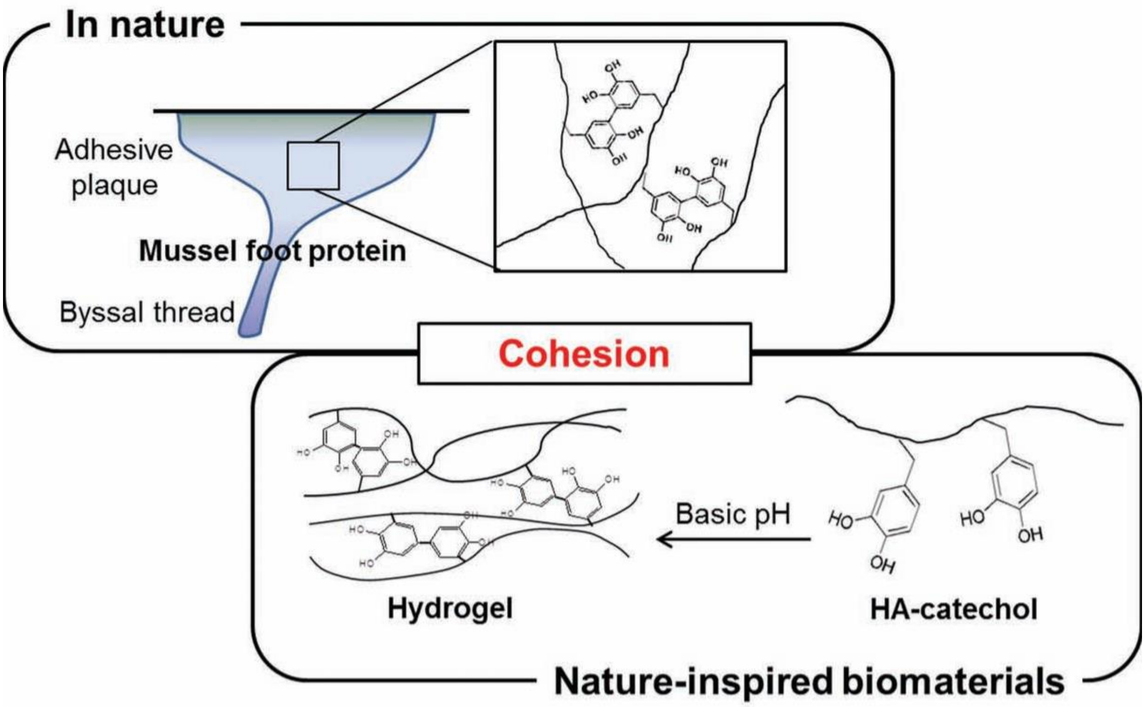

FIGURE 2.4

Schematic representation of the cohesive function of catechol groups when submitted under an alkaline environment. The catechol-modified HA forms a hydrogel by catechol-catechol covalent bonds. Reproduced from [72].

There are, however, other reactions between catechol groups that allow for the crosslinking of the HA chains (Figure 2.5). These non-covalent interactions comprise hydrogen bonds, π-π stacking, cation-π interactions and metal coordination [72]. Metal coordination, for instance, has been used as a crosslinking method to form hydrogels, namely through the addition of Fe^{3+} ions to the catechol-modified HA [73][74].

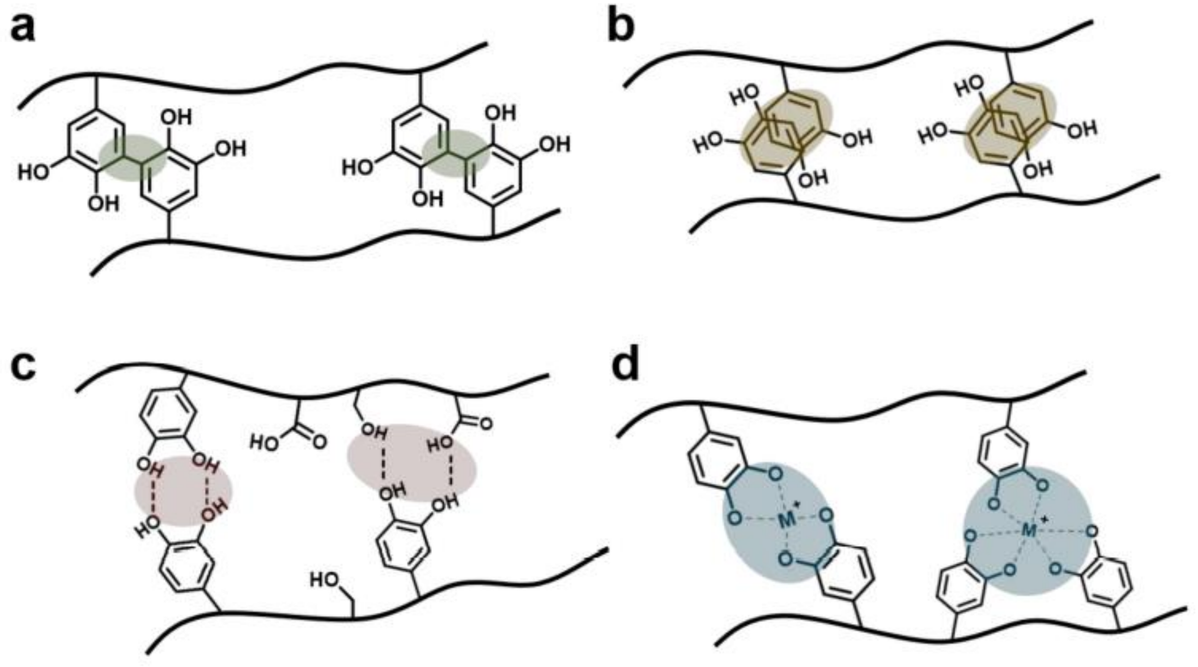

FIGURE 2.5

Schematic illustration of catechol-involving reactions of HA–catechol: (a) covalent bonds, (b) π–π stacking, (c) hydrogen bonds, and (d) metal coordination. Reproduced from [71].

2.2.3 | Electrically Conductive Hydrogels: The Path towards Functionalized Graphene

The electrical conductivity is an important factor that must be considered in the design of tissue engineering biomaterials as this may allow to mimic the electrophysiological characteristics of tissues, such as cardiovascular, skeletal muscle and neural tissues [75].

Under physiological conditions, neurons use electrical signals to communicate with each other and with other cell types through a complex and vast network [76]. CNS injuries may lead to the obstruction of this network, degrading its electrical properties and, hence, decreasing proliferation and migration of neuronal cells [77]. In addition, endogenous electric fields are known to be crucial during neural development. Thereby, an ideal hydrogel must support the endogenous electric field propagation in order to favour neural regeneration [78]. Suitable electric conductivities have been shown to promote neurogenesis in the lesion site as well as neuronal growth [79].

The appliance of exogenous biomimetic electrical signals has also been shown to activate proliferation, migration, and differentiation of neural cells, consisting therefore of a powerful tool to induce repairment after SCIs [80]. Moreover, electrical stimulation promotes cell adhesion to the biomaterial as well as neurite growth [81].

The electric conductivity of hydrogels can be increased through several strategies. Polypyrrole (PPy) and polyaniline are two conductive polymers with many attractive properties, such as high conductivity, easy synthesis, low cost, and easy availability [82]. However, a critical issue for the use of these polymers in neural tissue engineering is its suboptimal biocompatibility. Thereby, these polymers are usually combined with biodegradable polymers. For instance, Luo *et al.* have developed a natural biopolymer based soft hydrogel with PPy that was able to yield similar electrical conductivities to the ones found in the spinal cord. Moreover, *in vitro*, these hydrogels promoted neuronal differentiation, enhanced axon outgrowth and inhibited astrocyte differentiation [83].

Carbon-based nanomaterials are an alternative to PPy and other conductive polymers. In particular, carbon nanotubes (CNTs) and graphene have been increasingly applied in neural tissue engineering because of their inherent conductivity and flexibility, as well as good biocompatibility and outstanding mechanical properties [77][84].

CNTs are allotropes of carbon arranged in a cylindrical structure, and they have been shown to promote neurite outgrowth [77][85]. Moreover, Shin *et al.* demonstrated that a catechol-modified HA hydrogel with both CNTs and polypyrrole enhanced neurogenesis of human NSCs, showing good biocompatibility under small percentages of electroconductive motifs [86]. Sun *et al.* have also shown that a collagen hydrogel with CNTs up to 1 w/w % displayed more than 85 % of cell viability. However, for concentrations of CNTs up to 2 w/w %, cell viability was significantly decreased [87].

Graphene, on the other hand, is a carbon allotrope consisting of a single layer of carbon atoms arranged in a two-dimensional hexagonal lattice. It can sustain extremely high electric current densities (a million times higher than copper) and presents a high thermal conductivity, above 3000 W m^{-1} K^{-1}. In addition, most studies indicate that graphene and its derivatives are biocompatible and have lower toxicity, although no consensus has been reached yet [84]. Graphene also has remarkable bactericidal activity on a wide range of bacteria [88], antiviral properties [77], anti-inflammatory effects [89], and good mechanical properties, with a high elastic modulus (≈1 TPa) and a tensile strength of 130 ± 10 GPa [84].

As natural hydrogels usually have poor electrical and mechanical properties, the reinforcement of their networks with graphene and derivatives has been reported to optimize the primary properties. However, graphene is hydrophobic and presents poor dispersion in organic and aqueous solvents containing proteins, salts, or other ions, which makes it difficult to include the material in polymer-based hydrogels [84].

The functionalization of graphene, where functional groups are attached to the graphene surface, allows to overcome the hydrophobic behaviour of graphene. The functionalization provides reactivity towards molecules and polymers with biological activity, which allows the production of stable dispersions of graphene with the polymer matrix [90].

Graphene oxide, a covalently functionalized version of graphene, has been investigated for many biomedical applications (Figure 2.6). HA hydrogels combined with graphene oxide have been developed as a vehicle for smart drug release [91]. In addition, graphene oxide hydrogel has been shown to promote neurite outgrowth when functionalized with choline [92]. Zhang *et al.* developed a hydrogel with graphene oxide able to promote the growth of neurons and the remyelination of axons [76]. Yet, the oxidation of graphene leads to a significant loss of its attractive electrical properties due to the conversion of the planar sp^2 lattice into a sp^3 lattice, which results in a drastic reduction of electron mobility [93]. To overcome these shortcomings, reduced graphene oxide has been used as an alternative [94]. However, the reduction of graphene oxide only partially restores the unique properties of pristine graphene (PG) [95].

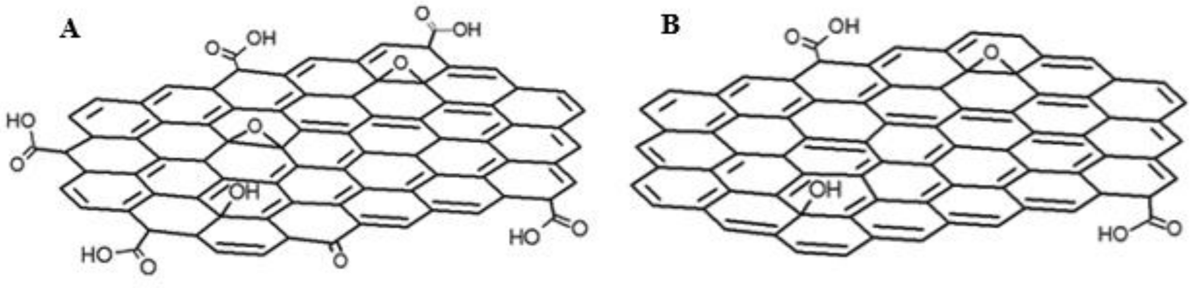

FIGURE 2.6

Schematic of graphene oxide (A) and reduced graphene oxide (B). Adapted from [95].

In addition to oxidation and reduction, there are several other ways to functionalize graphene. For instance, Silva *et al.* produced graphene functionalized with pyrrolidine (Figure 2.7) [96]. This covalent functionalization is based on 1,3-dipolar cycloaddition reaction of an azomethine ylide and this strategy increases the bioactivity of graphene while maintaining its inherent structure. Furthermore, they have also introduced a method to include metal nanoparticles, namely silver (Ag^+), into the graphene structure through the pyrrolidine groups [97]. Still, the application of FG besides graphene oxide and reduced graphene oxide in neural tissue engineering has been underexploited.

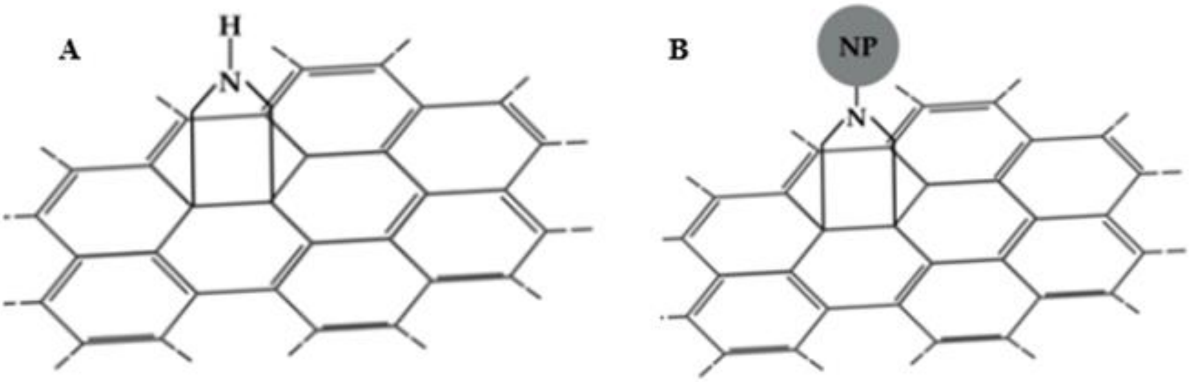

FIGURE 2.7

Schematics of FG without (A) and with the inclusion of metal nanoparticles (B). Adapted from [97].

While electroconductive materials optimize the electrical properties of the hydrogel, the rigidity and brittleness of the network are also increased. Thereby, conductive hydrogels usually have less flexibility. Since neuronal cells have been shown to prefer softer hydrogels, there is a need to find a compromise between the electrical and mechanical properties of the hydrogel [98].

2.2.4 | Hydrogels as Delivery Vehicles: The Immobilization of Nogo Receptor Antibodies

Hydrogels and, in particular, HA-based networks enable the localized delivery of therapeutic cargo, such as stem cells, drugs and growth factors to areas of CNS damage [99].

For instance, Zarei-Kheirabadi *et al.* demonstrated that the encapsulation of human embryonic stem cell derived-NSCs within HA-based hydrogels leads to increased differentiation of these cells into oligodendrocytes and improved locomotor function after a SCI [100]. In addition, Seidlits *et al.* have shown that HA-based biomaterials lead to long-term expansion and differentiation of NPSCs seeded within the hydrogel toward oligodendroglial and neuronal fates, while inhibiting astroglial fates [101].

Moreover, biomolecules such as growth factors can be tethered to the HA polymer chain or embedded in a hydrogel for local delivery. The drug release profile may be tuned by adjusting the degradation rate of the HA hydrogel, which can be tailored through chemical modifications [99]. Donaghue *et al.* used a HA-based hydrogel to deliver neurotrophin-3, a growth factor, and anti-Nogo-A, an antibody that targets the growth inhibitory molecule Nogo-A, which led to increased axon density and improved locomotor function in a SCI model [102]. Furthermore, hyaluronan hydrogels have been used as vehicles to deliver other growth factors such as brain-derived neurotrophic factor [103] and vascular endothelial growth factor [104].

As will be further discussed in Chapter 3, Nogo, myelin-associated glycoprotein (MAG) and oligodendrocyte myelin glycoprotein (OMGP) are myelin-associated proteins that hinder axonal growth, all of which interact with the NgR. Thus, NgR antibodies have been seen as a mean to promote the regeneration of the CNS after injury. Tian *et al.* included Nogo-66 receptor antibodies into a HA hydrogel by covalently attaching the antibodies to the HA backbone via the hydrolytically unstable hydrazone linkage. The antibody had to be previously oxidized. The hydrazone linkage formed between hydrogel and antibody is pH-sensitive and, thereby, at low pH, the antibodies were released quite fast, while in the neutral and alkaline environment the antibodies were released much slower. The bioactive antibody could be released from these hydrogels for at least 400 h [48].

Hou *et al.* confirmed that HA hydrogels modified with NgR antibodies supported attachment, survival, and neurite extension of neural cells, with both more neurites and longer neurite extension in the groups of modified HA hydrogels than those in unmodified controls. Moreover, while dorsal root ganglia and neuron cells adhered to the modified hydrogels and survived well, the same did not happen with unmodified HA hydrogels [105].

Another study conducted by Wei *et al.* have shown that HA-based hydrogels modified with poly-L-lysine (PLL) and Nogo-66 receptor antibodies when administered to rats after lateral hemisection of the spinal cord resulted in the enhanced extension of anti-neurofilament positive axons into the hydrogel when compared to HA-PLL hydrogel without antibodies. In addition, there were more cells and normal axons with myelin in the hydrogel with immobilized antibodies than that of HA-PLL hydrogel. In this study, the antibodies were once again immobilized on the backbone of HA hydrogels through its aldehyde group interaction with hydrazide groups of adipic dihydrazide (ADH) [106].

2.3 | Polyisocyanopeptides

As referred in Chapter 1, under the work at KU Leuven, PIC-based hydrogels were used to study the influence of salts on their microstructure.

These are novel synthetic fibrous hydrogels based on PICs, grafted with oligo(ethylene glycol) side chains, first published in 2013 by Kouwer and co-workers [21].

The PIC polymers are obtained through a nickel(II)-catalysed polymerization of isocyano-(D)-alanyl-(L)-alanines functionalized with the oligo(ethylene glycol) chains (Figure 2.8a). These polymers possess a stiff and helical architecture (Figure 2.8c), which is stabilized by a peptidic hydrogen-bond network along the polymer backbone (Figure 2.8b) [21].

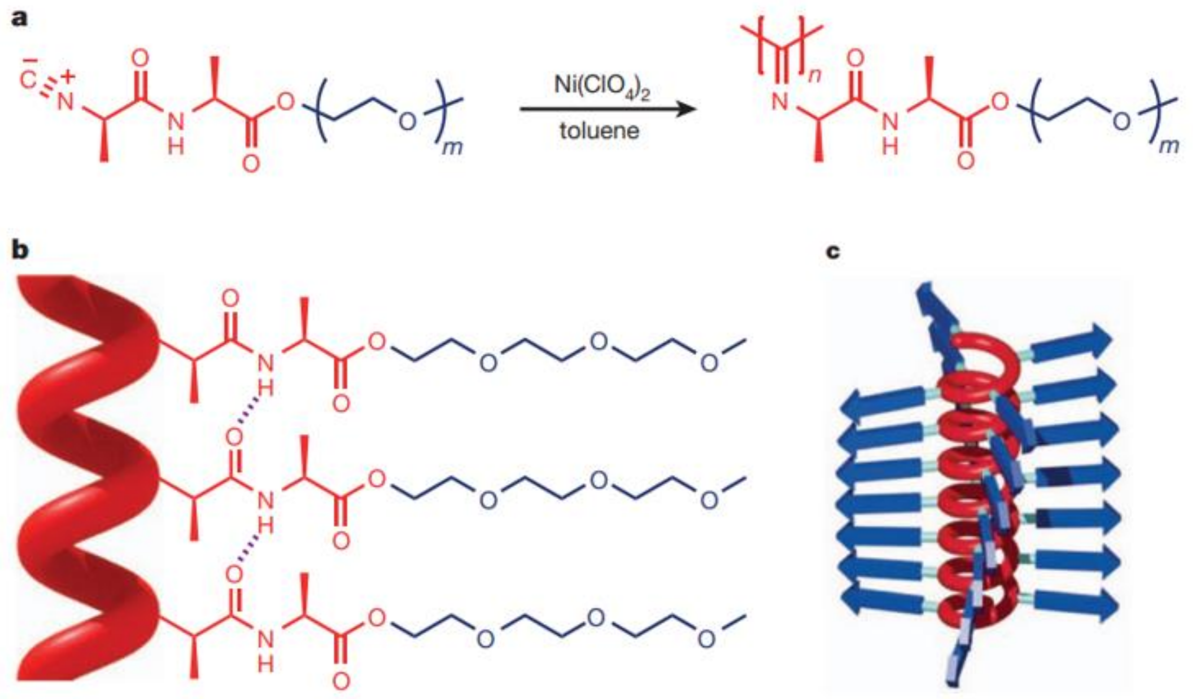

FIGURE 2.8

Polyisocyanopeptides with substituted oligo (ethylene glycol) side chains. In (a) the synthesis of the polymer is described, whereas in (b) the hydrogen-bond network that stabilizes the helical architecture is represented with dotted lines. (c) is a schematic representation of the beta sheet helix. Adapted from [21].

The beta helix architecture is, in addition to the alfa helix and the beta sheet, one of the structural motifs found in proteins. PICs synthetically reproduce this natural structure [107].

It must also be noted that when the polymer is formed by isocyano-(L)-alanyl-(L)-alanines instead of the alanine enantiomers D and L, the helix was found to be less stable. This is due to van der Waals contact between the methyl groups of the alanine units that leads to unfavorable steric interaction. When the enantiomers are used, this unwanted interaction is absent, and the structure is thereby more stable [107].

PICs, when dissolved in water, form transparent thermoreversible hydrogels at extremely low concentrations and upon heating [21]. With the increment of temperature, the polymers become increasingly hydrophobic and at the lower critical solution temperature (LCST) a network of entangled semi-flexible bundles of polymer chains is formed [20]. As so, bundle formation in the PIC hydrogels is thermally activated. Heating the polymers results in the entropic desolvation of the ethylene glycol arms, giving rise to more hydrophobic chains and stronger hydrophobic interactions, which drives the formation of the hydrogel. Therefore, the hydrophobic effects are caused by the ethylene glycol tails [21].

The temperature upon which hydrogel formation is activated depends on the length of the ethylene glycol tail. It shows little dependence on the polymer concentration. For the standard polymer length, the gelation temperature is around 18°C. In addition, the transition from hydrogel to solution and vice-versa is completely reversible [21].

The tunability of the pore size is another important parameter to consider. Herein, since the bundle dimensions are independent of the polymer concentration, the pore size in the hydrogel is directly controlled by the PIC concentration [21][108].

Unlike many networks of synthetic polymers, PIC-based hydrogels show a strong and well-defined nonlinear stress response after a critical stress has been applied, a behavior usually named stress-stiffening [21].

2.3.1 | The Stress-Stiffening Behaviour of Polyisocyanopeptide Hydrogels

It is well known that biological materials from several tissues stiffen under strain [109][110]. Mechanical studies have also confirmed that gels made of structural polymers, such as collagen, fibrin, and intermediate filaments, present this stiffening behavior [109]. These gels present a constant stiffness or storage modulus G' at small deformations. However, when an internal or external stress (or strain) is applied that exceeds a critical value, these biological gels show a nonlinear stiffening response that is usually named stress-stiffening [111].

From shear rheology experiments in the linear viscoelastic regime, the storage modulus G' is obtained as the ratio between the stress σ and the strain γ. For elastic gels, however, the term plateau modulus G_0 is often used for G' since the modulus is independent from the deformation frequency. In the nonlinear regime, the modulus is more accurately described by the differential modulus K', which is equal to $\partial\sigma/\partial\gamma$ (Figure 2.9a). It must be noted that in the linear regime, K' is equal to G' [111].

Overall, the mechanical properties of these fibrous networks can be described by three essential parameters (Figure 2.9b): (1) the storage modulus at low stress or strain (linear regime) or the so-called plateau modulus; (2) the critical stress σ_c or critical strain γ_c, which are the points at which the gels start to show the nonlinear strain response; and then (3) the extent of stiffening, expressed as the stiffening index *m*. This stiffening index can be considered the responsiveness of the hydrogel, whereas the critical stress or strain may be considered as its sensitivity. A low σ_c characterizes a highly stress-responsive gel and a high *m* indicates a strong response [111].

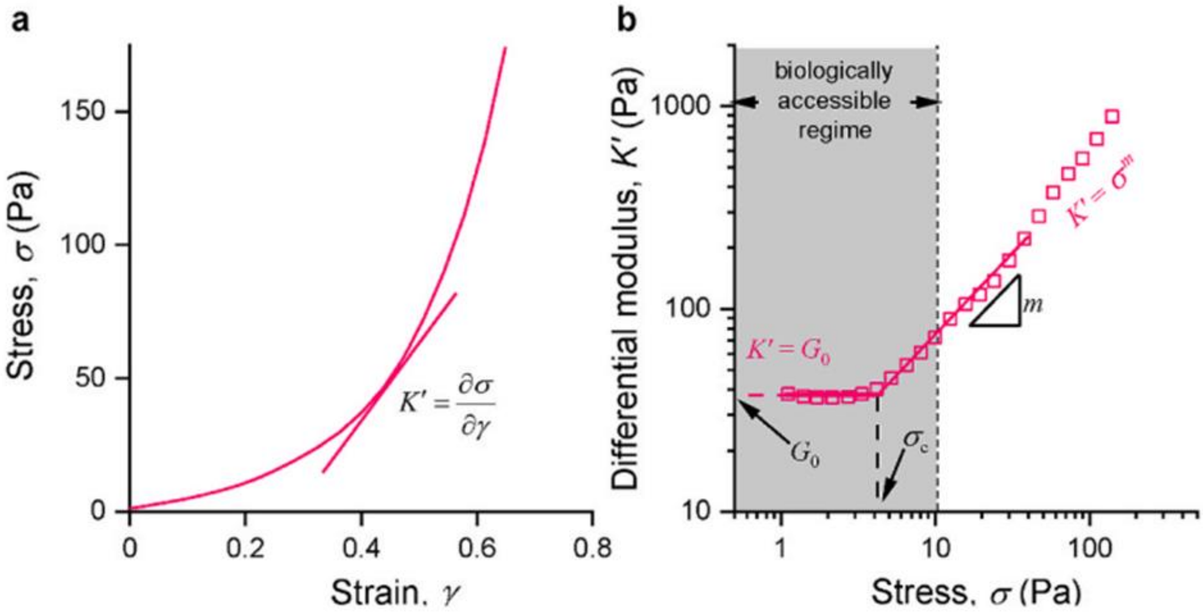

FIGURE 2.9

Basic concepts of the strain-stiffening behavior. (a) is the stress-strain curve of a fibrous matrix in a stress ramp, whereas in (b) the stiffness is represented as the differential modulus *K'*, as a function of stress, for the same polymer. At low stress, $K' = G_0$. However, beyond a critical stress σ_c, *K'* increases, following $K' \propto \sigma^m$, where *m* is the stiffening index. Reproduced from [111].

The precise biological functions of the nonlinear mechanical properties of the ECM remain mostly unknown for now [111]. Nevertheless, it is believed that they may be involved in the structural integrity of tissues [109], as well as in communication processes between cells [112].

PIC hydrogels developed by Kouwer *et al.* mimic the mechanical properties of biological gels, including the nonlinear mechanics at large stress or strain (Figure 2.10b), which is markedly different than that of other synthetic hydrogels. In addition, Figure 2.10 shows, as previously stated, that while the gelation temperature is mainly independent from the concentration of the polymer (Figure 2.10c), it is highly dependent on the length of the ethylene glycol tail (Figure 2.10a) [20].

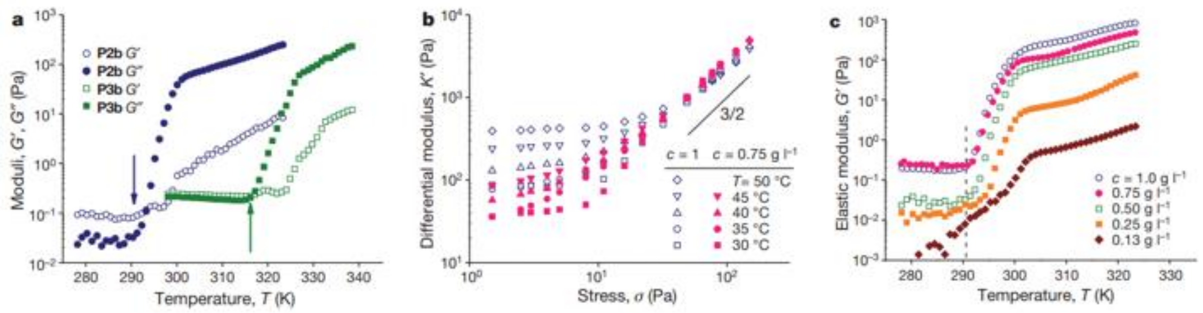

FIGURE 2.10

Rheological analyses of PIC hydrogels carried by Kouwer and co-workers. (a) Moduli *G′* and *G″* as a function of temperature *T* for P2b and P3b at c = 1.0 mg ml^{-1}. P2b and P3b are polyisocyanopeptide polymers with different side chain lengths. While P2b has three units of ethylene glycol as side chain, P3b has four. The arrows indicate the transition temperature, which can be rheologically determined as the onset of the step in *G′* at a frequency of 1 Hz. (b) Differential modulus *K′* as a function of stress for different values of *c* and *T*. (c) *G′* as a function of *T* for P2b at different concentrations. The gelation temperature is indicated by the dashed line, and it is nearly concentration-independent. Reproduced from [21].

The nonlinear mechanics of PIC hydrogels can be used to drive cell behavior as the ECM does. Das *et al.* used PIC matrices with similar stiffness but different critical stresses to study the effect of this mechanical parameter on cell behavior. They demonstrated that adipose-derived stem cells could be switched from adipogenesis to osteogenesis by changing the onset of stress-stiffening (through changes in polymer length) [113]. In addition, Liu and co-workers verified that PIC hydrogels with the strongest stiffening response to stress resulted in the strongest spreading of adipose-derived stem cells [114].

2.3.2 | Applications of Polyisocyanopeptide Hydrogels

The gelation of PICs is thermoreversible. When the PIC hydrogel is cooled below the gelation temperature, it turns into a polymer solution [21]. This streamlines cell harvesting, pointing the PIC hydrogel as a particularly suited matrix for 3D cell culture [114]. In addition, Zimoch *et al.* demonstrated that fibroblasts, endothelial cells, adipose-derived stem cells and melanoma cells do survive, thrive, and differentiate in optimized PIC hydrogels [115]. Liu and co-workers have also shown that the addition of $\alpha 5\beta 1$ integrin-selective bicyclic RGD peptide in PIC hydrogels resulted in enhanced stem cell spreading, showing that it was even faster than the spreading registered in the default RGD-decorated PIC hydrogel [116]. Studies have also confirmed the non-immunogenicity and fully biocompatibility of PIC hydrogels, as they do not induce inflammation when applied *in vivo* [117]. Therefore, PIC hydrogels are considered as artificial cytoskeleton models [118], for cancer therapeutics [119], and for 3D printing [120], wound healing [121][122], and periodontal [123][124] applications.

Upon gelation, PIC polymers in the bundles can be chemically crosslinked to keep the network architecture unchanged, as described by Schoenmakers *et al*. Covalent crosslinking allows to stabilize the hydrogels permanently but may result in hydrogels with smaller pores and with more limited application potential in 3D cell studies. However, the approach developed by Schoenmakers and co-workers consists of crosslink the polymers predominantly inside the bundles, generating open porous networks of semi-flexible bundles (Figure 2.11). Therefore, in this methodology, the bundle formation remains thermally induced and the crosslinking should take place above the gelation temperature. By changing the concentration and the nature of the crosslinkers, the mechanical properties of the hydrogels can be tailored, both in the linear and in the strain-stiffening regime [125].

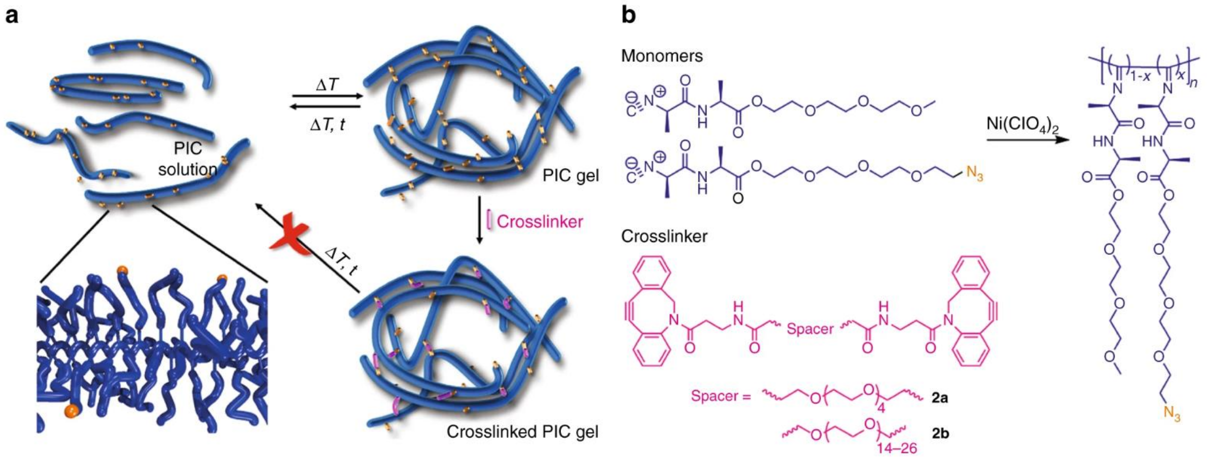

FIGURE 2.11

Crosslinking of a bundle network of PIC polymers. (a) Schematic representation of the crosslinking methodology, where azide (orange) decorated polymers (blue) are gelled and crosslinked selectively within the bundles by a crosslinker (pink). (b) Hydrogel components. It must be noted that some monomers include the azide groups, while others do not. The crosslinker may have different spacers, which allows to tailor the properties of the chemically crosslinked PIC hydrogels. Adapted from [125].

Schoenmakers *et al.* draw one interesting conclusion from their results. Upon cooling, only the thickest bundles of the crosslinked hydrogel remain. However, rheology experiments showed that the stiffness and the mechanical response to stress of the gels are barely impacted by the cooling. This suggests that in such networks the mechanical load is predominantly carried by the thickest bundles and that thinner bundles have a minor contribution to the linear and nonlinear mechanical properties of PIC hydrogels [125].

As a relatively young material, the number of studies using PIC is still limited. As so, its full potential across several applications is yet to be determined [111].

2.3.3 | The Hofmeister Effect on Polyisocyanopeptide Hydrogels

For the further development of smart materials for biomedical applications, it is important to study how simple and readily applicable stimuli can control the response of the material. One such stimulus is the addition of salts [20]. In 1888, it was discovered that salts have the ability to precipitate proteins from aqueous solutions [126]. This effect is named the Hofmeister effect and besides describing protein precipitation and stabilization, it can also be applied to describe the behavior of thermoresponsive aqueous systems [20], such as PIC hydrogels.

It has been shown that the addition of salts changes the lower critical solution temperature (LCST) of aqueous solutions of synthetic thermoresponsive polymers [127][128]. The nature of the salt and its concentration are the parameters that allows to tailor the transition temperature of polymer solutions [20].

In addition, Jaspers *et al.* described for the first time that the Hofmeister effect can be used to controllably manipulate the mechanical properties of PIC hydrogels. As expected, the addition of salts directly affected the gelation temperature of PIC hydrogels. However, in addition, they were able to construct hydrogels ranging from very soft to stiff, but all at identical concentration. There are other ways to vary the mechanical properties of the hydrogels without the addition of salts, namely by tuning polymer concentration, morphology, and bundle (or fiber) diameter. Still, some of these are difficult to control, while others simultaneously change many important network characteristics [20]. The addition of salts may offer an alternative method to tune some of the hydrogel properties and make it suitable for specific applications.

The Hofmeister effect is usually more pronounced for anions than for cations and some ions have a stronger effect than others. For that reason, a Hofmeister series was formulated (Figure 2.12) [127], where the ions on the left-hand side of the series are well-hydrated ions, usually named kosmotropes, and the ones on the right-hand side of the series, the poorly hydrated ions, are commonly named chaotropes. While the kosmotropes decrease protein solubility and the LCST of thermoresponsive polymers, the chaotropes ions increase both the protein solubility and the LCST of the polymers [20].

Jaspers *et al.* argue that three different interactions contribute to the Hofmeister effect in PIC hydrogels. Firstly, the added ions may destabilize the hydrogen bons between the polymer and its hydration water molecules (Figure 2.12a), which is expected to lead to a decrease in the solubility of the polymer and as a result a decrease in the gelation temperature of the PIC solution. This interaction will be stronger in the presence of well-hydrated ions. On the other hand, poorly hydrated anions have a strong affinity to the polymer; they can directly bind to the polymer (Figure 2.12b), adding extra charge and thereby increasing its solubility and gelation temperature. Finally, a third interaction is expected: depending on the nature of the salt, ions may interact with the hydration shell of the hydrophobic surface of the polymer (Figure 2.12c), leading to an increase or decrease of the gelation temperature. Salts that increase the interfacial tension at polymer/water interface reduce the gelation temperature. On the other hand, salts that decrease the polymer/water interfacial tension increase the gelation temperature [20].

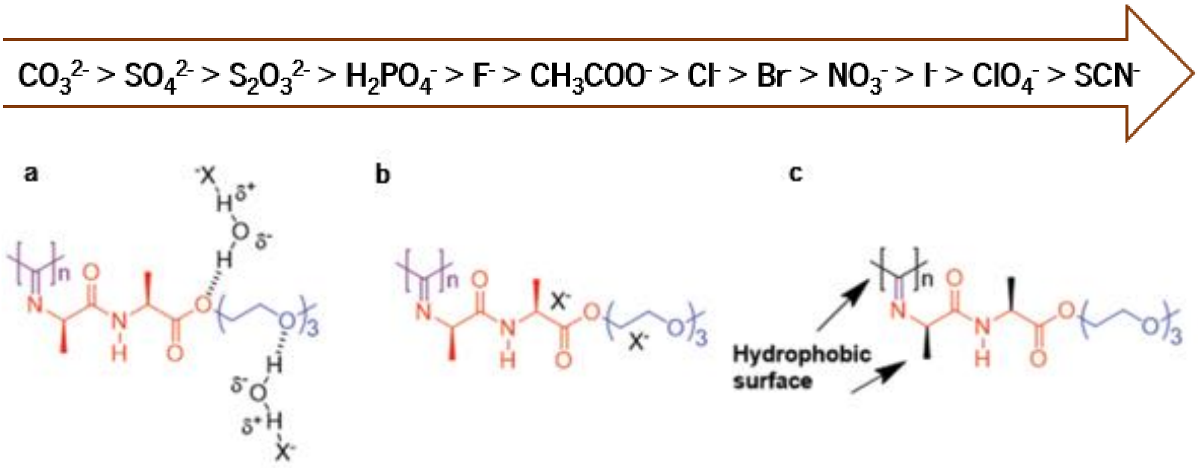

FIGURE 2.12

The Hofmeister series and the possible interactions between the Hofmeister series anions and ethylene glycol-functionalized polyisocyanide in water. The kosmotropes are on the left-side, whereas the chaotropes are represented on the right-side. (a) Hydrogen bonds between water molecules and the ethylene glycol side chains are destabilized through polarization by the anion X^-. (b) Direct binding of the anion to the polymer. The precise binding mechanism is yet unknown. (c) The anions can also interfere with the hydrophobic hydration of the polymer backbone by increasing or decreasing the surface tension at the polymer/water interface. Adapted from [20].

3. FUNCTIONALIZED HYALURONIC ACID-BASED HYDROGELS WITH CONTROLLABLE ELECTRICAL CONDUCTIVITY

In this chapter, the development of dopamine-modified HA hydrogels with graphene and NgR antibodies is presented, the production and evaluation methodologies are described and the obtained results are discussed.

3.1 | Introduction

The CNS comprises the brain, spinal cord and retina and it is the control panel of our bodies, responsible for cognition, movement, senses, and emotions [35]. The functional units of the CNS are neurons which are unique in their ability to transmit and store information. However, neurons are also very vulnerable to injury since the majority of them are post-mitotic cells incapable of cell division [14]. In addition, the vast majority of neurons are generated from NSCs during the embryonic and early postnatal stages. Only a small number of neurons is generated throughout the rest of human life. Consequently, the destruction of these cells can leave a patient with severe functional deficits [129].

The CNS is mostly composed by three main cell types, those being neurons, glial cells, and vascular cells [130].

Neurons are widely known electrically excitable cells. Across the nervous system, there are neurons with different morphologies and their size can range from 5 up to 130 μm. According to their function, they can be classified as motor, sensory or interneurons. However, despite their morphological and functional differences, they all possess a cell body, dendrites, axon, and axon terminals. The only exception is pseudounipolar neurons which have no dendrites [130]. In general, dendrites receive afferent signals while axons carry efferent signals. When the electrical signal, named the action potential, reaches the axon terminal, neurotransmitters, neuromodulators or neurohormones are released, thus translating the action potential to a chemical signal that can cross the synapse or neuromuscular junction [131].

Glial cells are quite different from neurons as they have complex branches extending from their bodies but are usually smaller than neurons and do not have axons and dendrites. In addition, these cells do not participate directly in synaptic interactions and electrical signalling. Glial cells include microglial cells, astrocytes, and oligodendrocytes [132].

Microglia are important for building and defending the CNS. These cells are the professional phagocytes of the CNS as they are able to sense and take up extracellular material, such as cell debris, apoptotic cells, as well as microbes and tumour cells [133]. They recognise antigens and initiate phagocytosis to remove foreign material [134]. When activated, they can also produce small molecules called cytokines that trigger cells of the immune system to respond to the injury site. Therefore, microglia are commonly defined as the resident tissue macrophages of the CNS, including the brain as well as the spinal cord and retina [133]. Following neuronal damage, the number of microglial cells at the injury site increases substantially. Microglia usually represent the majority of immune cells in the CNS, although there are others (Figure 3.1) [134], and perform a multitude of functions, with impactful participation in several physiological processes, such as neuroinflammation and degenerative diseases [133][135].

Astrocytes are restricted to the brain and spinal cord and its major function is to maintain in several and complex ways a suitable chemical environment for neuronal signalling [136]. They provide crucial support for the maintenance of neuronal homeostasis by regulating several processes and substances, including glutamate levels, which uncontrolled have lethal consequences for neurons [130].

In addition to microglia and astrocytes, oligodendrocytes are another important type of glial cells residing in the CNS. They produce and lay down a lipid-rich substance called myelin around axons in the CNS, which is crucial to augment the speed and conserve the electrical signal [132]. Apart from their myelinating function, oligodendrocytes also contribute for the maintenance of axonal and neuronal metabolism [130].

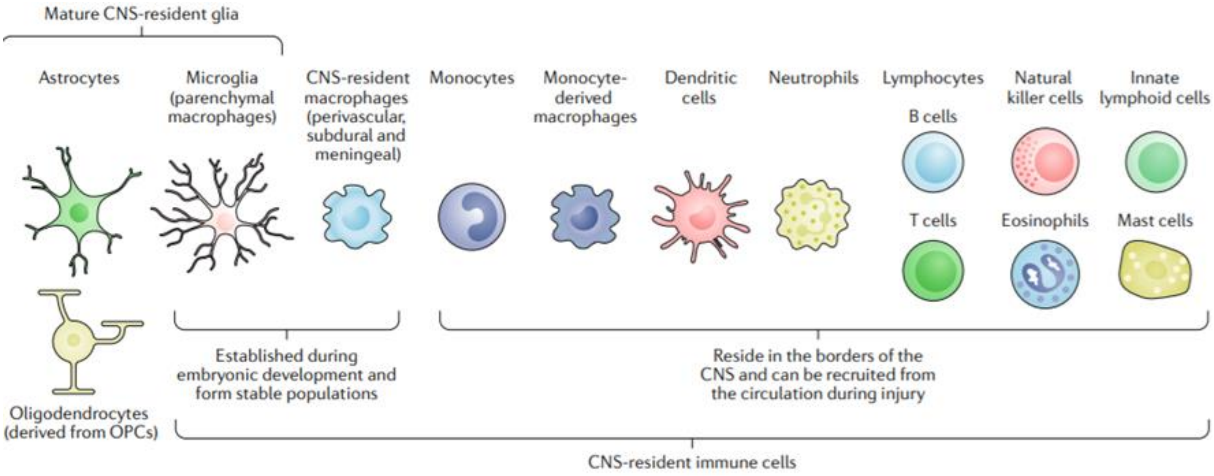

FIGURE 3.1

Central nervous system resident cell types. The various immune cells that reside in the borders of the CNS can be recruited from the circulation during disease and injury. Astrocytes, oligodendrocytes, and microglia represent the major glial populations of the CNS. Oligodendrocytes derive from OPCs. Reproduced from [134].

3.1.1 | Extracellular Matrix

The CNS extracellular matrix occupies the space between neurons and glial cells and both these cell types secrete molecules that contribute to the ECM [137]. It is a 3D structural framework that defines the environment for cells in the CNS [138]. The ECM plays an important role in the development of the CNS through regulating cell migration, axon guidance and synaptogenesis [137]. It is also deeply involved in regulatory signalling in mature and healthy CNS, whether in a direct way, through cell surface receptors, or in an indirect way as a carrier and reservoir for growth factors and molecules [138]. It regulates repair following injury by restricting in part aberrant remodelling [137].

Besides the ECM, its molecules also create specific compartments in the CNS extracellular space. These compartments include perineuronal nets (PNNs) and basement membranes (BMs) [137][138].

PNNs are pericellular condensed ECM structures that surround the soma and dendrites of some neurons, often including the axon initial segment. Neurons with PNNs, such as inhibitory interneurons in the cerebral cortex and motor neurons in the spinal cord, are present in almost all parts of the mature mammalian CNS [139]. These PNNs and the broad ECM are mainly composed of HA to which chondroitin sulphate proteoglycans (CSPGs), namely lecticans, are bound, as well as tenascin-R and link proteins (Figure 3.2) [137].

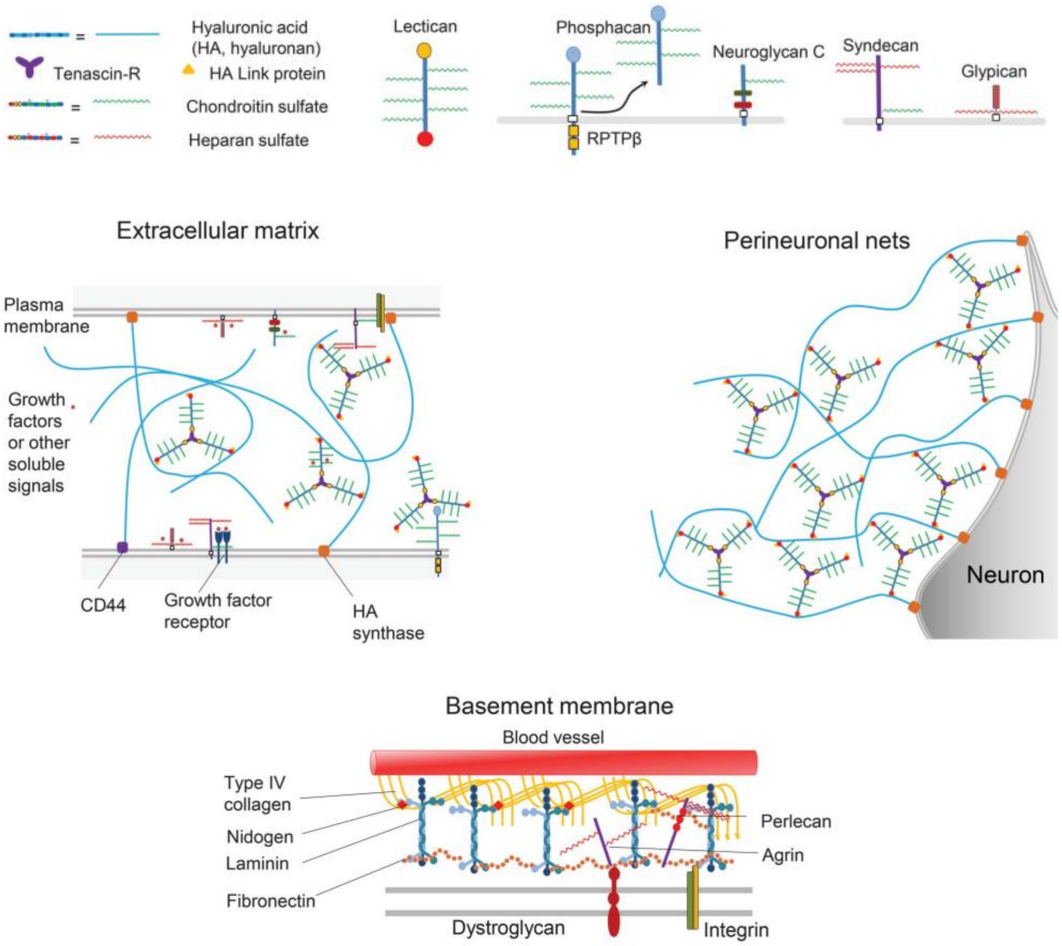

FIGURE 3.2

CNS extracellular matrix composition. HA is one of the main components of the CNS extracellular matrix, along with tenascin-R and sulphated proteoglycans, including CSPGs and HSPGs. HA can bind to cell membrane receptors such as CD44. Lecticans both in the ECM and PNNs bind to HA via interactions with tenascin-R, which are stabilized by link proteins. The BM surrounds endothelial cells of blood vessels, and it is mainly composed of laminin, collagen type IV and HSPGs. Reproduced from [137].

Although the ECM and PNNs share composition similarities, the ECM in PNNs is more compact with a higher concentration of CSPGs and other growth-inhibiting components [138]. PNNs may serve several functions such as regulating plasticity by stabilizing synaptic connectivity and protecting neurons and synapses by forming a physical and ionic shield to preserve the integrity of synaptic junction [140].

The BM is a thin layer of cell-adherent ECM that serves as a boundary between endothelial cells and parenchyma. It is composed primarily of collagen, laminin, fibronectin, dystroglycan and heparan sulphate proteoglycans (HSPGs), such as agrin or perlecan [137][138].

CPSGs and HSPGs are therefore the two main proteoglycans in the CNS. Proteoglycans consist of a core protein covalently linked to charged glycosaminoglycan (GAG) chains that are variably sulphated. There are several groups of CSPGs and HSPGs, being lecticans the most abundant CSPGs. In the CPSGs the amino sugar is N-acetylgalactosamine, while in the HSPGs is N-acetylglucosamine. The GAG chains are able to bind guidance molecules that regulate axon growth and pathfinding, including growth factors and others, and while HSPGs promote axonal growth and cell migration, CSPGs inhibits both [137]. Thereby, PNNs provide a nonpermissive environment for axonal growth as well as for the formation of new synapses, restricting structural plasticity and synaptic remodelling [137][138].

3.1.2 | Nogo-66 Receptor

Nogo-A, Nogo-B and Nogo-C are the three main protein products of the RTN4 gene, also known as Nogo (Figure 3.3). These three proteins have the same last 188 amino acids in the carboxyl terminus and this common domain is called RTN. It contains two long hydrophobic stretches linked together by a 66-amino acid segment called Nogo-66. Nogo proteins are present in the endoplasmic reticulum as well as at the cell surface. On the cell surface, the N termini of Nogo-A and Nogo-B and the sequence of Nogo-A encoded by exon 3 have been found to face the extracellular space [141].

Nogo-A, in particular, has been confirmed as a major obstacle to nerve regeneration after injury in the adult mammalian CNS due to its inhibitory behavior when it comes to axonal regeneration. Both Nogo-66 loop and Nogo-A specific Nogo-Δ20 exert inhibitory effects on neurite growth and induce growth cone collapse [141][142].

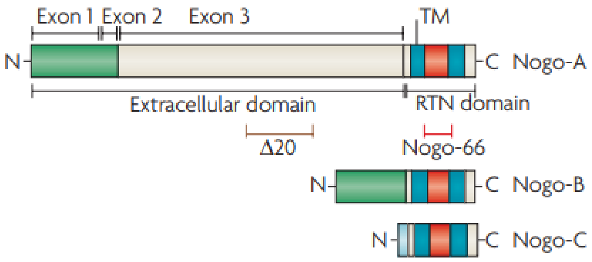

FIGURE 3.3

Structure of the three main Nogo isoforms and their functional domains. The fragment Nogo-Δ20 is shown in brown and the Nogo-66 loop is shown in red. These segments are the ones associated with neurite growth inhibition. Adapted from [141].

Nogo-66 exerts these inhibitory effects by binding to Nogo-66 receptor [142]. This receptor is a 473-residue protein expressed mainly in the grey matter of the CNS. Oligodendrocytes have minimal NgR1 expression. This receptor is mostly found in a tripartite complex (Figure 3.4), comprised of LINGO-1 and either p75 or TROY [143]. These transmembrane proteins are associated with Nogo-66 receptor because they are needed to induce Nogo signaling, since Nogo-66 receptor has no transmembrane domain [141]. In addition to functioning as a co-receptor for Nogo-66 receptor, LINGO-1 plays an important role in the inhibition of oligodendrocyte differentiation and myelination [143].

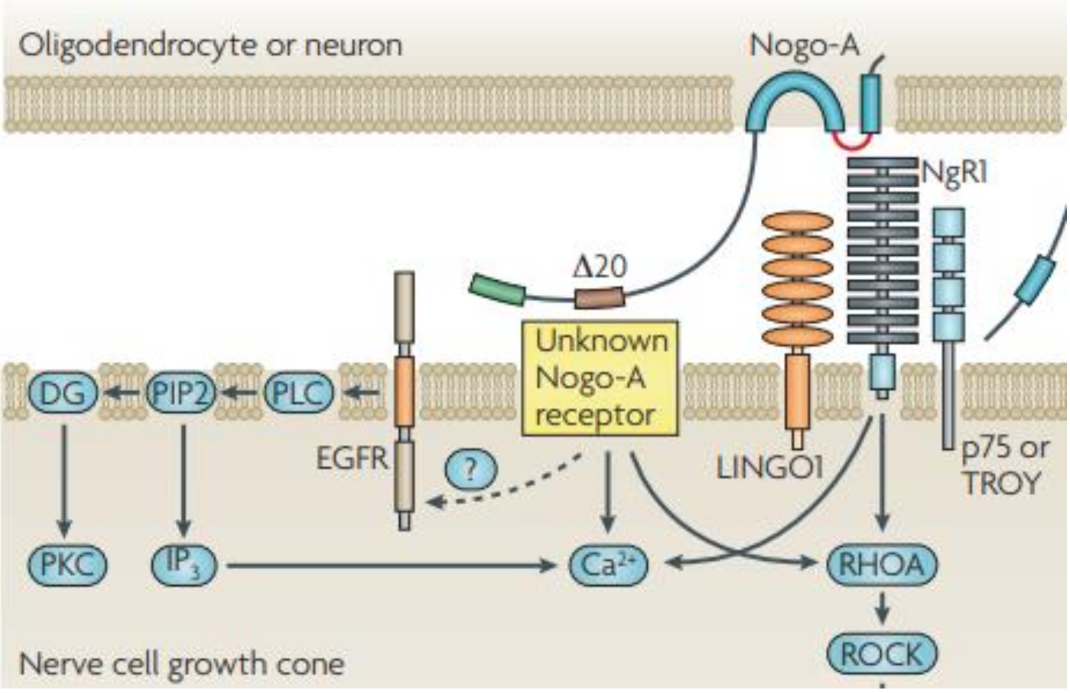

FIGURE 3.4

Signalling pathway of Nogo-A. Nogo-A inhibits neurite outgrowth through binding of its inhibitory Nogo-66 domain to Nogo-66 receptor. In addition, the fragment Nogo-Δ20 binds to an unknown receptor, also resulting in Ras homolog A (RHOA) activation. Adapted from [141].

While Nogo-66 receptor interacts with all three nogo isoforms, it has a greater binding affinity with Nogo-A due to the sequence in the C-terminal part of Nogo-A that is encoded by exon 3. During the main outgrowth phase of central and peripheral neurons, Nogo-A is expressed by many neuron types. However, this expression decreases to low level after birth. Nevertheless, some neurons, such as interneurons in the hippocampus and spinal motor neurons, retain high levels of Nogo-A expression. In the postnatal CNS, Nogo-A is mainly expressed in oligodendrocytes [141].

The binding of the Nogo-66 domain to Nogo-66 receptor leads to an increase in intracellular Ca^{2+} and RHOA activation (Figure 3.4). Through RHOA signaling, the actin cytoskeleton is destabilized, and this leads to growth cone collapse, neurite outgrowth inhibition, and oligodendrocyte differentiation inhibition. The Nogo-A specific segment Nogo-Δ20 interacts with an unknown Nogo-A receptor, also resulting in RHOA activation and increased intracellular Ca^{2+} levels, as well as transactivation of the epidermal growth factor receptor (EGFR) with a detailed pathway still unknown [141][143]. More recently, Kempf *et al.* identified sphingosine 1-phosphate receptor 2 (S1PR2) as a Nogo-A-Δ20 specific receptor and their interaction results in RHOA activation. However, the study did not approach calcium release and activation of EGFR and thus it is premature to conclude that this receptor is the unknown receptor identified in Figure 3.4 [144].

Interestingly, it has been confirmed that, besides Nogo-A, Nogo-66 receptor also binds to the growth-inhibitory molecules MAG and OMGP, resulting in the same signaling pathway [143]. MAG, however, binds with higher affinity to another receptor from the same family called Nogo Receptor 2 (NgR2) [141].

Nogo-66 receptor is therefore the common binding receptor for Nogo-A, OMGP and MAG, all of which are growth inhibitory molecules. Thus, targeting this receptor has been viewed as a potential strategy to promote axonal regeneration and neurite outgrowth [141][143].

3.1.3 | Spinal Cord Injury

SCI causes neural cell death and tissue architecture destruction, thereby resulting in functional impairments. Endogenous restoration after SCI is limited due to the low repair capacity of the CNS and the growth-inhibitory environment that impedes the regrowth of axons [138].

An injury of the spinal cord triggers a series of complex cellular and biochemical reactions that are usually divided into two phases: primary and secondary injuries. The primary injury leads to cell damage or death at the injury epicentre as well as local blood vessel damage [12]. It may also compromise the blood-spinal cord barrier. Then, together, these events initiate a sustained secondary injury cascade. The destruction of the local micro-vascular supply leads to ischemia, which together with pro-apoptotic signalling causes cell dysfunction and death. Blood vessel injury may also cause severe haemorrhages. These haemorrhages and the migration of blood cells to the injury site through the broken blood-spinal cord barrier leads to an influx of inflammatory cells, such as macrophages and lymphocytes, and pro-inflammatory cytokines. Dying neurons and astrocytes release high levels of glutamate that are poorly reabsorbed by surviving astrocytes, leading to excitotoxic cell death [145]. Furthermore, ongoing necrosis of neurons and glia due to ischaemia, inflammation, and excitotoxicity releases adenosine triphosphate (ATP), DNA, and potassium, which can activate microglial cells and hence propagate the inflammatory response, deepening the ongoing apoptosis of neurons and oligodendrocytes [145][146]. The death of oligodendrocytes causes axons to lose their myelination, which greatly impairs the conduction of electrical signalling. While cleaning myelin debris at the injury site, phagocytic inflammatory cells may release cytotoxic by-products, including free radicals, inducing further damage to the spinal cord [145]. Reactive astrocytes overexpress cytokines and chemokines, attracting more inflammatory cells to the lesion site [137]. These events cyclically propagate the secondary injury cascade [145].

The degradation of the ECM components leads to further disruption of the spinal cord-blood barrier, intensifies the inflammation, and disrupts synaptic homeostasis. Fragmentation of HA occurs due to the overactivation of hyaluronidases or inducible matrix metalloproteinases (MMPs) released from inflammatory cells and activated microglia. These MMPs are proteases that process ECM proteoglycans, and they are held in an inactive state unless activated by products of inflammation such as free radicals and cytokines. Therefore, when a lesion occurs, the basement membrane and ECM matrix are degraded, leading to further inflammation. Low molecular weight HA species activate microglia and macrophages, promoting inflammation. Reactive astrocytes upregulate CSPGs and other inhibitory molecules, preventing axonal repair and remyelination. GAG chains are released from their core protein backbone, promoting further inflammation [137].

The vast cell death and degeneration in the acute phase of injury promote the formation of cystic cavities that are an extremely poor substrate for axonal regrowth filled with extracellular fluid, thin bands of connective tissue and macrophages [145].

In the acute phase, signalling from activated microglia, astrocytes and macrophages causes the secretion of ECM proteins that are inhibitory to axonal growth. These inhibitory biostructures, such as

CSPGs and tenascin, condense with astrocytes to form the glial scar (Figure 3.5) [145]. In the beginning, glial scars isolate the injury site from the healthy tissue, locking inflammatory cells within areas of damaged tissue and protecting adjacent viable neural tissue [146]. However, overtime, they act as a physical barrier that blocks the outgrowth, penetration, and reconnection of axons. The glial scar also constitutes a biochemical barrier due to the presence of molecules such as Nogo, MAG, OMGPs and CSPGs, all of which are potent inhibitors of neurite outgrowth [12]. Therefore, the glial scar potently restricts both axon regeneration (that is, the repair or regrowth of existing neural pathways, or the development of new pathways) and anatomical plasticity by inhibiting neurite outgrowth [145].

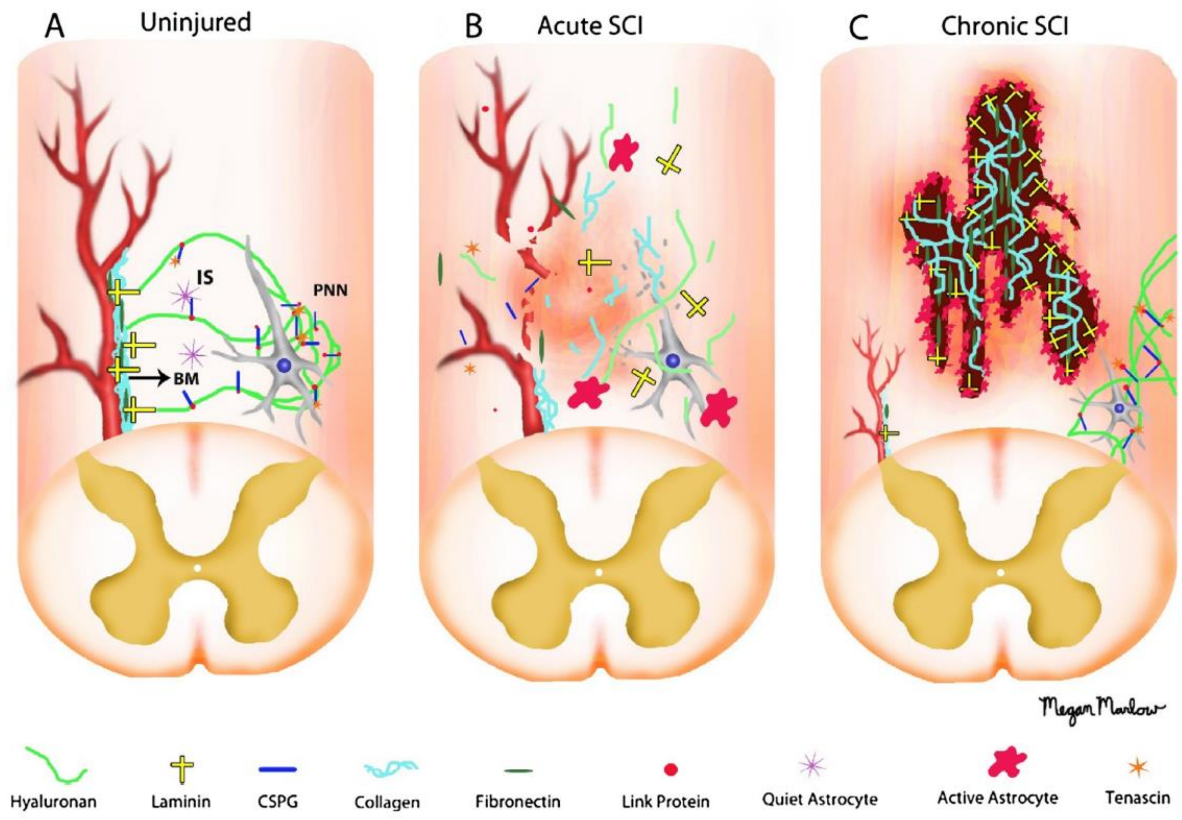

FIGURE 3.5

Schematic illustration of the ECM in healthy spinal cord and at the acute and chronic stage of SCI. (A) Uninjured spinal cord, with representation of PNN, interstitial space (IS) and the BM of blood vessels. (B) In acute SCI, the ECM is compromised, and blood vessels are damaged. Astrocytes become reactive. (C) In chronic SCI tissue damage is extensive. Scar tissue rich in growth inhibitory molecules has formed at the injury site. Reproduced from [138].

3.1.4 | Treatments for Spinal Cord Injuries

CNS injuries, such as SCIs, are one of the leading causes of long-term disability and death worldwide [9]. The impact on the individual quality of life and the social costs of these conditions are enormous. Indeed, damage to the CNS usually results in severe neurological impairments which commonly cause limitations such as paralysis, limited mobility, and sensory loss. Moreover, completely functional restoration in damaged CNS is not yet possible in most clinical cases [12].

Recently, ambitious therapies for the treatment of SCIs are in development or under clinical trials. Some, such as the administration of HGF or granulocyte colony-stimulating factors, focus on neuroprotection. Others, however, focus on neuroregeneration, such as spinal cord stimulation and the administration of OPCs or anti-Nogo antibodies. In addition, biomaterials have been increasingly investigated as they constitute a biodegradable and cytocompatible tool able to fill cavitation defects and reproduce the complex structural architecture of the ECM, while delivering treatments in a controlled and non-invasive manner [13].

One of the biomaterials with higher research record for the treatment of CNS injuries is HA. HA is a polysaccharide comprised of repeating disaccharide units of D-glucuronic acid and N-acetyl-D-glucosamine [46]. It is the main component of the central nervous system ECM, thus being able to mimic the neuronal natural environment [15]. Indeed, research has proved that HA is a suitable polymer for scaffold-based therapies in the CNS. Lower molecular weight HA has been shown to promote angiogenesis [50][147] and the application of this polymer to the injury site have been confirmed as effective in reducing the glial scar formation following CNS damage [51]. In addition, crosslinked HA scaffolds were shown to promote neurite outgrowth [55]. Moreover, HA-based hydrogels are usually mechanically soft, with storage modulus typically lower than 1 kPa [1][47][104]. Lower mechanical properties favour neuronal cells over astroglial populations [62][63][64]. Furthermore, HA is chemically versatile, and biomolecules, such as NgR antibodies, can be attached to it through different mechanisms. Indeed, several studies have successfully immobilized NgR antibodies on the HA backbone [48][106], and they were shown to support attachment, survival, and neurite extension of neuronal cells, with both more neurites and longer neurite extension in the groups of modified HA hydrogels than those in unmodified controls [105].

Therefore, the aim is to develop and assess HA-based hydrogels with graphene and NgR antibodies to induce axonal development and neuronal growth in the inhibitive environment of the CNS and, in particular, to promote recovery after SCI. Catechol groups were incorporated in the HA backbone through the oxidation of the polymer followed by the addition of dopamine, as reported by Zhou *et al* [47]. This allowed for the crosslinking of HA chains through catechol-catechol adducts, while simultaneously conferring to the hydrogel higher adhesive properties. Graphene was dispersed within the hydrogel matrix to increase its electrical conductivity, as higher electrical conductivities have been shown to promote neurogenesis in the lesion site as well as neuronal growth [78][79]. Furthermore, graphene has remarkable bactericidal activity on a wide range of bacteria [88], antiviral properties [77], and anti-inflammatory effects [89].

3.2 | Material and Methods

Sodium hyaluronate with a molecular weight of 373 kDa (calculated by GPC) was purchased from LifeCore Biomedical and $NaIO_4$ was purchased from Sigma-Aldrich. Ethylene glycol, dopamine hydrochloride and sodium cyanoborohydride ($NaBH_3CN$) were also purchased from Sigma-Aldrich. PG was provided by Professor Conceição Paiva from the Department of Polymer Engineering of University of Minho (Portugal). FG with pyrrolidine was produced according to Silva *et al.* by the 1,3-dipolar cycloaddition reaction of an azomethine ylide [96] and was also provided by Professor Conceição Paiva. Hyaluronidase from bovine tests, NHS and EDC were purchased from Sigma Aldrich. NgR antibodies were purchased from LifeCore Biomedical, LLC.

3.2.1 | Synthesis of Dopamine-Conjugated Hyaluronic Acid (DHA)

DHA was synthesized according to the method reported by Zhou *et al* [47]. This strategy has two steps: the oxidation of sodium hyaluronate which forms dialdehyde-HA and then the inclusion of catechol groups through the addition of dopamine, forming DHA. Briefly, 1.0 g of sodium hyaluronate was dissolved in 100 mL of ultrapure water for 4 h, followed by the addition of 50 mL of 2.67 % $NaIO_4$ solution. After 30 min, ethylene glycol (1 mL) was added into the reaction solution to neutralize the excess amount of $NaIO_4$. The reaction solution was dialyzed against ultrapure water for 3 days and lyophilized to obtain dialdehyde-HA.

DHA was synthesized by the Schiff base reaction between dopamine and dialdehyde-HA. Specifically, 1.0 g of dialdehyde-HA was dissolved in 100 mL of phosphate buffer saline (PBS, pH = 5), followed by the addition of 0.55 g of dopamine hydrochloride. The reaction was stirred for 24 h under dark conditions at room temperature (25 °C). Dialysis (3 days) and then lyophilization were performed. ^1H NMR spectrums were recorded and the degree of substitution of dopamine was determined by UV-vis spectrophotometry. Briefly, a standard curve UV absorbance per concentration was generated by measuring through a microplate reader (BIO-TEK Instruments) the absorbance of dopamine and DHA solutions with known concentrations at λ_{max} of 280 nm, which is the maximum absorbance wavelength of catechol. These curves, with a slope m, were used to determine the concentration of dopamine in DHA and the substitution degree of DHA was calculated by the following equation:

$$Degree\ of\ Substitution\ (\%) = \frac{m_{dopamine}}{m_{DHA}} \times 100\ \%$$

3.2.2 | Synthesis of Reduced Dopamine-Conjugated Hyaluronic Acid (RDHA)

RDHA was synthesized through the usage of a reducing agent, $NaBH_3CN$. Briefly, 1.0 g of DHA was dissolved in 100 mL de PBS and 225 mg of $NaBH_3CN$ was added to the solution. The reaction was stirred for 2 h under dark conditions at room temperature (25 °C). Dialysis (3 days) and then lyophilization were performed. ^{1}H NMR spectrums were recorded, and the substitution degree of dopamine was determined.

3.2.3 | Hydrogels Formulation

To form hydrogels, DHA macromers (5%, w/v) were dissolved in deionized water for 24 h [47]. Graphene was added in different concentrations (1, 5, and 50 %, w/w) and dispersed through vortex for 4 h. Then, the solution was mixed with an equal volume of a 16 mg mL^{-1} $NaIO_4$ solution (pH = 8.5, adjusted with sodium hydroxide) in order to oxidize the hydroxyl groups of catechol and thereby allowing the formation of catechol-catechol adducts, which results in the crosslinking of DHA chains. RDHA hydrogels were formulated according to the exact same procedure.

3.2.4 | Electrical Conductivity Assays

The electrical conductivity of DHA hydrogels with PG and FG was determined by applying a voltage potential and subsequently measuring the current through the gels. The hydrogels were exposed to a 1 V continuous potential difference using the Digilent Waveform Generator hardware and software. Simultaneously, the current through the gels was measured using a UNI-T UT39 Digital Multimeter. The electrical conductivity was determined through the following relation based on the Ohm's Law:

$$\sigma\ (S\ m^{-1}) = \frac{I\ (A) \times l\ (m)}{V\ (V) \times A\ (m^2)}$$

Where I is the measured current (A), l is the length (m) of the hydrogels, V is the exposed potential (1 V) and A is the cross-sectional area (m^2) of the hydrogels.

3.2.5 | Dynamic Mechanical Characterization

The mechanical properties of DHA-FG hydrogels were investigated in the compression mode using a dynamic mechanical analyzer (DMA) (Q800, PerkinElmer, USA) with a 0.2 N preload force and at 1 Hz. Prior to and during the analysis, the samples were immersed in Dulbecco's Modified Minimum Essential Medium (DMEM)/Ham's F12 (Thermo-Fisher Scientific) culture medium.

3.2.6 | Adhesive Mechanical Tests

The adhesion properties of the DHA hydrogel (0 and 5 % of FG) were tested using an Universal Mechanical Testing Equipment (INSTRON 5540) with a load cell of 50 N operating in the tensile mode, following the standard test method ASTM D1002 with slight modifications. Briefly, porcine skin was used as a tissue model. A fresh porcine skin, without fat layers, was immersed in PBS solution (pH =7.4) for 1 h prior to the test. Then, porcine skin was cut into strips of 35 mm in length and 10 mm in width. The hydrogel was placed between two pieces of porcine skin (bonding area = 1.5 x 1 cm^2), and a weight of 60 g was applied for 24 h at 37°C. Then, the two pieces of samples were fixed between two grips positioned 2 cm in length axis. The crosshead speed of 3 mm min^{-1} was applied until the hydrogel detached from the porcine skin. The resulting stress-strain curve allows us to determine the adhesion strength of hydrogels. Each test was repeated three times. The adhesive strength was obtained by using the following equation:

$$Lap - Shear\ Adhesion\ (Pa) = \frac{Force\ (N)}{Area\ of\ Adhesive\ Overlap\ (m^2)}$$

3.2.7 | Swelling, Stability and Biodegradation

The swelling, stability and biodegradation studies were conducted for DHA hydrogels without and with 5 % of FG. Lyophilized DHA gels (weighted as w_0) were immersed in 3 mL of PBS (pH = 7.4) at 37 °C. At each time point, the swollen hydrogels were taken out, the excess amount of medium was removed with filter paper, and the hydrogels were weighted as w_s. The degree of swelling, Q, was calculated as follows:

$$Q = \frac{w_s - w_0}{w_0} \times 100$$

To assess their stability, lyophilized gels, weighted as m_0, were placed in 3 mL of PBS (pH = 7.4) at 37°C. The PBS was renewed every 72 h. At each time point (1, 3, 7 and 14 days), the hydrogel was taken out, lyophilized, and weighted as m_x.

For *in vitro* degradation tests, lyophilized gels, weighted as m_0, were placed in 3 mL of 0.125 mg/mL hyaluronidase PBS solution (pH = 7.4) at 37°C. The solution was renewed every 72 h. At each time point (1, 3, 7 and 14 days), the hydrogel was taken out, lyophilized, and weighted as m_x.

The degradation ratios were calculated as follows:

$$Weight\ Loss\ (\%) = \left(\frac{m_0 - m_x}{m_0}\right) \times 100\%$$

3.2.8 | Cell Culture and Seeding

A SH-SY5Y neuroblastoma cell line (ATCC® CRL-2266™, passage 31) was used to test the *in vitro* cytotoxicity of hydrogels. Cells were cultured in DMEM/Ham's F12 culture medium (1:1, v:v) supplemented with 10% of fetal bovine serum (FBS, Thermo-Fisher Scientific) and 1% of Antibiotic-Antimycotic solution (Thermo-Fisher Scientific). The cells were grown in a T150 flask and incubated at 37 °C in a humidified air atmosphere of 5% CO_2. The medium was changed every 4 days. At 80% of confluence, the cells were washed with Dulbecco's Phosphate Buffered Saline (DPBS, Thermo-Fisher Scientific) and subsequently detached with 5 mL of trypLE™ (Thermo-Fisher Scientific) express solution for 5 min at 37 °C. To inactivate the trypLE™ express solution effect, 10 mL of culture medium were added. The cells were centrifuged at 150 relative centrifugal force (rcf) for 5 min and the obtained pellet was resuspended in the culture medium. Before cell seeding, the samples were sterilized for 1 h by ultraviolet radiation (UV) and washed with DMEM:F12 medium without FBS and with 10% of antibiotic, and then washed several times with DPBS and new immersion in DMEM:F12 medium without FBS for 72 h to remove the excess $NaIO_4$ of the hydrogel. Afterwards, 100 µL of supplemented DMEM containing a cell suspension with a density of $5x10^5$ cells mL^{-1} was added dropwise carefully above the surface of the samples, and the tissue culture polystyrene surface (TCPS) was used as a control. Then, the samples were incubated at 37 °C in a humidified air atmosphere of 5% CO_2. After 3 h of seeding, a fresh culture medium was added to each well until reaching a volume of 600 µL.

3.2.9 | Metabolic Activity

The metabolic activity of neuronal cells seeded on DHA hydrogels with 0, 1, 5 and 50 % of FG was determined using the Alamar-Blue method. After 1, 3, and 7 days of culture, the culture medium was removed and a fresh medium supplemented with 20 % of Alamar-blue (Bio-Rad) reagent was added to the culture wells, followed by incubation at dark for 4 h at 37 °C in a humidified air atmosphere of 5% CO_2. Then, aliquots of 100 µL were transferred to a 96-well black plate and the fluorescence was measured at 590 nm emission wavelength and 530 nm excitation wavelength using a microplate reader (BIO-TEK Instruments).

3.2.10 | Cell Viability

Live/dead assay was used to assess the viability of cells cultured on the DHA hydrogels with 0, 1, 5 and 50 % of FG. While Calcein AM stains the live cells in green, propidium iodide (PI) was used to stain the dead cells in red. After 1, 3, and 7 days of culture, the culture medium was removed, and a fresh medium supplemented with 0.2% Calcein AM and 0.1% PI (Thermo-Fisher Scientific) was added to immerse the seeded hydrogels. These immersions lasted for 30 min in the dark and then washed with DPBS and analysed using an inverted confocal microscope with incubation (TCS SP8, Leica, Germany).

3.2.11 | Cell Morphology and Adhesion

The morphology and the adhesion behaviour of neuronal cells on the surface of the DHA-FG hydrogels were observed by scanning electron microscopy (SEM). After 1, 3, and 7 days of culture, the samples were washed carefully with DPBS solution and incubated with 2.5% glutaraldehyde solution for 1 h to fix the cells to the material. Afterward, the hydrogels were dehydrated in a graded ethanol solution (50, 70, 90, and 100%). The hydrogels were immersed in each ethanol concentration twice for 15 min each time. Then, the samples were left to air dry and were ready to mount by sputter coat to be analysed by SEM.

3.2.12 | Immobilization of Nogo Receptor Antibodies

NgR antibodies were immobilized on the carbonyl groups of DHA through the EDC/NHS coupling chemistry. Briefly, DHA hydrogels with 5 % of FG and antibodies were formulated according to the following procedure: (1) DHA macromers (5%, w/v) were dissolved in deionized water for 24 h. (2) EDC

(20%, w/w) and NHS (14.5%, w/w) were added and (3) after 1 h, 20 μL of 0.369 μg μL^{-1} antibody solution was added. The solution was agitated during 4 h and then FG (5%, w/w) was dissolved in the reaction mixture. Finally, an equal volume of a 16 mg mL^{-1} $NaIO_4$ solution (pH = 8.5) was added to allow the gelation of the solution.

To confirm the immobilization of the antibodies to the DHA backbone, the samples were stained with a secondary antibody, Alexa Fluor 405, Goat anti-Rabbit IgG (H+L) (1 μg mL^{-1}, 1 h at RT, Molecular Probes). Samples were also stained with biotinylated HA binding protein from bovine nasal cartilage (1 μg mL^{-1}, 1 h at RT, Millipore) followed by incubation with Streptavidin-AlexaFluor® 594 conjugate (1 μg mL^{-1}, 1 h at RT, Thermofisher). Images were acquired using an Inverted Confocal Microscope (TCS SP8, Leica). The negative control (DHA-FG hydrogel without NgR antibodies) was analysed using the same conditions.

3.2.13 | Statistical Analysis

Presented data were expressed as average ± standard deviation (SD) of at least three replicates. The error bars in the graphics denote the SD. For statistical comparison, two-way Anova followed by Tukey's test were employed. The statistical analysis was performed using the software GraphPad Prism 8.0 for Windows. Statistical significance was accepted for a (*) $p < 0.0332$.

3.3 | Results and Discussion

3.3.1 | Synthesis of Dopamine-Conjugated Hyaluronic Acid

There are some methods through which dopamine can be grafted to HA. Previous studies have reported the effectiveness of this conjugation through carbodiimide coupling chemistry [72]. However, herein DHA was produced through a different method, reported by Zhou *et al.*, via the Schiff base reaction between the amine group in dopamine and dialdehyde groups in dialdehyde-HA (Figure 3.6a) [47]. Through this strategy, the catechol grafting ratio is highly controllable, depending on the amount of time at which the HA is under oxidation by $NaIO_4$.

The ^1H NMR spectrum of the synthesized DHA (Figure 3.6b) confirms the conjugation of dopamine to HA, as indicated by the presence of catechol aromatic-proton peaks at $\delta \sim 7$ parts per million (ppm) and catechol methylene-proton peaks at δ 3.1 and 2.8 ppm [47].

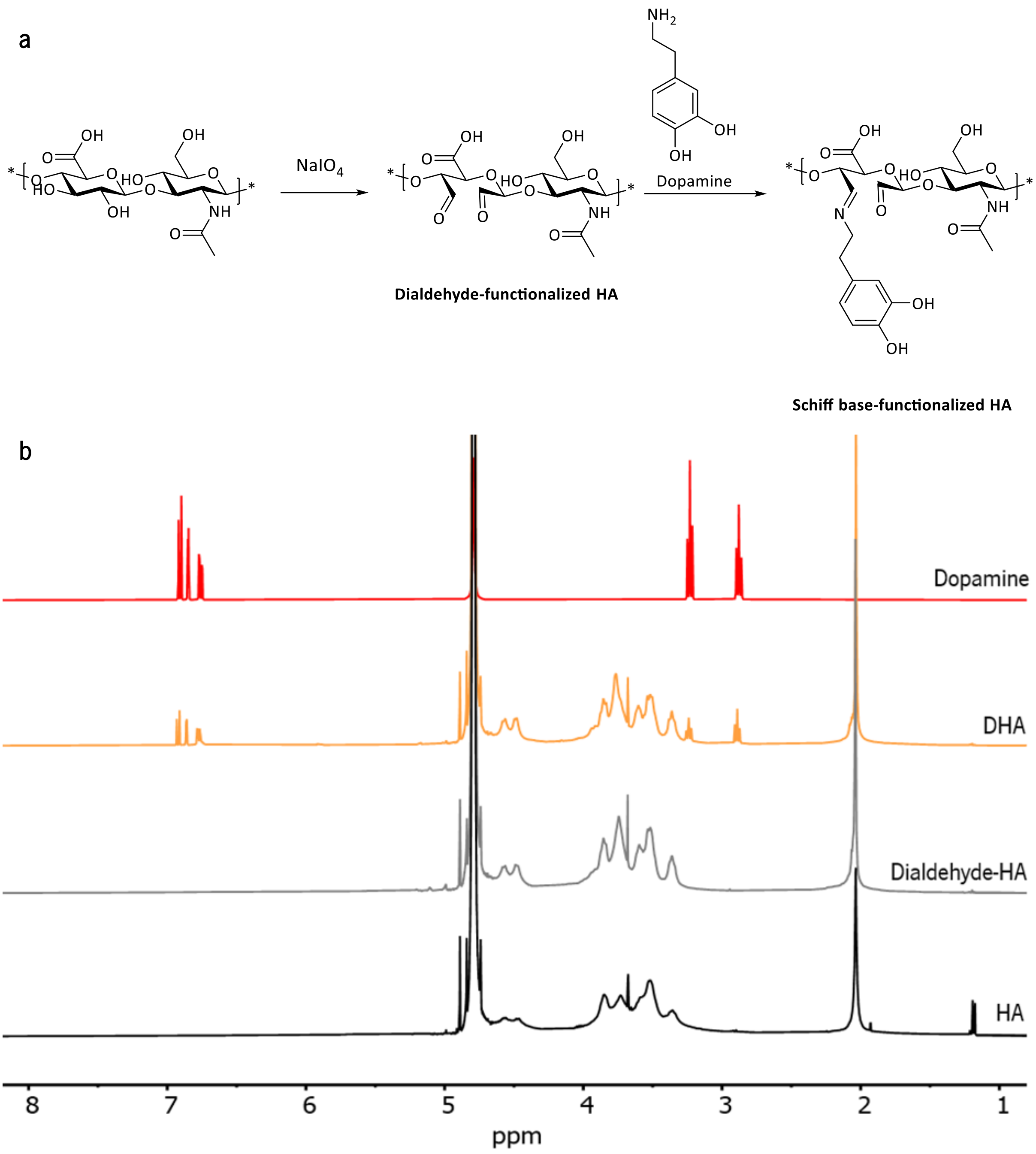

FIGURE 3.6

Synthesis route of DHA (a) and ^{1}H NMR spectra of HA, dialdehyde-HA, DHA, and dopamine (b). The conjugation of dopamine is confirmed by the proton peaks at δ 2.8, 3.1 and approximately 7 ppm.

The substitution degree of catechol groups of DHA was determined by UV-vis spectrophotometry (Figure 3.7), from a standard curve built by using solutions of dopamine with known concentrations. Zhou *et al.* proved that DHA with higher degree of substitution has higher adhesive properties [47]. However, a high quantity of catechol groups may be cytotoxic and require the usage of higher quantities of $NaIO_4$

to achieve their full oxidation, which could increase cytotoxicity [148][149]. Therefore, a balance between adhesive and biological properties must be found. In order to obtain a lower degree of substitution than Zhou and co-workers have reported, HA was under oxidation only during 30 min and the obtained substitution degree of catechol groups was 2.2 %.

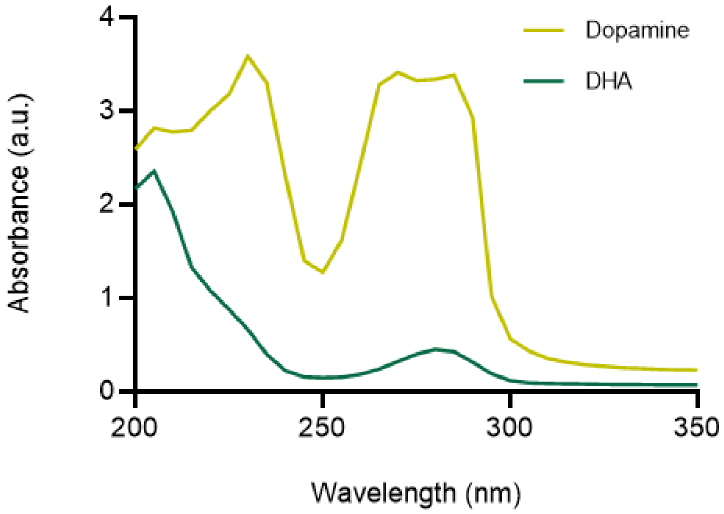

FIGURE 3.7

UV-visible spectra of the conjugate (2 mg mL^{-1} of DHA) and the control (2 mg mL^{-1} of dopamine).

3.3.2 | Synthesis of Reduced Dopamine-Conjugated Hyaluronic Acid

RDHA was synthesized by the reaction between DHA and a reducing agent, $NaBH_3CN$, which modifies the imine bond between dopamine and the polymer backbone to an amine (Figure 3.8a) that may be more stable against hydrolysis and biodegradation.

The substitution degree of the synthesized RDHA was 7.5 % and the ^1H NMR spectrum (Figure 3.8b) confirms the conjugation of dopamine to HA, as indicated by the presence of catechol aromatic-proton peaks at δ ~ 7 parts per million (ppm) and catechol methylene-proton peaks at δ 3.1 and 2.8 ppm. Furthermore, the reduction of the imine to an amide bond is confirmed by the proton peaks between δ 1.0 and 1.5 ppm.

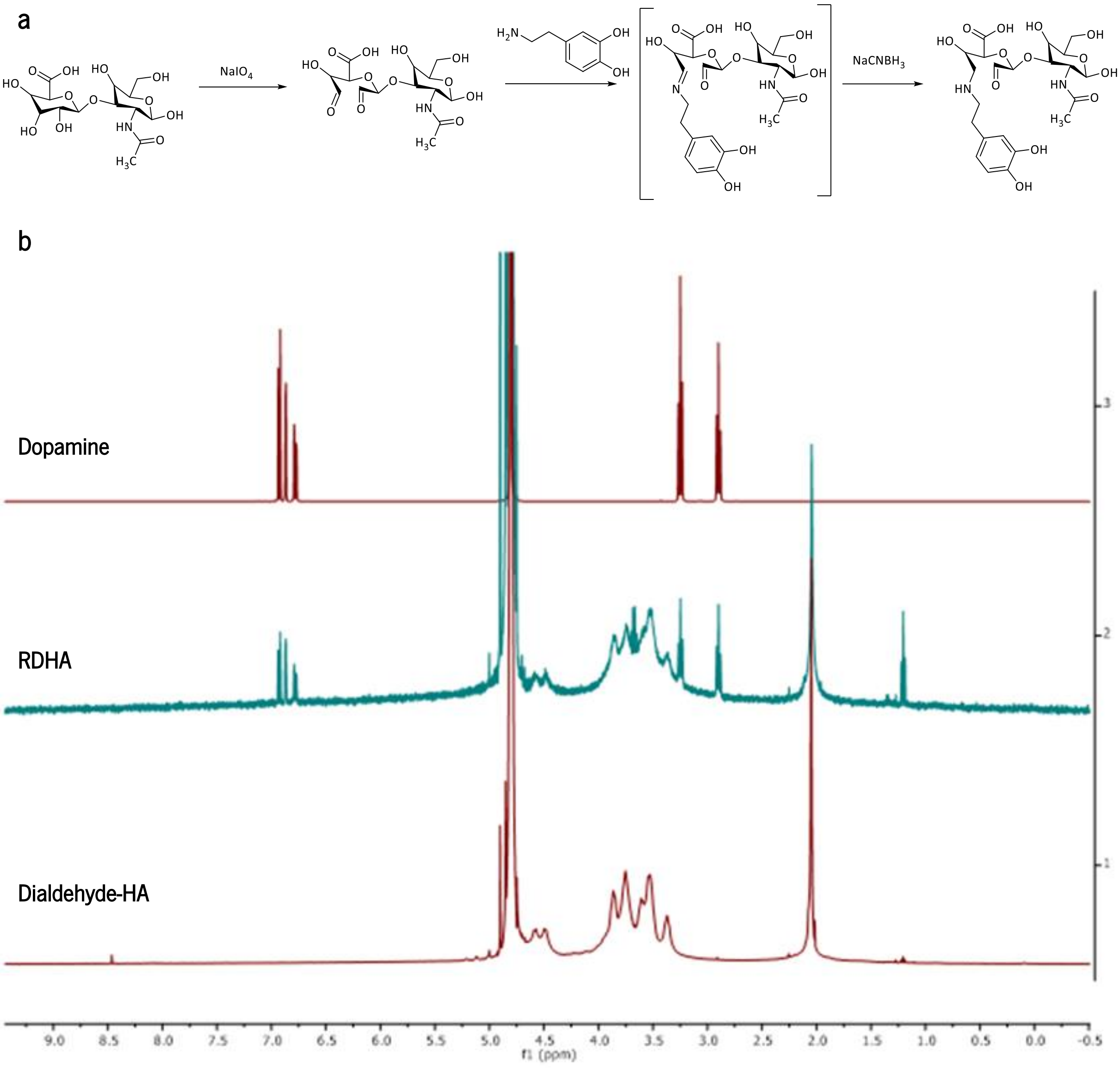

FIGURE 3.8

Synthesis route of RDHA (a) and ^{1}H NMR spectra of dopamine, dialdehyde-HA, and RDHA (b). The conjugation of dopamine is confirmed by the proton peaks at δ 2.8, 3.1 and approximately 7 ppm. The amine bond is confirmed by the proton peaks between δ 1.0 and 1.5 ppm.

3.3.3 | Formation of the Hydrogels

DHA macromers can be crosslinked to form a hydrogel in the presence of $NaIO_4$ under an alkaline pH of 8.5 [47]. This allows the formation of catechol-catechol adducts, which in turn allows for the gelation of the solution in approximately 2 min. Figure 3.9 illustrates the process.

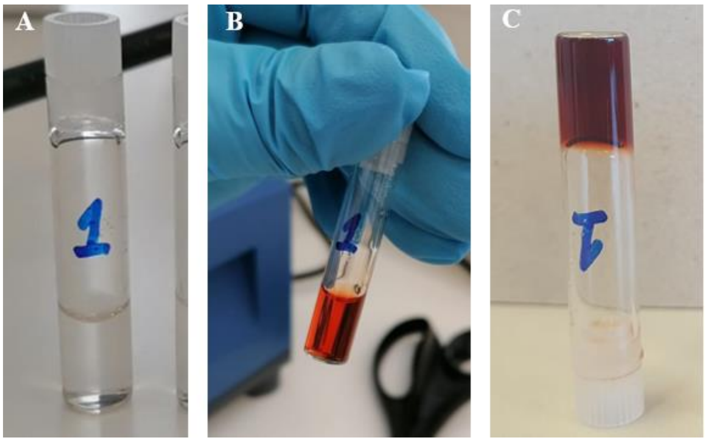

FIGURE 3.9

Photographs of (A) DHA solution in deionized water, (B) DHA oxidized solution and finally (C) DHA hydrogel. Firstly, DHA is dissolved in deionized water. Then, a solution of $NaIO_4$ in deionized water is added and a change of color confirms the start of the oxidation process. Finally, after a few minutes, the DHA hydrogel is formed.

RDHA hydrogels were produced according to the same procedure. However, when placed in PBS or cell culture medium, these hydrogels dissolved after a few hours. Therefore, only DHA-based hydrogels were further characterized.

DHA hydrogels with 1, 5 and 50 w/w % of graphene were produced. In particular, two graphene formulations were tested: PG and graphene functionalized with pyrrolidine, a cyclic secondary amine that may better interact with the polymeric matrix. Graphene (PG or FG) was introduced after the complete dissolution of DHA, and before the addition of the $NaIO_4$ solution. During the production of these hydrogels, it was observed that PG did not disperse well in the DHA solution. In addition, when the $NaIO_4$ solution was added and the hydrogel was formed, it was verified that PG was mostly aggregated and mainly present either on the top or on the bottom of the hydrogel, which should be due to its highly hydrophobic behaviour [84]. On the other side, FG dispersed efficiently throughout the DHA hydrogel, a behaviour that may be granted to its functionalization with pyrrolidine.

3.3.4 | Electrical Conductivity Tests

The electrical conductivity is an important factor that must be considered in the design of tissue engineering biomaterials as this may allow to mimic the electrophysiological characteristics of tissues. For the treatment of lesions in the CNS, an ideal hydrogel must support the endogenous electric field propagation in order to favour neural regeneration [78]. Suitable electrical conductivities have been shown to promote neurogenesis in the lesion site as well as neuronal growth. Zhou and co-workers compared hydrogels with electrical conductivities from 0.05 to 0.18 S cm^{-1} and verified that the matrix with higher conductivity showed higher viability [79].

To this purpose and due to its electrical properties, graphene was included within the DHA hydrogel and the electrical conductivity was evaluated by measuring the current that passes through the hydrogel when submitted to a voltage of 1 V. The introduction of both PG and FG in the hydrogel resulted in the increase of its electrical conductivity (Figure 3.10). An increase from 1.16 ± 0.35 μS mm^{-1} to 2.53 ± 0.84 μS mm^{-1} and to 4.25 ± 1.21 μS mm^{-1} is obtained when 50 % of PG and FG is included, respectively. The inclusion of FG generally results in higher electrical conductivities than PG-included hydrogels, which may be due to the higher affinity of FG to the polymeric solution. During the production of the hydrogels, it is observable that PG, which is highly hydrophobic [84], did not disperse as well as FG throughout the DHA solution, probably resulting in a lower capacity to transmit charges. Therefore, from now forward, only DHA-FG hydrogels will be further characterized.

Despite its higher electrical conductivity than the DHA hydrogels without any graphene added, the semiconductive DHA-FG hydrogels do not yield conductivities similar to the spinal cord where charges can be conducted between 20 (vertebral bone) to 1800 (cerebrospinal fluid) μS mm^{-1} [150]. To further increase the electrical conductivity of the DHA hydrogels, higher w/w content of graphene should be tested and the addition in the hydrogel of other electroconductive materials besides graphene, such as CNTs, can be considered.

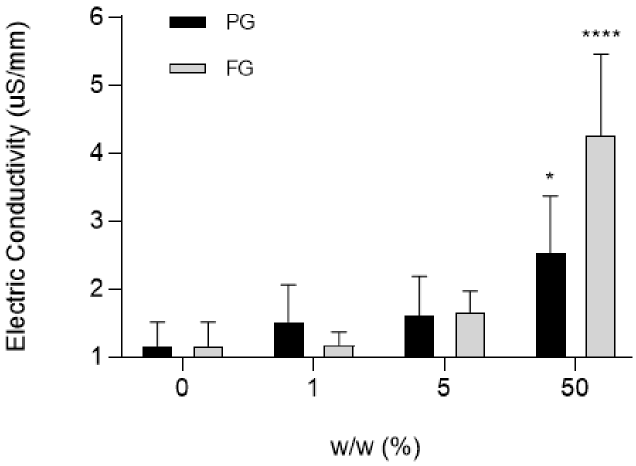

FIGURE 3.10

Electrical conductivity of the hydrogels with different w/w % of PG and FG. Data are displayed as mean ± SD. The significantly different groups are indicated in the graph, with * being $p < 0.03$, ** $p < 0.002$, *** $p < 0.0002$, and **** $p < 0.0001$. All experiments were performed in triplicate.

3.3.5 | Dynamic Mechanical Analysis

The solid-like elastic response of the hydrogels with and without FG was assessed via dynamic mechanical analysis of the storage modulus and loss factor or tan δ (Figure 3.11), which is the ratio between the storage modulus and the loss modulus [151]. The hydrogels were hydrated with DMEM/ Ham's F12 culture medium and the analysis was conducted at 37 °C to reproduce the physiological conditions.

In this study, all the DHA hydrogels exhibited a stable low loss factor, suggesting that they have good elastic recovery properties [151], even when higher w/w content of FG is included. The introduction of graphene significantly increases the storage modulus of the hydrogels, from 4.23 ± 2.20 to 26.33 ± 2.92 kPa when 50 % of FG is included. Since it has been proved that neuronal cells prefer softer hydrogels (storage modulus lower than 1 kPa) [62][63], a balance between electrical and mechanical properties must be found. From now forward, the characterization of the hydrogels will proceed with 5 % of FG, which is the content of graphene that simultaneously increases electrical conductivity without compromising the softness of the DHA hydrogel.

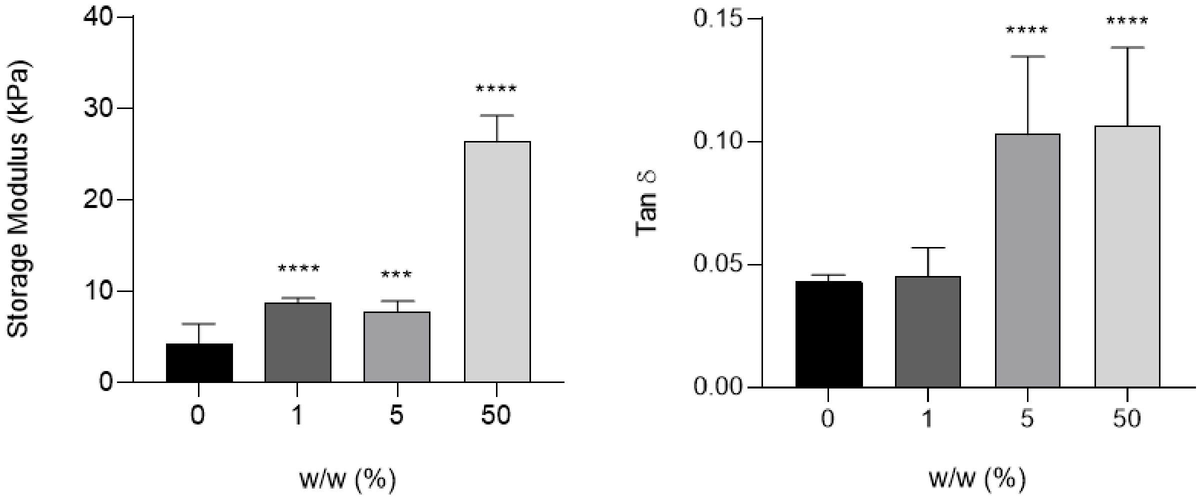

FIGURE 3.11

Storage modulus and loss factor of the DHA hydrogels with different w/w % of FG. Data are displayed as mean ± SD. The significantly different groups are indicated in the graphs, with * being $p < 0.03$, ** $p < 0.002$, *** $p < 0.0002$, and **** $p < 0.0001$. All experiments were performed in triplicate at 37 °C.

3.3.6 | Tissue Adhesion Study

In this study, lap-shear tests were used to assess the tissue adhesive properties of the DHA hydrogels (Figure 3.12). The adhesion strength of the hydrogel to the porcine skin was calculated through the stress-distance curves obtained. The results show that the slightly catechol-substituted DHA hydrogel has an adhesive strength of 4.6 ± 4.4 kPa, which is lower than the adhesive strengths of the hydrogels reported by Zhou and co-workers. This was predictable, as the DHA produced have substantially lower degree of substitution of catechol groups in comparison to the HA synthesized by Zhou *et al.*, where a minimum degree of substitution of 25 % was reported. In addition, the SD is remarkably high, which further difficult the comparison of results.

Interestingly, the inclusion of FG in the DHA hydrogel increased substantially its adhesive strength up to 10.1 ± 4.7 kPa, which is a 54.5 % increase from the DHA hydrogel without any graphene added.

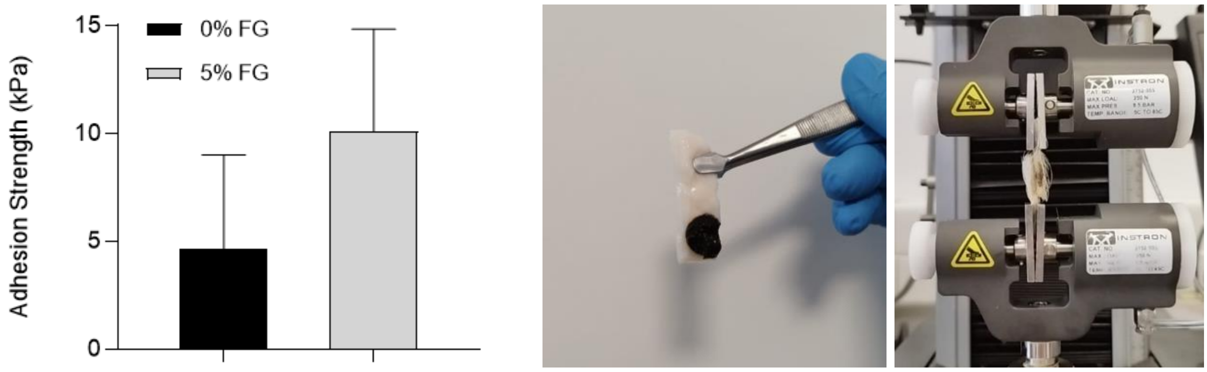

FIGURE 3.12

Lap-shear adhesion tests of the DHA hydrogels without and with 5 % (w/w) of FG. Data are displayed as mean ± SD. Adhesion strength results of the hydrogel to the porcine skin and photographs of the procedure applied are represented.

3.3.7 | Swelling Behaviour

Swelling is a typical feature of hydrogels that must be analysed for biomedical applications. The swelling profile over time of the DHA hydrogels without and with 5 % of FG was followed up to 14 days of incubation in PBS at 37 °C. The hydrogels exhibited an initial fast swelling over the first 16 h (Figure 3.13). After 48 h of incubation, an equilibrium state of swelling was reached, and it kept approximately constant over time. As proved by Zhou *et al.*, this equilibrium swelling ratio can be increased if the degree of substitution of catechol groups of DHA is also increased [47]. Moreover, the introduction of 5 % of FG to the hydrogel did not affect, at least to a great extent, the swelling behaviour of the hydrophilic network.

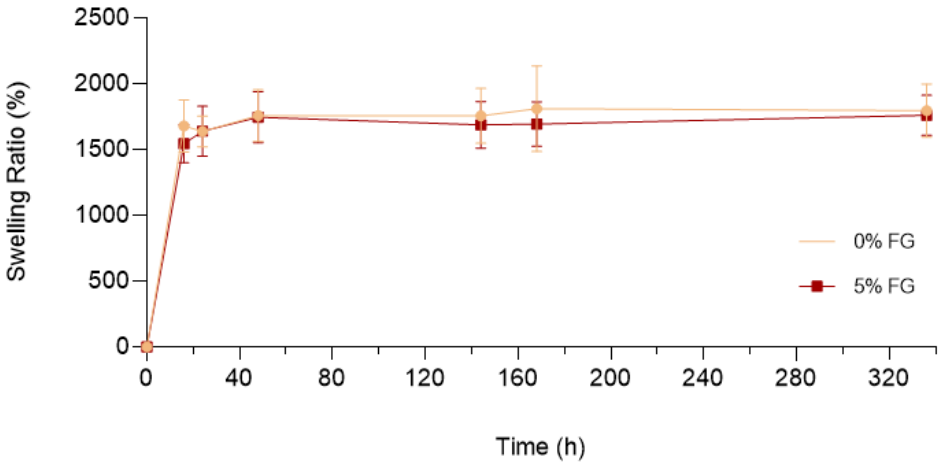

FIGURE 3.13

Swelling kinetics of DHA hydrogels without and with 5 % (w/w) of FG. Data are displayed as mean ± SD.

3.3.8 | Stability and Biodegradation

The degradability of the scaffold is of utmost importance in tissue engineering applications. It is crucial that the hydrogel degrades during and according to tissue regeneration. There are two main mechanisms contributing to the degradation of hydrogels: hydrolysis and enzymatic cleavage. Both mechanisms degrade the polymer backbone of the network and contribute to the weight loss over time of the hydrogel [151]. To assess the degradation behaviours of the DHA hydrogel, *in vitro* stability was investigated by monitoring the percent weight loss during incubation in PBS (pH 7.4) at 37 °C. In addition, degradation by enzymatic cleavage was also studied by immersing the hydrogels in hyaluronidase solution at physiological concentrations.

Stability results (Figure 3.14a) show that after 1 day in PBS the DHA hydrogel has a weight loss of 45.01 ± 5.49 % in comparison to its initial weight. Indeed, during the first day is when the weight loss is higher, stabilizing then at approximately 50 % of its initial weight throughout the rest of the time. The addition of 5 % of FG to the hydrogel have minor effects on the stability of the network. Nevertheless, a slightly higher resistance towards degradation is verified for the DHA hydrogel with FG at each time point.

Upon the presence of hyaluronidase, the degradation profile of the DHA hydrogel is as expected more accentuated due to enzymatic cleavage (Figure 3.14b). While the DHA hydrogel remains after 7 days in PBS with 48.16 % of its initial weight, when placed in an enzymatic solution over the same period of time the hydrogel is left with only 21.76 % of its initial weight. The DHA hydrogels developed by Zhou *et al.* with higher content of catechol groups showed a slower degradation behaviour in comparison to the low-substituted hydrogels produced, which was expected as a lower substitution of catechol groups results in lower crosslinking density and thus diminished resistance towards degradation [47]. The introduction of FG in the hydrogel did not have a significant impact on its enzymatic degradation behaviour.

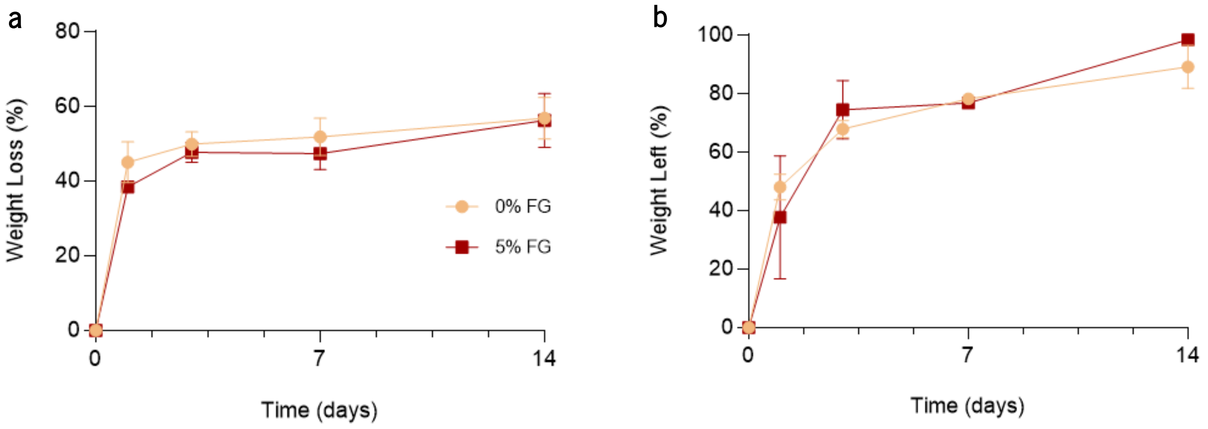

FIGURE 3.14

Stability (a) and *in vitro* degradation (b) behaviours of DHA hydrogels without and with 5 % (w/w) of FG. Data are displayed as mean ± SD, except for the seventh day on the enzymatic degradation profile, where only a single value is plotted because the other two hydrogels dissolved in the medium.

3.3.9 | Metabolic Activity and Cytotoxicity

The metabolic activity of neuronal cells seeded on the DHA hydrogels was determined using the Alamar-Blue method. The hydrogels, however, were first placed under medium culture for 3 days to allow for the diffusion and removal of residual $NaIO_4$ and iodate ion derived from the oxidative reaction that results in the crosslinking of DHA macromers [47]. The results show that the cellular metabolism is higher on the third day after the seeding. On the seventh day, the metabolism is diminished to approximately first-day levels (Figure 3.15).

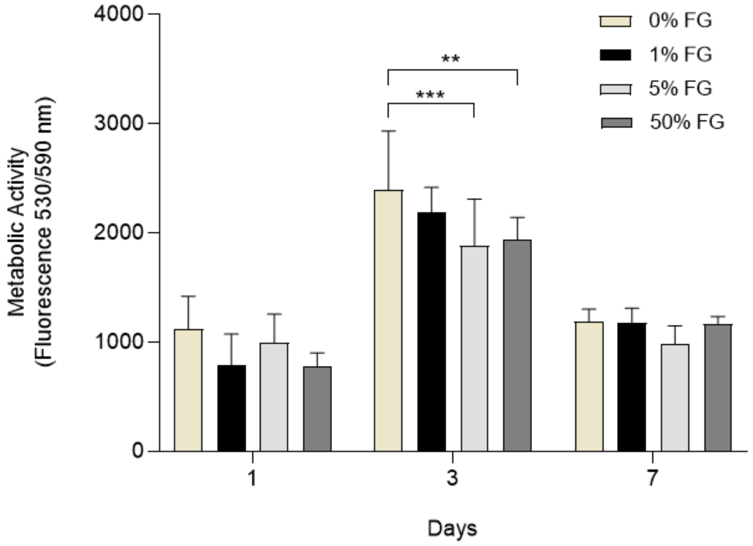

FIGURE 3.15

Metabolic activity of neuronal cells seeded on DHA hydrogels. Data are displayed as mean ± SD. The significantly different groups are indicated in the graph, with * being $p < 0.03$, ** $p < 0.002$, *** $p < 0.0002$, and **** $p < 0.0001$.

The metabolic activity in % of DHA-FG hydrogels in comparison to DHA hydrogels with no graphene added indicates that FG is not cytotoxic. According to International Standard ISO 10993-5 (2009), reduction of cell viability by more than 30% is considered a cytotoxic effect. As this reduction of at least 30 % is not verified, it is concluded that no graphene-included hydrogel produced is cytotoxic (Figure 3.16). Several studies have shown that high content of carbon-based materials in hydrogels have cytotoxic effect. For instance, Sun *et al.* have also shown that a collagen hydrogel with carbon nanotubes up to 1 w/w % displayed more than 85 % of cell viability. However, for concentrations of CNTs up to 2 w/w %, cell viability was significantly decreased [87]. The DHA-FG hydrogels are not cytotoxic, not even with 50 % of FG, confirming the potential of graphene functionalized with pyrrolidine as a suitable material for tissue engineering applications.

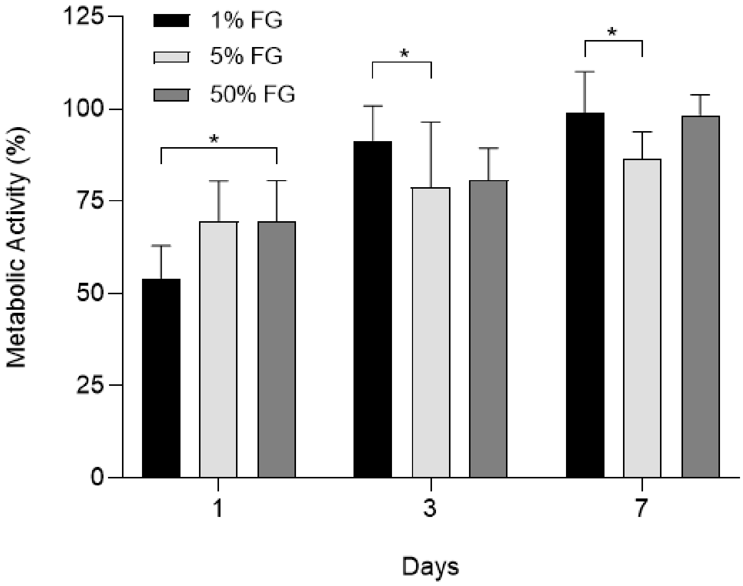

FIGURE 3.16

Metabolic activity (%) of neuronal cells seeded on the DHA hydrogels with different w/w % of FG in comparison to the control DHA hydrogel with no graphene added. Data are displayed as mean ± SD. The significantly different groups are indicated in the graph, with * being $p < 0.03$, ** $p < 0.002$, *** $p < 0.0002$, and **** $p < 0.0001$.

3.3.10 | Cell Viability

The Live/Dead assay was employed to visualise the distribution of living and dead neuronal cells after 1, 3 and 7 days of their seeding on the hydrogel (Figure 3.17). Calcein AM fluoresces green upon the reaction of intracellular esterase, thus staining live cells as green [152], while PI stains dead cells as red. The results clearly show that even after 7 days of seeding living cells are still thriving in the DHA hydrogels. Moreover, a higher quantity of living cells is found on the DHA hydrogels with FG than on the hydrogel with no graphene added, further confirming the potential of this material for neuronal applications.

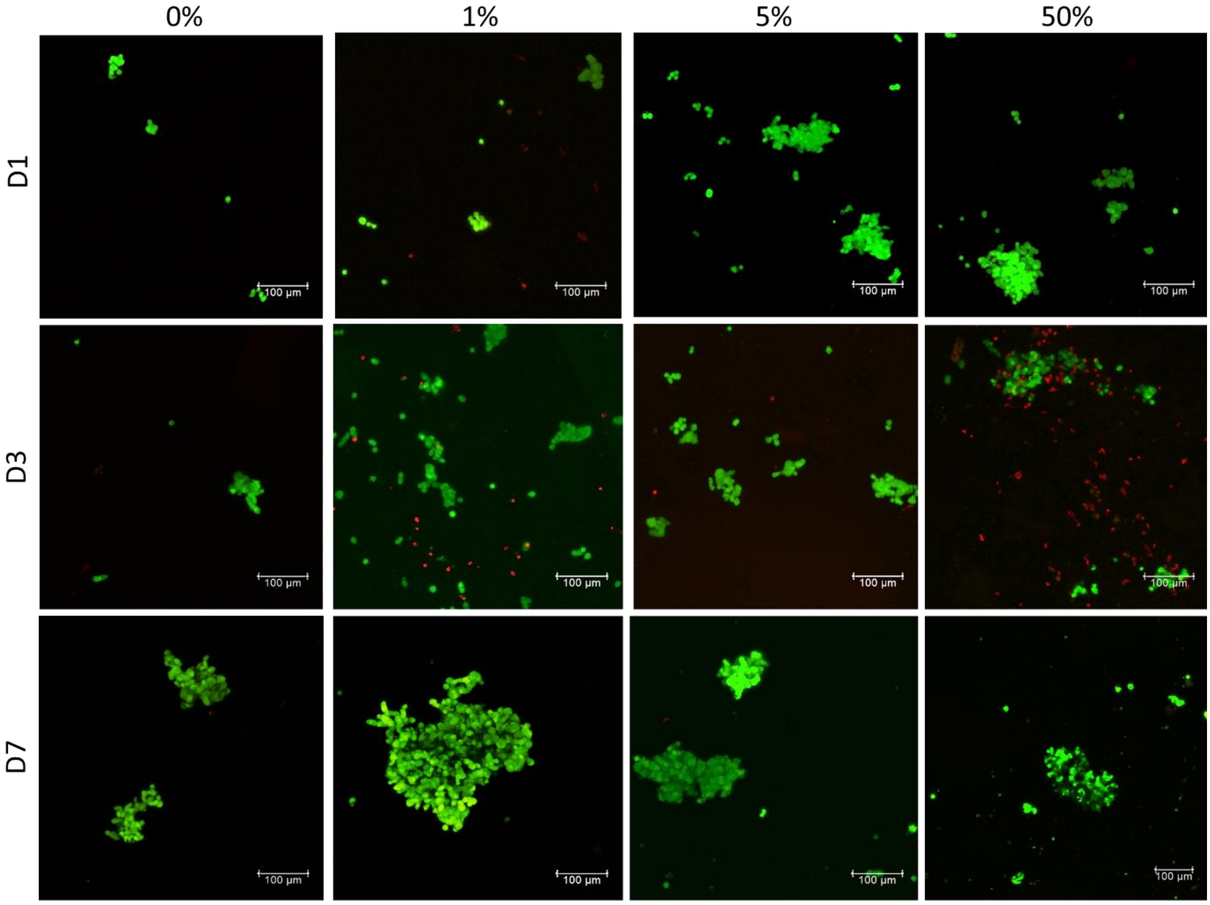

FIGURE 3.17

Cell viability analysis with the Live/Dead assay after 1, 3 and 7 days of neuronal cells seeded on the DHA hydrogel with different w/w % of FG (indicated on the top). Live cells (green) were stained with Calcein AM, while dead cells (red) were stained with PI. The scale bar is 100 µm.

3.3.11 | Cell Morphology and Adhesion

Attachment of the cells onto the DHA hydrogels was evaluated through SEM imaging. The images (Figure 3.18) reveal that neuronal cells seeded on the hydrogel adhered to its surfaces. However, their rounded morphology indicates that this adhesion is not sufficiently strong as neuronal cells usually have a more elongated and branched phenotype. Indeed, previous studies indicated that HA lacked cell adhesion sites [56][153] and the introduction of 2.2 % of catechol groups in the DHA is not yet sufficient to enhance substantially its adhesive properties. Further optimizations should be performed to increase the adhesion of neuronal cells to the hydrogel surfaces. Since the developed DHA-FG hydrogels have reinforced electrical conductivity, electrical stimulation after cell seeding should be considered [80][81].

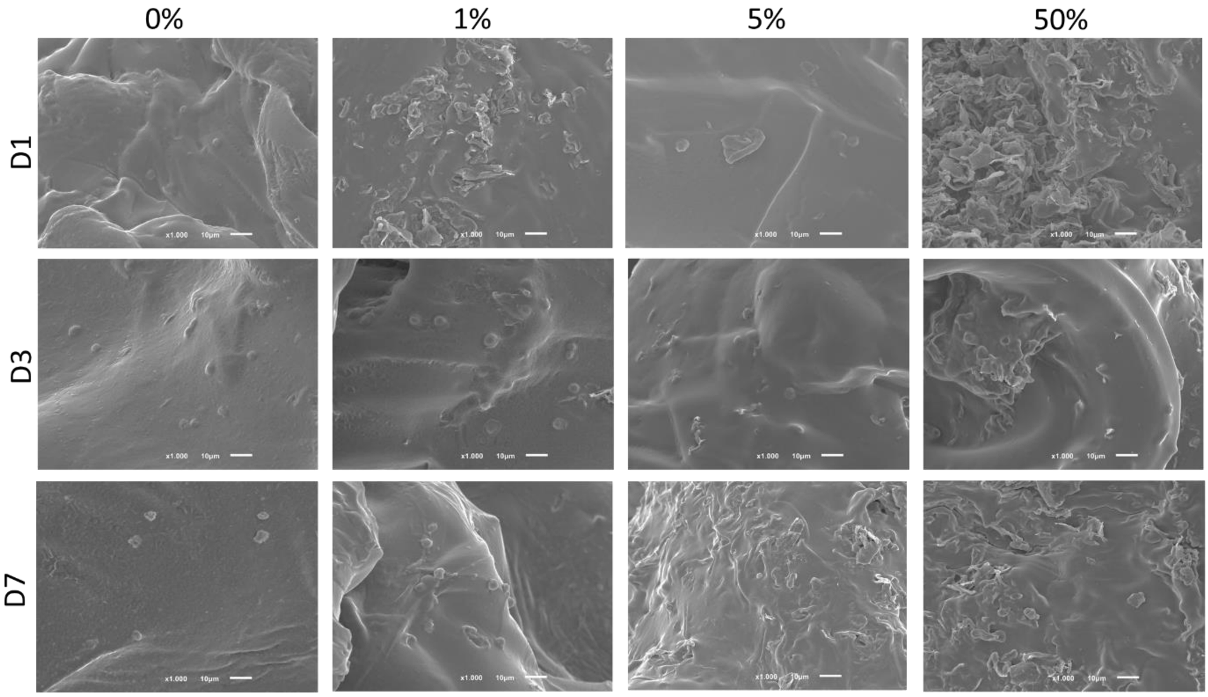

FIGURE 3.18

SEM images of neuronal cells adhered on the DHA hydrogel surfaces. The scale bar is 10 µm.

3.3.12 | Antibody-Conjugated Hyaluronic Acid Hydrogel with Functionalized Graphene

The covalent immobilization of NgR antibodies to HA-based hydrogels promotes attachment, survival, and neurite extension of neuronal cells [105][106]. Herein, a novel unreported chemistry to include NgR antibodies in the DHA hydrogel by reacting the amine-end of the antibody with the carbonyl group of DHA was employed. The immobilization was confirmed by the usage of a secondary antibody, Alexa Fluor 405 (blue), and DHA was also stained with other two antibodies (red) (Figure 3.19). The results show that while Alexa Fluor 405 is not present in the control hydrogel with no NgR antibodies added (Figure 3.19a), it is visible in the DHA-FG hydrogel with NgR antibodies attached (Figure 3.19b), confirming the immobilization of NgR antibodies to the DHA backbone. Figure 3.20 shows two microscopic images of the DHA-FG hydrogel samples with NgR antibodies without the red signal from the DHA. In these images, the Alexa Fluor 405 and subsequently the NgR antibodies can be clearly visualized in blue.

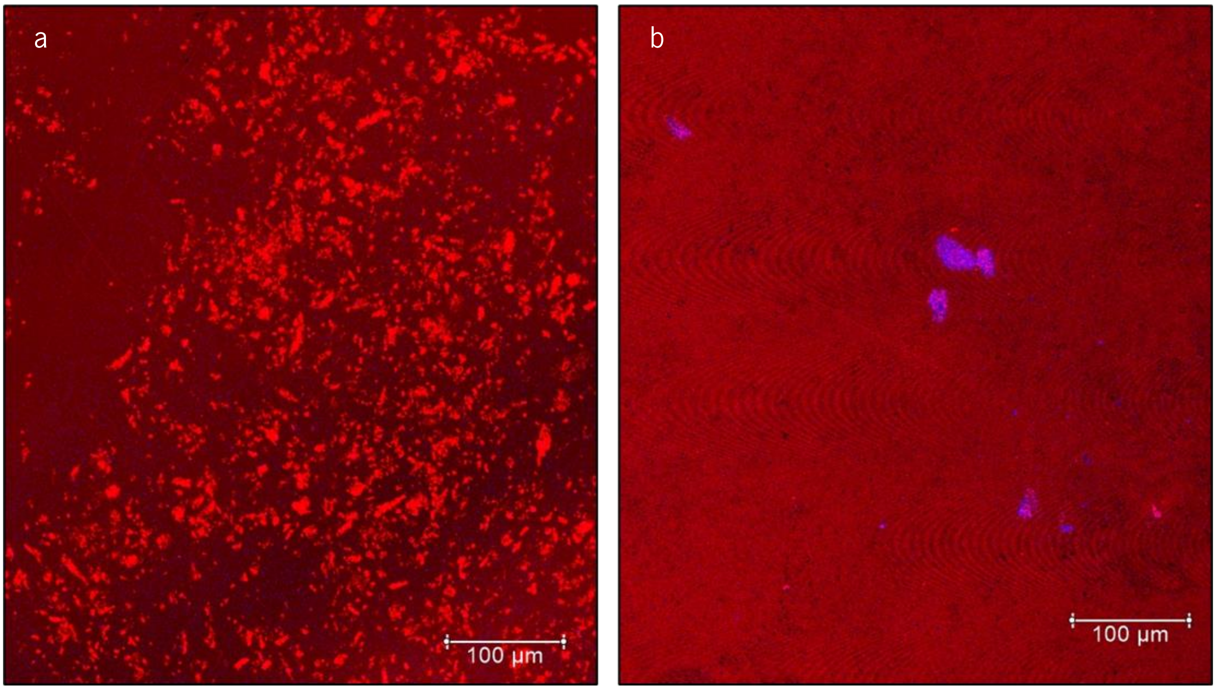

FIGURE 3.19

Microscopic images of the DHA-FG hydrogel without (a) and with (b) NgR antibodies. The DHA was stained with the usage of Biotinylated HA-binding protein followed by incubation with Streptavidin-Alexa Fluor 594 Conjugate. NgR antibodies were stained with Alexa Fluor 405 Goat Anti-Rabbit IgG (blue). The scale bar is 100 µm.

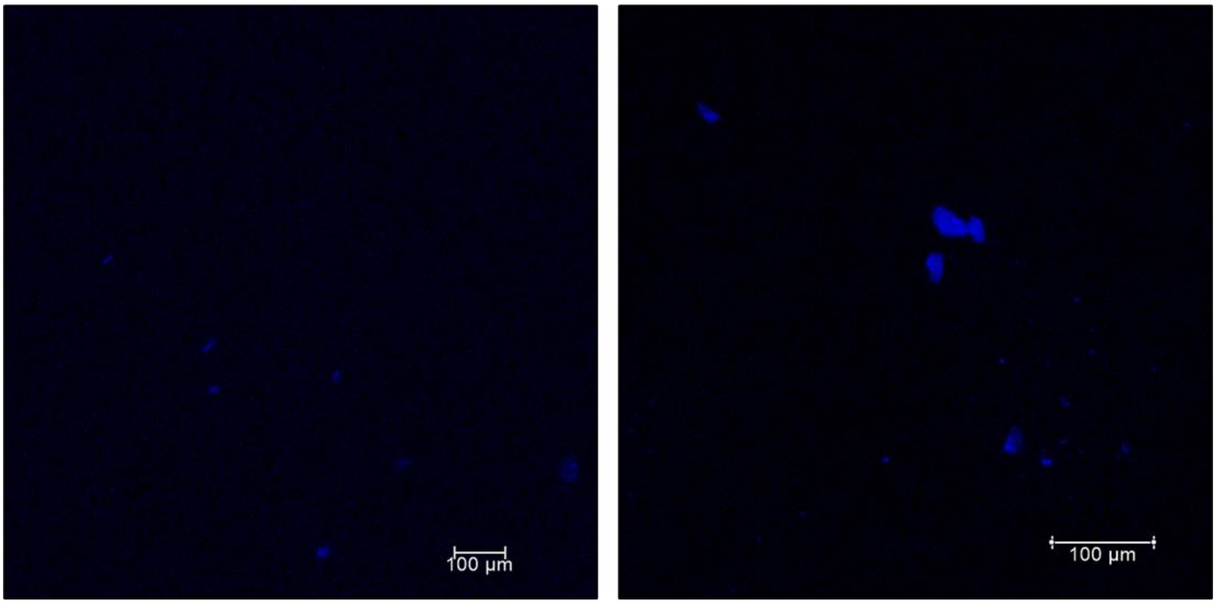

FIGURE 3.20

Microscopic images of the DHA-FG hydrogel with NgR antibodies. NgR antibodies were stained with Alexa Fluor 405 Got Anti-Rabbit IgG (blue). The scale bar is 100 µm.

3.4 | Conclusions

In this work, dopamine-modified HA-based hydrogels with FG were developed as a potential smart scaffold-based therapy for SCIs through a simple and quick crosslinking methodology. It was shown that mussel-inspired hydrogels have reinforced adhesive and electrical properties. The mechanical properties were also found to be adequate for the envisaged application. Furthermore, while the majority of electroconductive materials included so far on hydrogels to increase their electrical properties have been confirmed as cytotoxic at higher quantities [86][87], the results show that the inclusion of FG into the hydrogel do not present a toxic effect to neuronal cells, even with w/w percentages as high as 50 %. Moreover, the DHA hydrogel is stable against hydrolytic and enzymatic degradation at least for 14 days and presents a stable swelling profile. The introduction of NgR antibodies into the DHA-FG hydrogel was successful. Therefore, HA-based hydrogels show a promising potential to improve neuroregeneration and functional outcomes on SCI patients.

4. THERMOSENSITIVE POLYISOCYANOPEPTIDE-BASED HYDROGELS WITH CONTROLLABLE MICROSTRUCTURE

This fourth chapter presents the methodology employed to evaluate the effect of added salts on the microstructure of polyisocyanopeptide hydrogels. Furthermore, the obtained data are presented and discussed.

4.1 | Introduction

The ECM is a key regulator for cellular differentiation, migration, growth, and survival [111]. This broad responsibility is due to its biochemical composition, but also its mechanical properties and structural organization. The physical information of the ECM is transferred via mechanotransduction processes to the residing cells through focal adhesions, which are molecular linkages at the cell-matrix interface [16]. Then, the information is intracellularly processed into biochemical signals that significantly impact the behaviour of cells [111].

Therefore, it is well known that living cells interact physically with their 3D microenvironment. As so, manipulating the physical properties of the surrounding environment does impact cell behaviour [17]. This has inspired strategies for tissue engineering applications. For instance, Fu *et al.* showed that the pore size significantly affects the ability of hydrogels to enhance vascularization [154]. Han and co-workers also proved that different cell types showed differential preferences for scaffold pore sizes. While chondrocytes exhibited higher viability on the 100-200 μm scaffold, tendon stem cells preferred a pore diameter of 300 μm [155]. In addition, Liu and co-workers have demonstrated that the differentiation of mesenchymal stem cells (MSCs) is highly dependent on the hydrogel stiffness [156]. Guvendiren *et al.* showed that mesenchymal stem cells differentiated into an osteogenic lineage when seeded in hydrogels with lamellar surface wrinkles, whereas in the same gels but with hexagonal wrinkles the cells differentiated into an adipogenic lineage [157]. Moreover, enhanced pore interconnectivity allows for cell ingrowth, vascularization, and nutrient diffusion for cell survival [158][159].

As the importance of the scaffold physical properties becomes increasingly recognized across tissue engineering strategies, several techniques have surged to allow for their tunability. For instance, the pore size and/or the porosity of hydrogels can be tailored by different approaches [18][160]: phase separation using so-called porogens (chemical additives that generate pores) [161], lyophilization (freeze-drying) [162], electrospinning [163], via foam formation [164] or via cryogelation [165].

Herein, the aim is to study the influence of added salts on the microstructure of hydrogels and their potential capacity to tailor the physical properties of these networks. Indeed, it is widely known that salts have the ability to precipitate proteins from aqueous solutions. This effect is named the Hofmeister effect [126] and besides describing protein precipitation and stabilization, it can also be applied to describe the behavior of thermoresponsive aqueous systems such as hydrogels [20]. Several studies already proved that the addition of salts to physical hydrogels is a successful method to tune some properties of these 3D hydrophilic networks, such as their swelling behaviour and mechanical properties

[19][20]. The objective of this project is to study how the addition of salts to hydrogels affects their structural parameters. This will be done by (1) formulating and imaging PIC hydrogel samples with different salts, NaCl, NaClO4 and NaI, and (2) introducing the microscopic stacks of each sample as input to the algorithm developed by Vandaele *et al* [108]. As output from the algorithm, several structural parameters of each sample are obtained and three of them, pore diameter, connectivity, and pore ratio, will be analyzed.

As a model system, we used a fully synthetic fibrillar hydrogel based on oligo (ethylene glycol)-grafted PICs [21]. Jaspers *et al.* already proved that Hofmeister salts have a strong influence on the gelation temperature and mechanical properties of PIC hydrogels [20]. However, their effect on the microstructure of PIC networks is vastly unknown.

4.2 | Material and Methods

4.2.1 | Preparation of the Stock Solutions

PIC macromers were dissolved in water for 24 h in a heating block (Thermal Shaker, VWR), at 4°C and at 900 rotations per minute (rpm) to a final solution of 2 mg ml^{-1}. Stock solutions of 3 salts with a concentration of 4 M were also prepared by dissolving NaI (Sigma Aldrich), NaCl (Sigma Aldrich) and $NaClO_4$ (Sigma Aldrich) in Milli-Q water.

4.2.2 | Polymer Labelling and Sample Preparation

Before each measurement, the sample was prepared, starting with the addition of Milli-Q water, following by the salt solution. Then, to fluorescently label the polymer molecules, carboxy tetramethyl-rhodamine (TAMRA) with a covalently attached DBCO linker (Sigma Aldrich) was added and the final component to be introduced was the 2 mg ml^{-1} PIC solution (Figure 4.1). The solution was then incubated at least for 5 min on ice to avoid early gelation.

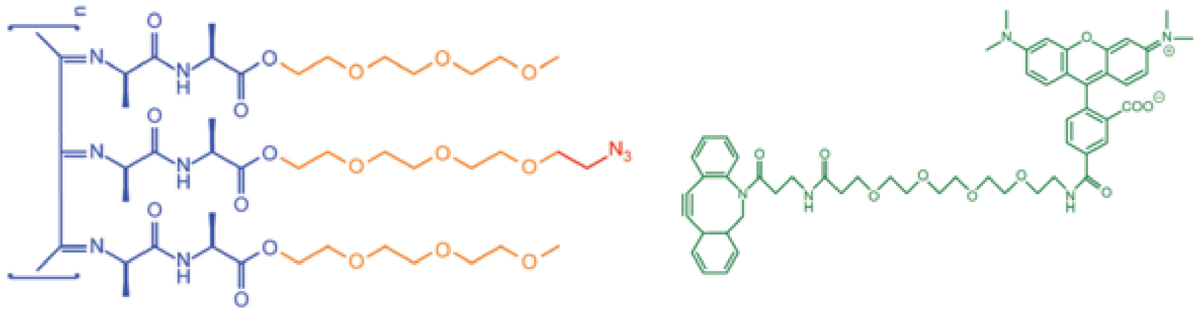

FIGURE 4.1

Chemical structure of PIC polymers and of the DBCO-TAMRA dye used. Dark blue represents the stiff helical polyisocyanide backbone stabilized with the hydrogen-bonded dialanyl group, whereas orange depicts the ethylene glycol substituent tails. Dark orange represents the azide groups, where the DBCO groups attach. The green structure is the DBCO-TAMRA dye used.

Two different polymer concentrations (0.5 and 1.0 mg ml^{-1}) and three different salt concentrations (0.5, 1 and 2 M) were assessed., for each salt.

In addition, each salt results in different gelation temperatures of the PIC solution. While the gelation temperature for the PIC solution with 2 M of NaI is approximately 33 °C (measured on a Leica TCS SP8 X confocal microscope), with the same concentration of $NaClO_4$ it increases up to 48 °C. Therefore, every sample was heated up to 35 °C, except for the ones with $NaClO_4$, which were heated up to 50 °C. The heating procedure was applied through the Vaheat Heating System (Interherence), starting from 25 °C until the final temperature was reached., with a rate of 1 °C min^{-1}. For each salt concentration, the same heating procedure and thereby the same final temperature (35 or 50 °C, depending on the salt) was applied in order to guarantee that differences in the results are due to different salt concentrations and not due to different temperatures applied to the samples.

Table 4.1 specifies the components introduced in the formulation of samples with a volume of 80 µL. It must be noted that for the samples with $NaClO_4$ the volume was doubled because these samples must be heated up to 50 °C. and at this temperature some degree of evaporation occurs. By trial and error during the measurements at the microscope, it was noticed that doubling the volume of the sample gives enough time to obtain all the necessary data before evaporation starts to occur, while preserving the same polymer and salt concentration.

Table 4.1. Composition of the samples. The quantities presented only apply to the samples with NaI or NaCl. For samples with $NaClO_4$, the volume of each component must be doubled.

Polymer Concentration (mg ml^{-1})	Salt Concentration [M]	Milli-Q Water (µL)	Salt Solution (µL)	TAMRA Solution (µL)	2 mg ml^{-1} PIC Solution (µL)
0.5	0.0	58	0	2	20
	0.5	48	10	2	20
	1.0	38	20	2	20
	2.0	18	40	2	20
1.0	0.0	38	0	2	40
	0.5	28	10	2	40
	1.0	18	20	2	40
	2.0	0	40	2	40

For each polymer and salt concentration, two PIC polymer lengths were tested: 145nm (short polymer) and 229nm (long polymer). For both lengths, the procedure applied was the same and the samples were equally formulated.

Furthermore, to assess the effect of chemical crosslink between PIC fibers on the microstructure of unsalted and salted hydrogels, samples with 0.5 mg ml^{-1} of short-PIC polymer and 1 M of each salt were formulated and the crosslink agent (Figure 5.2) was added in a ratio of 2 µL per 80 µL of solution. The experiments were performed at 35 °C, except for the PIC hydrogel samples with $NaClO_4$, which were measured at 50 °C to avoid early evaporation.

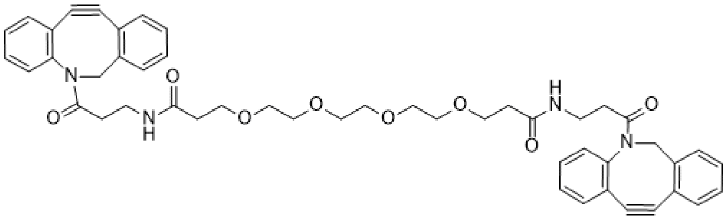

FIGURE 4.2

Chemical structure of the DBCO-PEG4-DBCO, the crosslinking agent used. Each DBCO bonds covalently to an azide group, thus crosslinking chemically PIC polymers.

4.2.3 | Confocal Fluorescence Imaging

Confocal fluorescence imaging was applied to image the samples and to measure 3D stacks, which are essential for the algorithm analysis. Fluorescence imaging was done with a Leica TCS SP8 X confocal microscope. An oil objective (HC PL APO 63x/1.40, motCORR, Leica) was used to acquire the images, as well as a hybrid photomultiplier tube as detector (HYD-SMD, Leica) and a field-of-view scanner (200 Hz, bidirectional). A white light laser (470-670 nm, pulsed, 80 MHz, NKT Photonics) was used as an excitation source. The TAMRA-labelled PIC polymers were excited at 552 nm, and the fluorescence was collected between 562 and 700 nm. All measurements were performed in a temperature-controlled environment at 23 °C.

At least five different areas of the sample were randomly selected and imaged for each sample in duplicate. Data was acquired with Leica Application Suite X software and ImageJ was then used for data visualization. The images were acquired with a pixel size of 107 nm in *XY* and a *z*-step of 150 nm, across 30.04 µm in *Z*, starting off from 30.00 µm.

4.2.4 | Polymer Network 3D Analysis

The analysis of the network was performed using the software developed by Vandaele and co-workers [108]. The software is freely available at https://github.com/BorisLouis/Segmentation and it was written in MATLAB. Every detail about the software can be consulted in the link provided. Briefly, after loading the data, the images are pre-processed through a 3D Gaussian filtering. Then, the smoothed images are segmented to distinguish pores from polymer fibers. After segmentation, the pores of the hydrogel become white on the images. For the segmentation, a global or adaptive threshold can be applied. While the global threshold do not consider the neighborhood of the pixel, the adaptive threshold does by considering in 3D the mean of *N* neighboring pixels and a sensitivity value to choose the threshold to be applied in each particular pixel. The global threshold is often sufficient to obtain segmentations with high accuracy. However, in the case of fluorescent images, the background signal is not uniform and as so the adaptive threshold provides better results. Therefore, an adaptive threshold for all the data analysis performed was used, with a pixel window of 6 x 6 x 6 ($N = 216$) and a sensitivity value of 0.5. These parameters were chosen after visual comparison between images processed with different sensitivities.

After segmentation, the images are binarized. Each pixel (2D) or voxel (3D) is classified as belonging to a pore or to a polymer fiber, depending on if its intensity is above or below the intensity threshold, respectively. In the first case an intensity of zero (minimum) is given to the pixel, while in the second case the intensity of the pixel becomes one (maximum).

Afterwards, for each pixel/voxel in the pore, the software calculates the distance to the closest pixel/voxel belonging to a polymer fiber. A distance map is constructed and used as input for a watershed transformation. This algorithm section each pore on the region where the diameter is narrower. Then, the local pore diameter is determined by calculating the diameter of the biggest circle/sphere that can fit in each section of the pore. Besides the diameter of the pores, the developed software outputs other structural parameters, namely the interconnectivity between pores and the pore ratio in the hydrogel.

4.2.5 | Statistical Analysis

Presented data were expressed as average ± SD of at least five values of two replicates. The error bars present in the graphics denote the SD. Non-parametric Kruskal-Wallis test followed by Dunn's multiple comparison test was employed. The statistical analysis was performed using the software GraphPad Prism 8.0 for Windows. Statistical significance was accepted for a (*) $p < 0.0332$.

4.3 | Results and Discussion

4.3.1 | Structural Characterization

In the first set of experiments, it was investigated how the architecture of the PIC hydrogel is influenced by polymer concentration and by temperature. No salts were added. While the influence of polymer concentration has already been proven [108], the effect of temperature is yet to be quantified. Two different concentrations (0.5 and 1.0 mg ml^{-1}) for two different polymer lengths at two different temperatures (35 and 50 °C) were compared. The results between polymer lengths were similar. Therefore, only results about the short-polymer hydrogel are herein presented. Data from long-polymer networks may be further consulted in the Supplementary Information.

Figure 4.3 shows microscopic images of PIC hydrogels, both constituted by short polymers but with different concentrations: while Figure 4.3a shows a hydrogel with a polymer concentration of 0.5 mg ml^{-1}, the network represented in Figure 4.3b has a polymer concentration of 1.0 mg ml^{-1}. Indeed, the images, which were both recorded at 35 °C, exhibit clear differences between the networks of the two different formulations. These differences can be highlighted by the quantification of some structural parameters, namely the average pore diameter of the hydrogel, the interconnectivity of its pores and the pore ratio in the network (Figure 4.4).

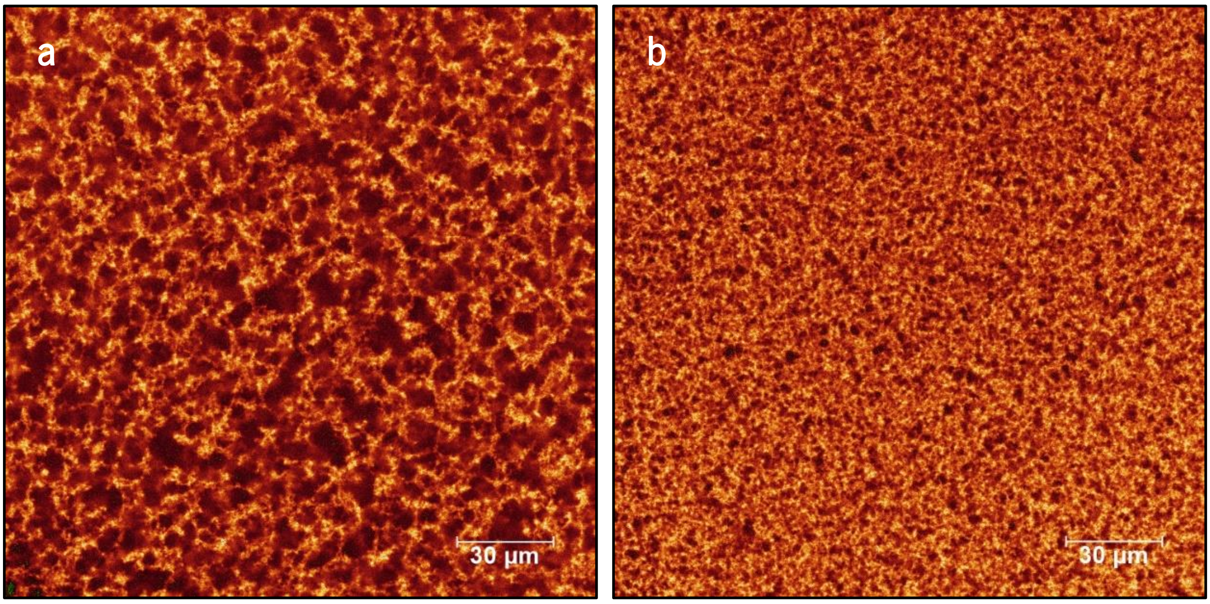

FIGURE 4.3

Representative fluorescence images of TAMRA-labelled and short-polymer PIC hydrogels, with a polymer concentration of (a) 0.5 mg ml^{-1} and (b) 1.0 mg ml^{-1}. Both images were recorded at 35 °C with the same settings.

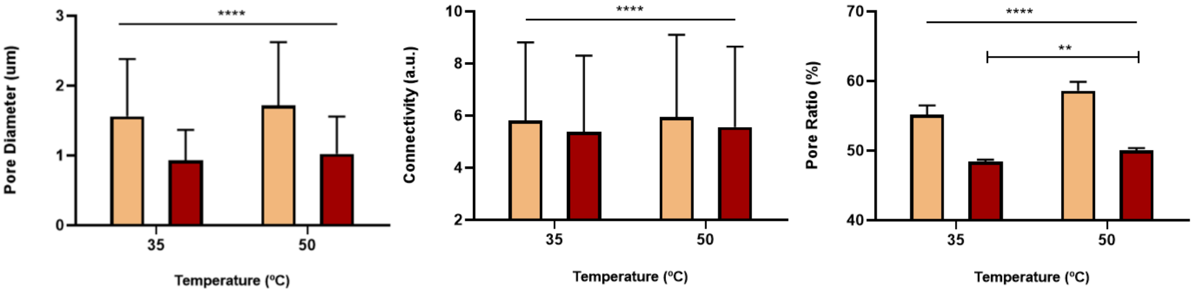

FIGURE 4.4

The average pore diameter, pore connectivity and pore ratio in the overall network of short-PIC hydrogels with two different polymer concentrations (0.5 and 1.0 mg ml^{-1}) at two different temperatures (35 and 50 °C). The orange (○) bars represent the 0.5 mg ml^{-1} PIC hydrogel, whereas the red (○) bars are respective of 1.0 mg ml^{-1} of polymer concentration. Data are displayed as mean ± SD. The significantly different groups are indicated in the graphs, with * being $p < 0.03$, ** $p < 0.002$, *** $p < 0.0002$, and **** being $p < 0.0001$. All experiments were performed in duplicate, with 5 different areas measured in each sample.

The presented data show that higher polymer concentrations yield significant decreases of the average pore diameter of the network. For instance, at 35 °C, the average pore diameter of the PIC hydrogel is reduced from 1.56 ± 0.82 to 0.93 ± 0.43 µm when the polymer concentration is increased from 0.5 to 1.0 mg ml^{-1}, respectively. At 50 °C, an even higher decrease is registered. Therefore, the results show, as proven elsewhere [108], that polymer concentration allows for the tunability of the pore size in the PIC hydrogel. Nevertheless, even with lower polymer concentrations, the pores of PIC hydrogels remain significantly smaller than what is required for several tissue engineering applications. For instance, CNS tissue engineering usually requires pores greater than 40 µm [166] and for angiogenesis the hydrogel must present at least 5 µm of pore diameter [167]. The addition of salts to the PIC hydrogel may allow for the increasement of its average pore diameter.

In addition, the pore ratio of the PIC hydrogels can vary significantly between different polymer concentrations. Higher polymer concentrations yield networks with lesser pore ratios and the effect is once again more pronounced at higher temperatures. From a concentration of 0.5 to 1.0 mg ml^{-1}, the pore ratio decreases as much as 6.72 % at 35 °C and 8.58 % at 50 °C. Nevertheless, PIC hydrogels remain overall highly porous, even with high polymer concentrations, which makes them very attractive for 3D cell culture applications [18].

Moreover, the pore connectivity of the polymer network was also analyzed. Here, the connectivity of a given pore is defined by the number of pores in contact with the respective pore. Higher connectivity values indicate, therefore, a more branched network. From a polymer concentration of 0.5 to 1.0 mg ml^{-1} and at 35 °C, the average connectivity decreases slightly from 5.80 ± 3.01 to 5.38 ± 2.92 (a.u.). As the concentration increases, the pore ratio decreases and therefore the interconnectivity between pores also decreases.

For the long-polymer PIC hydrogel, identical results are obtained (Appendix 4.B). Higher polymer concentration translates into lower average pore diameter, connectivity, and porosity.

Indeed, polymer concentration has a statistically significant effect on the overall microstructure of PIC hydrogels. However, although for a less extent, the temperature at which the hydrogel is has also some influence on the analyzed structural parameters (Table 4.2). With the increasement of temperature, higher averages of pore diameter, pore connectivity and pore ratio are obtained. An increment of 15 °C of a short-PIC hydrogel with 0.5 mg ml^{-1} of polymer results in higher pore diameters by approximately 10 %. It may be hypothesized that, with higher temperatures, the hydrophobic effects associated with the glycol tails of PIC polymers become stronger. Consequently, polymer bundles may become more compact, leading to an increase in pore diameter and pore ratio, which translates into higher pore connectivity. Although polymer concentration has a much stronger influence, the temperature at which the hydrogel is has a structural effect on the PIC hydrogel than must not be negligible.

Table 4.2. The influence of polymer concentration and temperature expressed by the increment or decrement percentage of the structural parameters of the short-polymer PIC hydrogel. The signal of each value is referred to the difference between the group on the line (reference) versus the group on the column.

	Pore Diameter	
	0.5 mg ml^{-1} at 50 °C	1.0 mg ml^{-1} at 35 °C
0.5 mg ml^{-1} at 35 °C	+10.1 %	-40.2 %
1.0 mg ml^{-1} at 50 °C	+67.5 %	-9.1 %
	Pore Connectivity	
	0.5 mg ml^{-1} at 50 °C	1.0 mg ml^{-1} at 35 °C
0.5 mg ml^{-1} at 35 °C	+2.6 %	-7.2 %
1.0 mg ml^{-1} at 50 °C	+7.1 %	-3.2 %
	Pore Ratio	
	0.5 mg ml^{-1} at 50 °C	1.0 mg ml^{-1} at 35 °C
0.5 mg ml^{-1} at 35 °C	+6.2 %	-12.2 %
1.0 mg ml^{-1} at 50 °C	+17.2 %	-3.1 %

The average values of these structural parameters may, however, hide some fundamental differences, since the PIC hydrogel is highly heterogeneous, and its pores can present a broad variation of diameters and connectivity [108]. The graphics in Figure 4.5 represent distributions of these parameters. They clearly demonstrate that polymer concentration has a strong influence on pore diameter, while temperature has a slighter effect on this structural parameter. Interestingly, these graphics show that the influence of both temperature as well as polymer concentration on the pore connectivity distribution is far less pronounced. Indeed, Table 4.2 shows that pore connectivity is the structural parameter where both polymer concentration and temperature influence less. However, the number of connections that each pore can establish within the network has an utmost importance that must not be underestimated. Studies show that scaffolds with higher porosity and well-interconnected pores promote cell ingrowth and better regeneration of tissue [158][159]. The addition of salts to the hydrogel may constitute a way to tune the pore connectivity of the PIC hydrogel, along with its porosity and pore diameter.

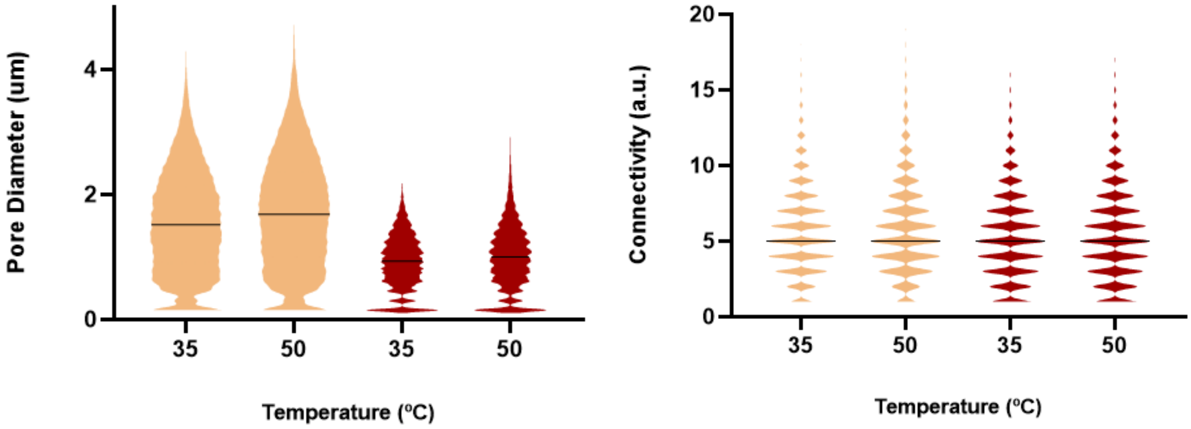

FIGURE 4.5

The diameter and connectivity distributions of all the pores in the short-polymer PIC hydrogel with two different polymer concentrations (0.5 and 1.0 mg ml^{-1}) and at different temperatures (35 and 50 °C). The orange (○) bars represent the 0.5 mg ml^{-1} PIC hydrogel, whereas the red (○) bars are respective of 1.0 mg ml^{-1} of polymer concentration. The black straight line represents the median of the distribution. All experiments were performed in duplicate, with 5 different areas measured in each sample.

4.3.2 | The Influence of Salts on the Microstructure of Polyisocyanopeptide Hydrogels

It is widely known that salts influence the behavior of aqueous systems, such as hydrogels. Indeed, several studies have been performed to clarify these effects. The majority of these focuses, however, on their influence on the swelling and rheology of hydrogels [19]. In the case of PIC hydrogels, Jaspers *et al.* proved the strong effect of Hofmeister ions on their gelation temperature and mechanical properties [20]. Nevertheless, the influence of salts on the microstructure of PIC hydrogels remains vastly unknown and its knowledge might help to explain their effect on the thermal and mechanical behavior of these 3D networks.

PIC hydrogels with and without salts were formulated, labeled with fluorescent TAMRA, and consequently imaged through confocal microscopy in order to assess the influence of three different salts, NaI, NaCl, and $NaClO_4$, on the architecture of the network. Figure 4.6 highlights strong differences between these different formulations. Figure 4.7, on the other hand, quantifies these differences through the average of some structural parameters that characterize the architecture of the network.

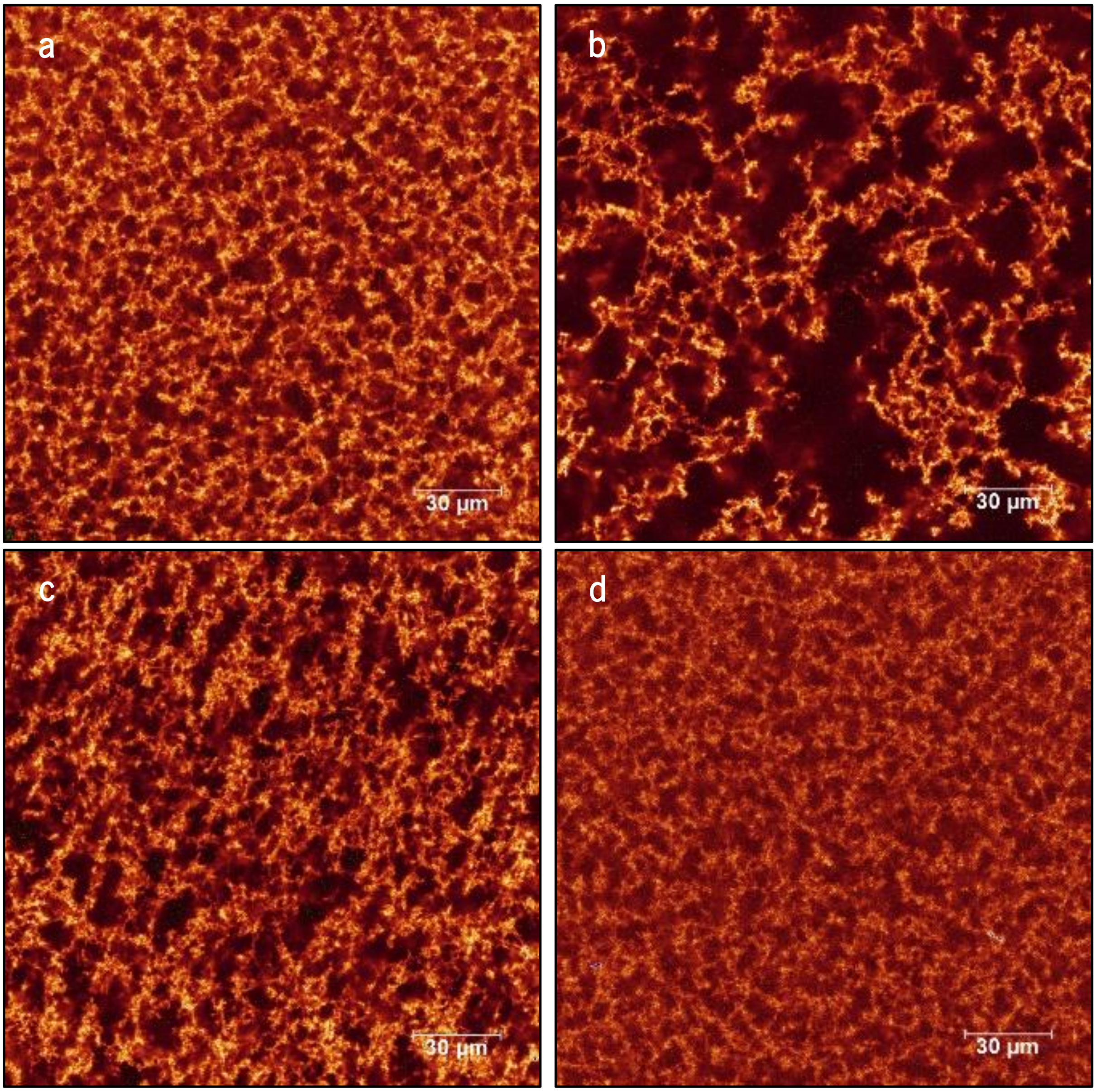

FIGURE 4.6

Representative fluorescence images of TAMRA-labelled and short-polymer PIC hydrogels, with a polymer concentration of 0.5 mg ml^{-1}. (a) represents the PIC hydrogel without any salt added. In (b) the PIC hydrogel was formulated with 1 M of NaCl, (c) with 1 M of $NaClO_4$ and (d) with 1 M of NaI. (a), (b) and (d) were recorded at 35 °C. (c) was recorded at 50 °C due to the high increasement of the gelation temperature induced by this salt. The same settings were employed for the four measurements.

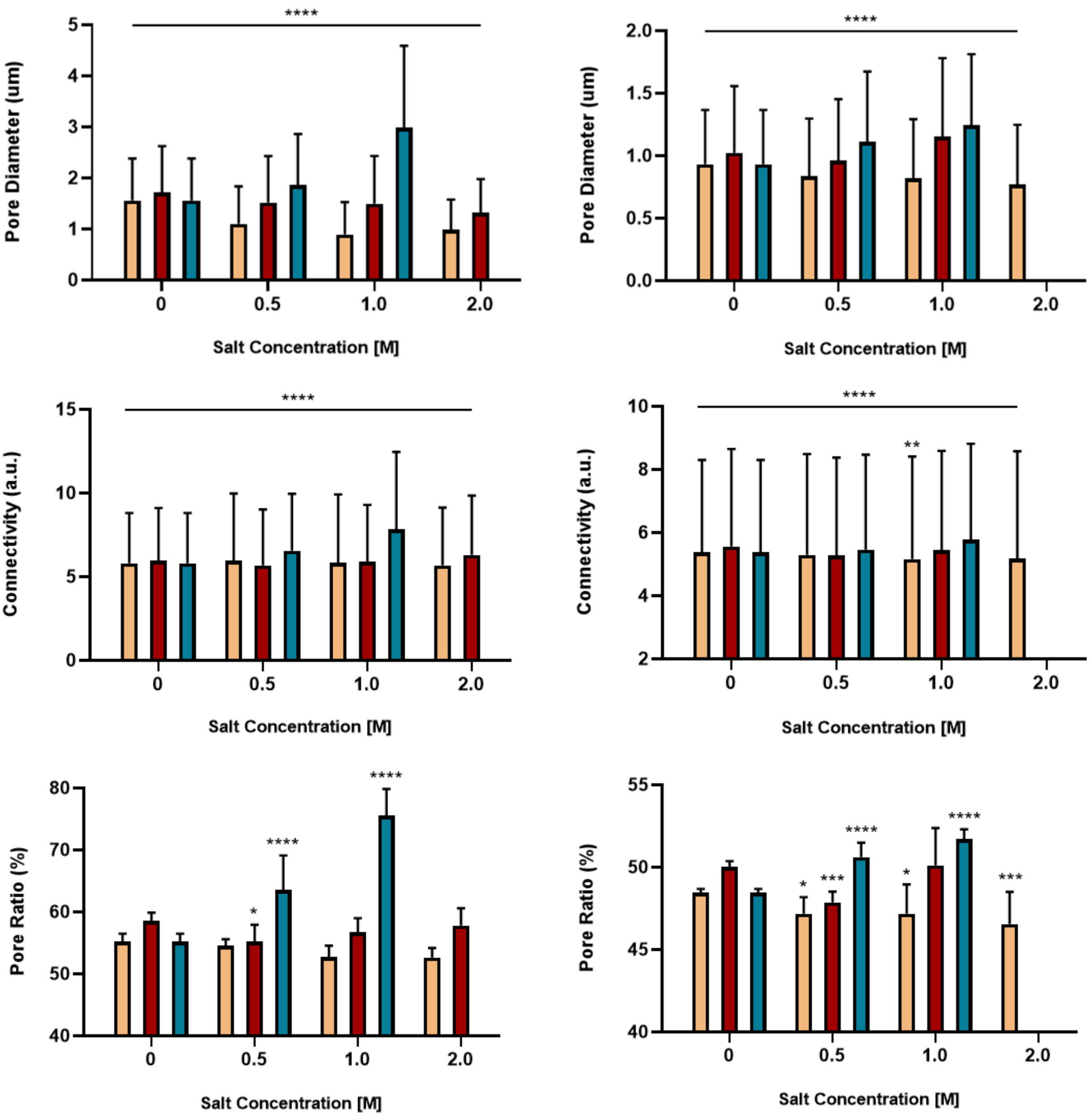

FIGURE 4.7

The average pore diameter, pore connectivity and pore ratio in the overall network of short-PIC hydrogels with different salt concentrations. Data are displayed as mean ± SD. The first column refers to the data obtained for a polymer concentration of 0.5, while the second column refers to a concentration of 1.0 mg ml^{-1}. The orange (○) bars are respective to NaI and the red (○) bars are respective to $NaClO_4$, whereas the PIC hydrogel with NaCl is represented by the blue (○) bars. The significantly different groups are indicated in the graphs, with * being $p < 0.03$, ** $p < 0.002$, *** $p < 0.0002$, and **** being $p < 0.0001$. Every statistical comparison is related to the respective control group (which have no added salts). All experiments were performed in duplicate, with 5 different areas measured in each sample.

Both the qualitative (Figure 4.6) and quantitative (Figure 4.7) analysis demonstrate that while NaI and $NaClO_4$, which are chaotropes, decrease the average pore diameter of the network, NaCl, a kosmotrope, has the opposite effect. This resembles the influence of these two different types of Hofmeister salts on other properties of the PIC hydrogel, such as gelation temperature and mechanical behavior, where kosmotropes and chaotropes have also opposite effects [20]. Indeed, the results obtained prove that this opposite influence between the two groups of anions also extends to the microstructure of the network and its pores. For instance, the addition of 1 M of NaCl to the 0.5 mg ml^{-1} short-PIC hydrogel results in an average pore diameter of 2.98 ± 1.61 μm, in comparison to a value of 1.56 ± 0.82 μm when no salt is added. On the other hand, 2 M of $NaClO_4$ decrease the average pore diameter from 1.56 ± 0.82 μm to 1.32 ± 0.66 μm. Despite their opposite effects, both NaI as well as $NaClO_4$ have a sharply lesser influence on the diameters of the pores than NaCl. For the hydrogels composed of long PICs, the same opposite effect on the pore diameter between NaI or $NaClO_4$ and NaCl is verified (Appendix 4.C).

Furthermore, the three salts also affect the porosity of the hydrogel. For a polymer concentration of 0.5 mg ml^{-1}, the addition of 1 M of NaCl into the short-polymer hydrogel increases its porosity from 55.17 ± 1.31 % to an astonishing 75.53 ± 4.30 %. However, while NaCl increases the porosity of the PIC hydrogel, NaI has once again the opposite effect: 2 M of this salt decrease the pore ratio by 2.52%. When comparing both salts, NaCl has a significantly stronger influence on the porosity of the hydrogel than NaI. Interestingly, $NaClO_4$ has a different effect on the pore ratio of the hydrogel: at small quantities, it decreases the porosity of the hydrogel; however, at higher concentrations, this salt starts to increase its porosity and at 2 M it almost reaches the pore ratio of the control hydrogel, which has no added salt. Similar results in terms of variation are obtained with long PICs (Appendix 4.C). On pore ratio, the only major difference between the two polymer lengths is that NaI, when added to long-PIC hydrogels, actually increases pore ratio, instead of decreasing it as it occurs when added to short-polymer hydrogels.

The added salts also influence the interconnectivity between pores. NaCl increases the connectivity significantly from 5.80 ± 3.01 with no added salt to 7.82 ± 4.64 with 1 M of this salt, for a short-polymer concentration of 0.5 mg ml^{-1}. For 1.0 mg ml^{-1} of polymer, the same trend is verified, although the increment is slighter. The other two salts are not so reliable when it comes to pore connectivity: NaI, at lesser concentrations, increases pore connectivity, while $NaClO_4$ decreases it. However, at higher concentrations, NaI decreases pore connectivity within the network, while $NaClO_4$ increases it. In addition, the described influence of NaI upon the pore connectivity is only true for a polymer concentration of 0.5 mg ml^{-1}. For 1.0 mg ml^{-1} of polymer, NaI decreases pore connectivity, whatever the salt concentration.

The influence of the salts on the analyzed structural parameters of the PIC hydrogel may be described by polynomial regressions (Figure 4.8). Quadratic regressions, in particular, are the approximations that better represent the obtained data, achieving higher R squares. However, even quadratic models do not have a sufficiently high R square to be a reliable approximation. To build more accurate statistical models a higher quantity of data points should be measured across a broader range of salt concentrations. Nevertheless, these models confirm that NaCl is the most reliable of the three salts assessed and it can be predictably used to increase the diameters and connectivity of the pores, as well as the whole porosity of the PIC hydrogel. On the other hand, NaI can be applied to achieve the opposite, although much higher concentrations of this salt may be needed to achieve the same magnitude of influence of NaCl.

It is increasingly important to characterize these aqueous scaffolds to be able to tune them according to the requirements of each application. The equations of these regressions (Appendix 4.C) can be employed to approximately determine the amount of salt needed to achieve a certain value of the three structural parameters analyzed.

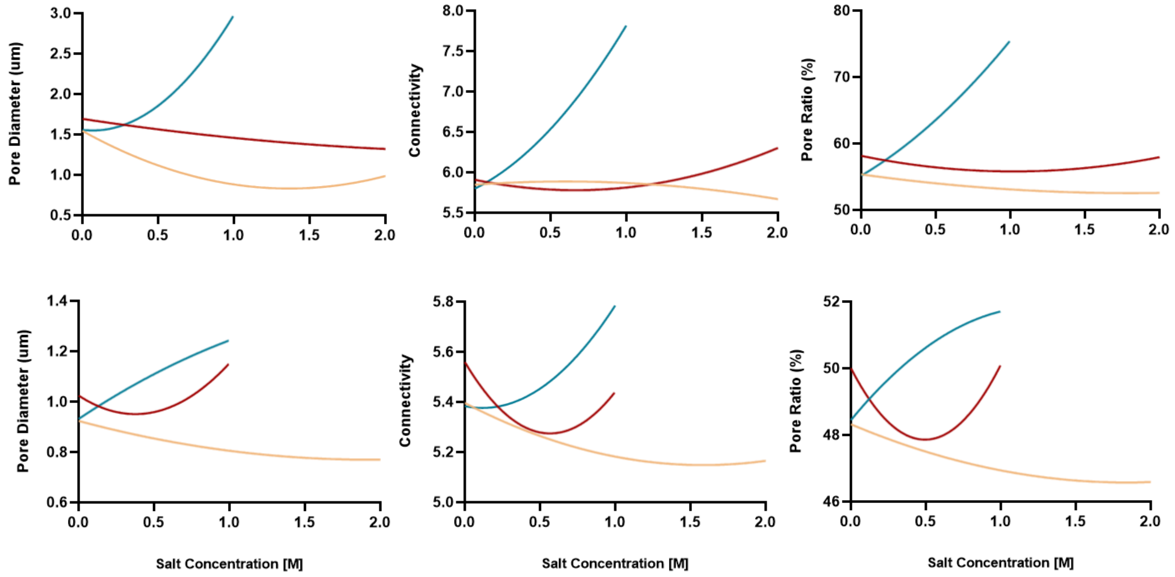

FIGURE 4.8

Quadratic regressions of the averaged pore diameter, pore connectivity and pore ratio of the short-polymer PIC hydrogel per salt concentration. The graphics on the top are representative of a polymer concentration of 0.5 mg ml^{-1}, whereas the bottom three graphics represent data of hydrogels with 1.0 mg ml^{-1} of polymer. The orange (○) curves are respective to NaI and the red (○) curves are respective to NaClO$_4$, whereas the PIC hydrogel with NaCl is represented by the blue (○) curves.

The salts influence on the microstructure of the short-PIC hydrogel is summarized in Table 4.3 and can achieve remarkable magnitudes. For instance, 1 M of NaCl, when added to 0.5 mg ml^{-1} short-PIC hydrogel, increases its average pore diameter by 91% of its original value, from 1.56 ± 0.82 to 2.98 ± 1.61 µm. It also increases pore connectivity by approximately 35% and pore ratio by 37%. On the other hand, 1 M of NaI diminishes the pore diameter by 43% of its original value. Furthermore, data indicate that while NaI has a more impactful effect on the average pore diameter of the short-PIC hydrogel than $NaClO_4$, the latter has a stronger influence on pore connectivity.

Table 4.3. The influence of NaI, $NaClO_4$ and NaCl in the analysed structural parameters of the short-PIC hydrogel, expressed in percentage related to the original values of the hydrogels with no added salts.

0.5 mg ml^{-1}									
	NaI			$NaClO_4$			NaCl		
Salt Concentration	0.5	1.0	2.0	0.5	1.0	2.0	0.5	1.0	2.0
Pore Diameter	-29.5 %	-42.6 %	-36.8 %	-11.9 %	-13.0 %	-23.2 %	+19.2 %	+91.2 %	-
Pore Connectivity	+2.8 %	+0.5 %	+2.1 %	-4.5 %	-1.2 %	+5.8 %	+12.7 %	+34.8 %	-
Porosity	-1.1 %	-4.5 %	-4.6 %	-5.7 %	-3.3 %	-1.3 %	+15.2 %	+36.9 %	-
1.0 mg ml^{-1}									
	NaI			$NaClO_4$			NaCl		
Salt Concentration	0.5	1.0	2.0	0.5	1.0	2.0	0.5	1.0	2.0
Pore Diameter	-10.2 %	-12.1 %	-17.5 %	-6.4 %	+12.5 %	-	+19.1 %	+33.5 %	-
Pore Connectivity	-1.7 %	-4.1 %	-4.0 %	-5.1 %	-2.1 %	-	+1.3 %	+7.5 %	-
Porosity	-2.6 %	-2.6 %	-3.9 %	-4.3 %	+0.2 %	-	+4.5 %	+6.7 %	-

The distributions of the diameters of the pores in the short-polymer PIC hydrogel with 1 M of the three different salts are represented in Figure 4.9. It is evident that while the PIC hydrogel with NaCl has a more symmetric distribution relative to the median of its values, hydrogels with $NaClO_4$ or NaI have a higher quantity of smaller pores that drive down the median of this structural parameter.

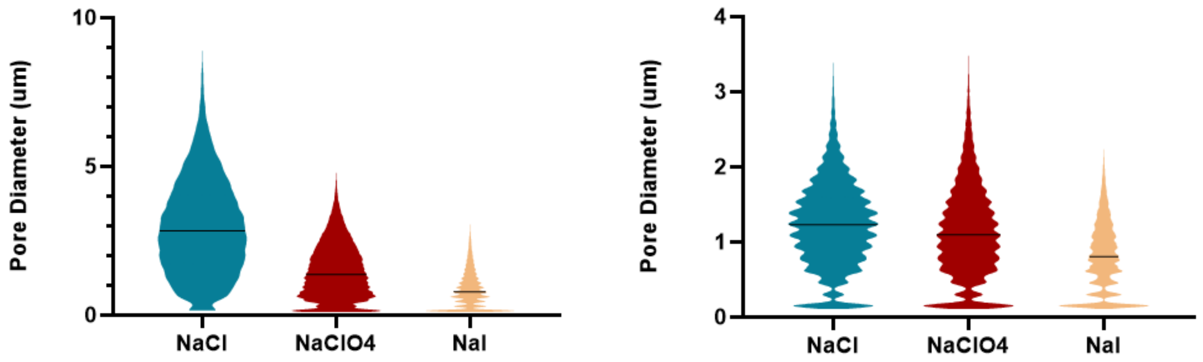

FIGURE 4.9

The diameter distribution of all the pores in the short-polymer PIC hydrogel with 0.5 mg ml^{-1} (left) and 1.0 mg ml^{-1} (right) of polyisocyanopeptides and with 1 M of three different salts. The black straight line represents the median of the distribution. All experiments were performed in duplicate, with 5 different areas measured in each sample.

The reason why NaI or $NaClO_4$ and NaCl have an opposite effect on the hydrogel average pore diameter may lie on the Hofmeister series. Chaotropes (NaI and $NaClO_4$) are able to bind to PICs, adding extra charge to the polymer and increasing its solubility. By increasing the solubility of the polymer, chaotropes increase the gelation temperature of the PIC solution [20]. It may be hypothesized that both iodide and perchlorate anions, as chaotropes able to bind to the PIC polymer, lead to charge repulsion between PIC macromers in the network, which in turn dilate the fibers and reduce the diameter of the pores.

On the other hand, chloride is a kosmotrope anion. Kosmotropes destabilize the hydrogen bonds between the polymer and its hydration water molecules, rendering the polymer less soluble [20]. As the hydrophobic forces increase, the polymer fibers tend to compact, leading to an increase in pore diameter, pore connectivity and the overall porosity of the PIC hydrogel. This effect is far more pronounced than the charge repulsion derived from chaotropes, leading to a much stronger influence of NaCl in the microstructure of the PIC hydrogel in comparison to NaI and $NaClO_4$.

4.3.3 | The Hofmeister Effect on Covalently Crosslinked Polyisocyanopeptide Hydrogels

The results show that the addition of salts greatly influence the microstructure of the physically crosslinked PIC hydrogel. However, while the hydrophobic effects that allow for the physical gelation of PIC solutions might not be strong enough to restrict the influence of salts on the hydrogel microstructure, covalent bonds between the PIC macromers may confer to the network a more resilient behavior. Therefore, it is important to study the influence of the Hofmeister salts on the covalently crosslinked PIC hydrogel. For that purpose, hydrogels with the three different salts previously used and with a crosslinking agent were formulated.

The microscopic images of these samples already provide some information (Figure 4.10). Indeed, for the hydrogel with NaCl (Figure 4.10a), the size of the pores and the overall pore ratio of the hydrogel seems to sharply decrease when comparing the physically crosslinked hydrogel with the PIC hydrogel with the crosslinking agent. For the other two salts, differences between the images are noticeable but not as significant. However, the quantification of structural parameters may provide more accurate information.

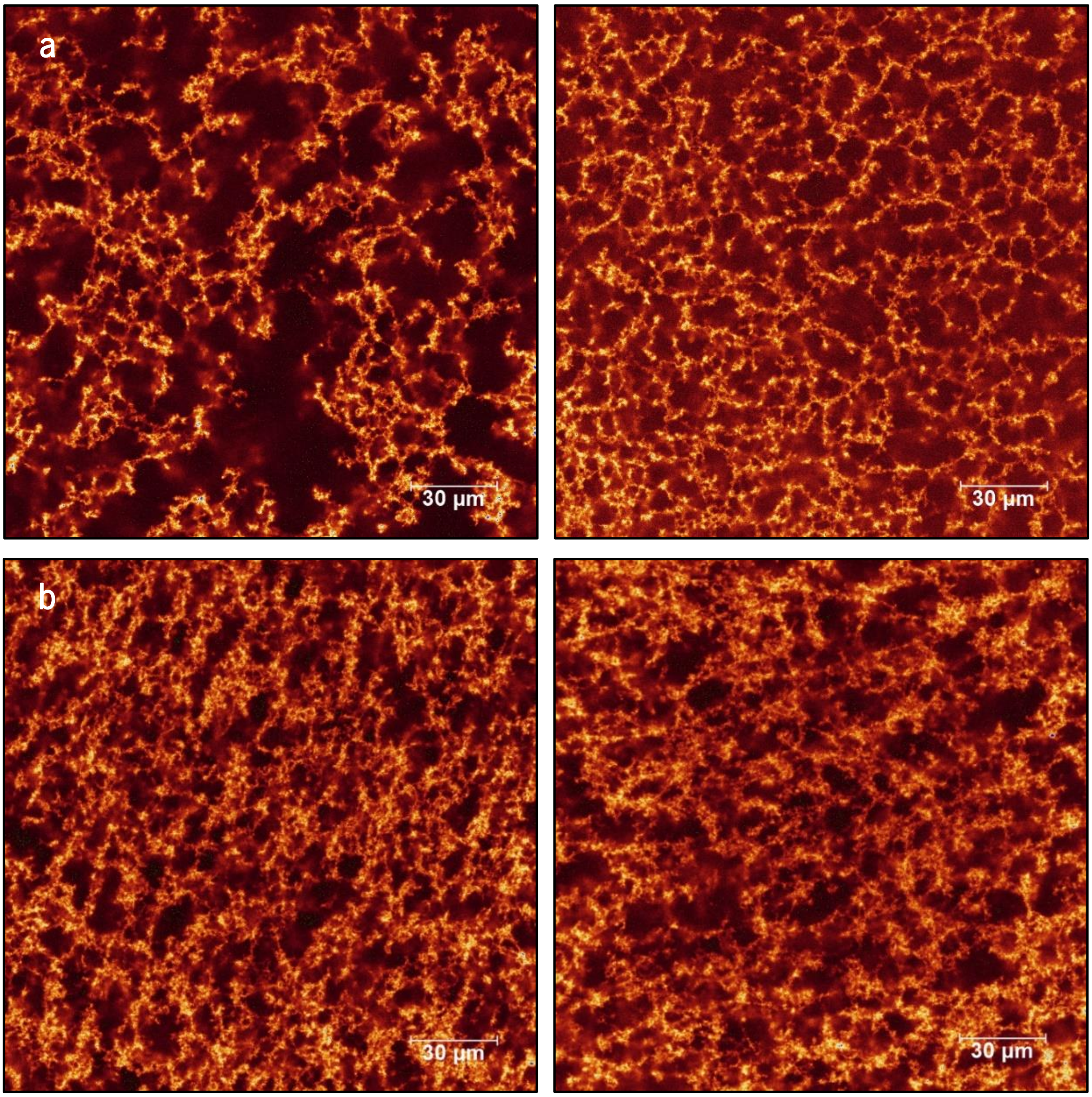

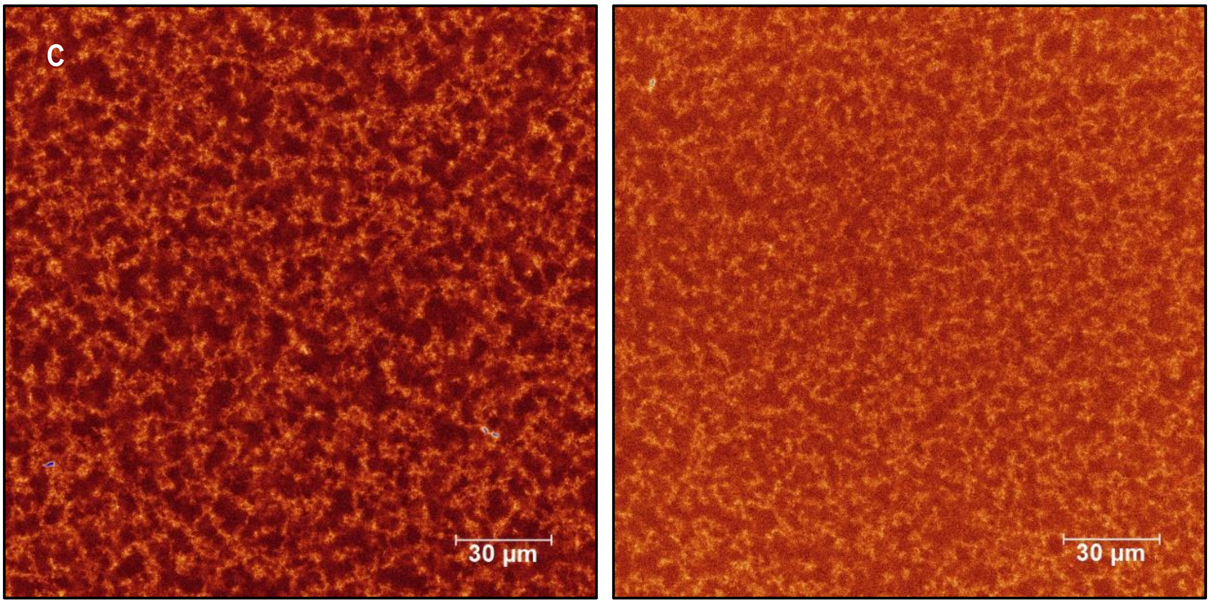

FIGURE 4.10

Representative fluorescence images of TAMRA-labelled and short-polymer PIC hydrogels, with a polymer concentration of 0.5 mg ml^{-1}. On the left column, the images represent the PIC hydrogel without the crosslink agent and with 1 M of (a) NaCl, (b) $NaClO_4$ and (c) NaI. On the other hand, the chemically crosslinked hydrogel is represented on the right column. (a) and (c) were recorded at 35 °C and (b) was recorded at 50 °C. The same settings were employed for all measurements.

Figure 4.11 shows that the chemical crosslink by itself diminishes the average pore diameter of the unsalted PIC hydrogel as much as 0.21 µm at 35 °C and 0.06 µm at 50 °C. Moreover, the average pore diameter of the PIC hydrogel with the added salts approaches the one of the unsalted PIC hydrogel when the crosslinking agent is included. However, this is only observed for $NaClO_4$ and NaCl. For instance, the chemically crosslinked NaCl-PIC hydrogel have an average pore diameter of 1.77 ± 0.84 µm, whereas the same hydrogel but without crosslinking agent has a pore diameter of 2.98 ± 1.61 µm. Interestingly, the chemical crosslink of the hydrogel does not restrict the effect of NaI on the pore diameter of the PIC hydrogel. Even for the crosslinked hydrogel with $NaClO_4$ and with NaCl, a statistically significant difference is still observed when comparing their average pore diameter with the unsalted hydrogel. It may be hypothesized that this difference may be further reduced if the concentration of crosslinking agent on the hydrogel is increased.

In terms of connectivity and porosity of the hydrogel, it is also observable that the chemical crosslink of the PIC fibers results in a structural approximation to the unsalted PIC hydrogel, especially for NaCl since the other two salts do not have as high influence on these two structural properties.

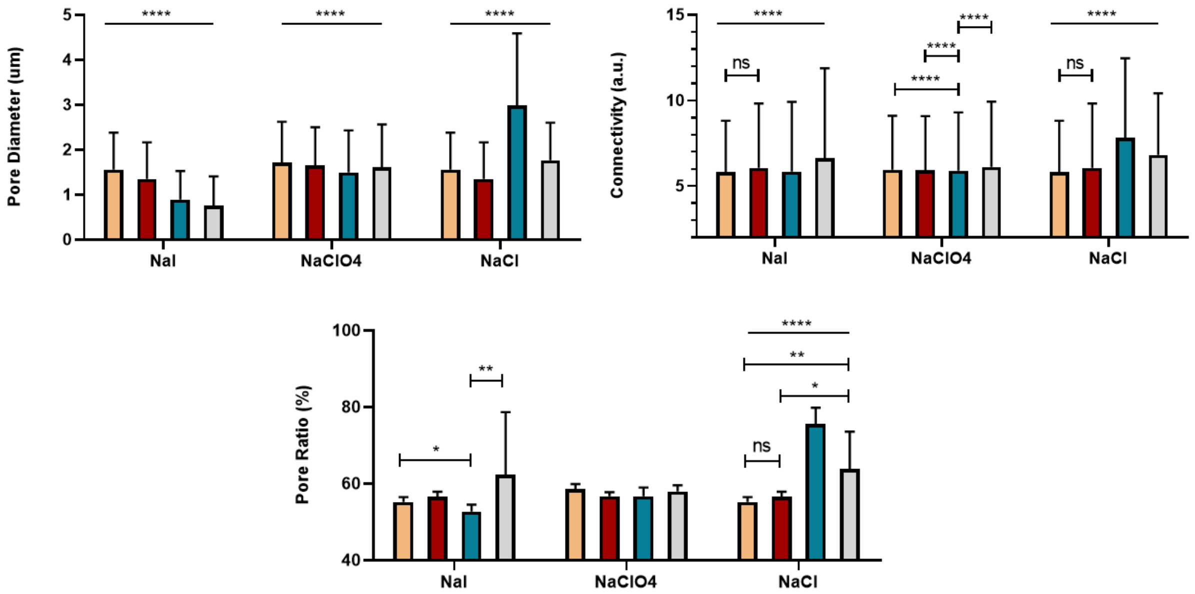

FIGURE 4.11

The average pore diameter, pore connectivity and pore ratio in the overall network of short-polymer chemically crosslinked 0.5 mg ml^{-1} PIC hydrogels without and with the three different salts. Data are displayed as mean ± SD. Note that (○) is respective to the PIC hydrogel with no salt and no crosslink agent added, whereas (○) represents the unsalted chemically crosslinked PIC hydrogel. Moreover, the PIC hydrogel with 1 M of the respective salt is denoted by (○) and the same formulation but with crosslink agent added is represented in (○). The significantly different groups are indicated in the graphs, with * being $p < 0.03$, ** $p < 0.002$, *** $p < 0.0002$, and **** being $p < 0.0001$. All experiments were performed in duplicate, with 5 different areas measured in each sample.

Generally, the chemical crosslink of the PIC hydrogel does restrict the Hofmeister effect of added salts (Table 4.4). NaI, however, do not have its influence restricted by covalent bonds between PIC fibers. Instead, its effect on pore diameter, connectivity and porosity of the PIC hydrogel is actually increased. Therefore, the restriction of salts influence provided by the chemical crosslink of the network must not be assumed universal and further studies with a broader range of salts ought to be performed.

Table 4.4. The influence of NaI, $NaClO_4$ and NaCl in the analysed structural parameters of the short-PIC chemically crosslinked hydrogel, expressed in percentage related to the original values of the physically crosslinked hydrogels with no added salts.

	NaI		$NaClO_4$		NaCl	
	No Crosslinker	W/ Crosslinker	No Crosslinker	W/ Crosslinker	No Crosslinker	W/ Crosslinker
Pore Diameter	-42.6 %	-51.2 %	-13.0 %	-6.2 %	+91.2 %	+13.4 %
Pore Connectivity	+0.5 %	+14.3 %	-1.2 %	+2.7 %	+34.8 %	+17.5 %
Pore Ratio	-4.5 %	+12.8 %	-3.3 %	-1.0 %	+36.9 %	+15.6 %

4.4 | Conclusions

It is widely known that salts influence the behaviour of aqueous systems such as hydrogels and this has been known as the Hofmeister effect. Several studies have been performed to clarify and quantify this influence. Most of the published research focuses on their influence on the swelling, transition temperature (in case of thermoresponsive systems) and mechanical properties of hydrogels [19][20]. Therefore, the effect of salts on their microstructure is until now vastly unknown. Through the usage of fluorescence microscopy and analysis algorithms, it was possible to three-dimensionally visualize and quantify the influence of three salts, sodium iodide, perchlorate, and chloride, on the architecture of hydrogels.

As a model system, PIC-based hydrogels were used. These are biomimetic materials that form fibrous hydrogels [21]. The analysis performed revealed that the three different salts have significantly different effects on the structure of PIC hydrogels. NaCl increases the diameters of the pores, as well as the connectivity between them and the overall porosity of the network. This is true for every polymer length and/or concentration assessed. On the other hand, NaI has the opposite effect: it decreases pore diameter, for every polymer length and/or concentration evaluated. On the connectivity between pores, NaI generally increases it. Moreover, this salt decreases the porosity of the hydrogel when the short-polymer is used, but it increases the pore ratio when the hydrogel is composed by the long-polymer. Finally, the inclusion of $NaClO_4$ in the hydrogel results in smaller pores, whereas its effect in the connectivity and porosity of the network is not so constant and is heavily dependent on the salt concentration, polymer concentration and polymer length employed.

Therefore, the addition of salts to the PIC hydrogel constitutes a straightforward and effective alternative to tune the microstructure of PIC-based networks. Since one of the main limitations of the PIC hydrogel is the small size of its pores, the addition of salts is an easy to apply answer to this shortfall. For instance, our results show that the use of NaCl can sufficiently increase the average pore diameter and porosity of PIC hydrogels to meet better conditions for endothelial and CNS tissue engineering, where 5 and 40 μm of average pore diameter are recommended, respectively [166][167]. Indeed, several studies have used NaCl to build macroporous hydrogels and the results obtained confirm the potential of this salt as a porogen [161][168]. Nevertheless, the small pores of the PIC hydrogel remain a limitation of this system for its application in tissue engineering, even with the usage of NaCl.

Furthermore, the influence of NaCl and $NaClO_4$ on the microstructure of the hydrogel is substantially lower when the PIC fibres are covalently crosslinked. The results show that these salts should not be used to tune the pore structure of the chemically crosslinked-PIC hydrogel.

PIC hydrogels are thermoresponsive and mechanosensitive and both of these smart behaviours can be tuned through the addition of salts [20]. It is now proved that its microstructure can also be manipulated by the same technique. Due to its stimuli-responsiveness and its readily functionalization, PIC hydrogels present a strong potential for biomedical purposes, where they may be used for instance as microfluidic actuators [5][169] or as smart valves for lab-on-a-chip applications that change their status in response to a critical temperature [4][170].

5. CONCLUSIONS AND FUTURE PERSPECTIVES

In this final chapter the most relevant conclusions from the results obtained are presented. Afterwards, future perspectives of the work developed are described.

5.1 | Conclusions

The present project had two aims: (1) to develop and assess a scaffold-based therapy with reinforced electrical conductivity for the treatment of SCIs and (2) to study how the addition of salts to fibrous physical thermosensitive hydrogels influences their microstructure.

Under the first objective, HA substituted with 2.2 % of catechol groups was synthesized and DHA-based hydrogels with graphene were formulated to promote neuroregeneration. The developed hydrogels reveal reinforced electrical conductivity up to 4.25 ± 1.2 µS mm^{-1} when 50 % (w/w) of FG is included. Moreover, their adhesive strength to porcine skin achieves approximately 10.1 kPa upon the inclusion of 5 % of FG, while the DHA hydrogel with no graphene added shows an adhesive strength of 4.6 kPa. It was already proved that higher degree of substitution of catechol groups results in higher adhesive properties. The results obtained demonstrate that the addition of FG have a similar outcome. However, further adhesion studies of DHA hydrogels with higher w/w content of FG should be conducted in the future to confirm this conclusion. Furthermore, upon the seeding of neuronal cells on the networks, DHA hydrogels with FG did not show cytotoxicity. Actually, live/dead assays prove that the inclusion of FG in the hydrogel increases neuronal cell viability. Despite these successful properties of the DHA-FG hydrogel, SEM images of the seeded cells and their rounded morphology demonstrate that further optimizations should be performed to increase cell viability over time. Nevertheless, the produced DHA-FG hydrogel shows overall a promising potential for the treatment of SCIs.

For the second part of the project, PIC-based hydrogels were used as a model system to study the effect of added salts on the pore diameters, pore connectivity and overall porosity of the network. These are thermoresponsive hydrogels with potential for a broad range of smart applications. Samples of this hydrogel with three different sodium salts, NaCl, $NaClO_4$ and NaCl, were formulated and imaged through fluorescence microscopy. The stacks obtained were the input to the algorithm used to analyse the networks. As output, pore diameter, connectivity and pore ratio were obtained, and the data were organized. The results show that the three different salts influence the microstructure of PIC hydrogels. In particular, among the three salts studied, NaCl has the highest influence on the studied parameters, capable of increasing the average pore diameter of the 0.5 mg ml^{-1} short-PIC hydrogel from 1.56 ± 0.82 to 2.98 ± 1.61 µm when 1 M of this salt is added. However, even this increase is not sufficient to meet requirements for some tissue engineering applications and in addition the chemically crosslinking of PIC macromers results in a high decrease of the salts effect on the structural parameters. Therefore, it can be concluded that the addition of salts, in particular NaCl, is an effective strategy, easily applicable and readily available to researchers, to manipulate to a certain extent the microstructure of physical hydrogels, namely the pore diameter, connectivity and porosity of these networks.

5.2 | Future Perspectives

The work developed has potential for future improvement. Herein, some suggestions are presented.

Firstly, in relation to the DHA-FG hydrogel, the attention should focus on the improvement of cell viability and adhesion. To this end, several options may be considered. As $NaIO_4$ may increase cytotoxicity [47], the amount used in the formulation of the hydrogel can be decreased. To formulate the hydrogels, 16 % (w/w) of $NaIO_4$ relative to the amount of DHA was used. Hydrogels with a $NaIO_4$ content of 7.5 % (w/w) were also produced, but they were not stable when placed in medium culture and degraded in a few hours. Therefore, w/w % of $NaIO_4$ between 7.5 and 16 % should be considered and assessed. In addition, electrical stimulation on the hydrogels with neuronal cells seeded may promote cell adhesion and increase their viability over time, as some studies have reported [80][81]. Also, the degree of substitution of catechol groups of DHA could be increased as higher quantity of these moieties may strengthen the adhesion of neuronal cells to the hydrogels surface [47].

In order to improve cell adhesion and functional outcome of SCI patients, NgR antibodies were successfully included in the DHA-FG hydrogel, specifically to the carbonyl group of DHA where the amine-end of the antibodies can bond through the usage of EDC and NHS. As future work, neuronal cells must be seeded on these DHA-FG hydrogels with NgR antibodies to evaluate if their viability and adhesion is increased as expected.

Finally, in case the chemistry employed to attach the antibodies to the DHA is not successful on the increasement of cell viability and adhesion, a different mechanism through which the NgR antibodies can be attached to the carboxyl group of the DHA is proposed below. Studies have reported the covalent immobilization of these antibodies to ADH-modified HA hydrogels via oxidation of the antibodies through $NaIO_4$, which provides them with an aldehyde group that can then react with the amine group present in the ADH-modified HA [48]. As so, a similar but novel approach to attach NgR antibodies to the DHA backbone is herein proposed: EDS and NHS shall be added to DHA to act as intermediaries and then 1,4-diamianobutane becomes easily bonded to the carboxylic acid of the HA (Figure 5.1). Dialysis for 3 days and lyophilization should follow. This material was already produced and the ^1H NMR spectrum confirmed the attachment of diaminobutane to the DHA structure. As future work, NgR antibodies should be oxidized through $NaIO_4$ and included in the DHA-aminobutane/FG hydrogel to compare the influence of the two different immobilization mechanisms on cell viability and adhesion and to overall increase the effectiveness of this scaffold on its potential treatment of SCIs.

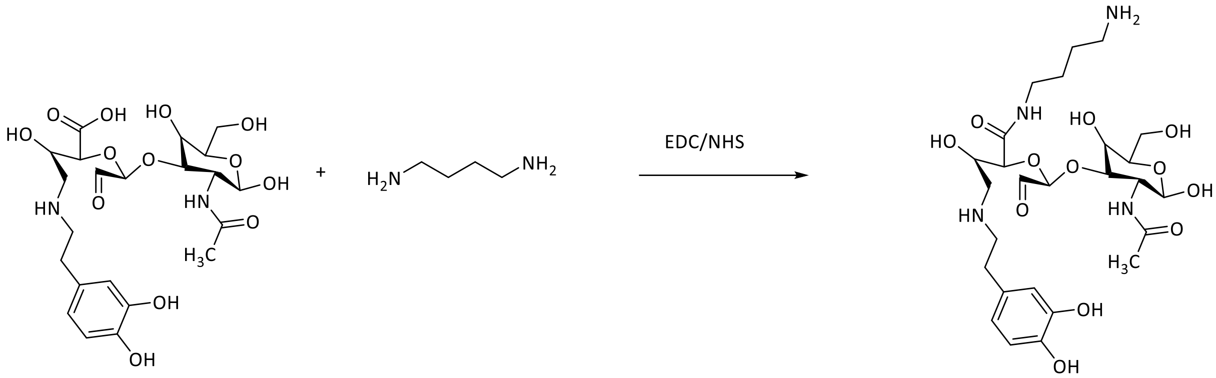

FIGURE 5.1

Synthesis of DHA substituted with 1,4-diaminobutane groups.

Secondly, to better understand how the addition of salts influence the microstructure of PIC hydrogels, a broader range of salts should be tested, as well as PIC hydrogels with more salt concentrations. Evaluating the influence of other salts may also allow for the formulation of hydrogels with higher pore diameter, since the results obtained show that although increments on this structural parameter are registered when NaCl is used, these are not yet sufficiently high for most tissue engineering applications. Moreover, the mechanical and thermal smart behaviour of PIC networks should be further exploited for biomedical applications, such as lab-on-a-chip devices, where self-actuated smart valves and microfluidic actuators are of utmost importance [4][5][170].

Therefore, DHA-FG and PIC-based hydrogels are suited for several biomedical applications and in the future these networks have the potential to be included in lab-on-a-chip applications or as biosensors where antibodies and/or other biomolecules can be immobilized to.

REFERENCES

[1] C. R. Silva *et al.*, ‘Injectable and tunable hyaluronic acid hydrogels releasing chemotactic and angiogenic growth factors for endodontic regeneration’, *Acta Biomater*, vol. 77, pp. 155–171, Sep. 2018, doi: 10.1016/j.actbio.2018.07.035.

[2] J. Erfkamp, M. Guenther, and G. Gerlach, ‘Enzyme-functionalized piezoresistive hydrogel biosensors for the detection of urea’, *Sensors (Switzerland)*, vol. 19, no. 13, Jul. 2019, doi: 10.3390/s19132858.

[3] L. Han *et al.*, ‘Transparent, Adhesive, and Conductive Hydrogel for Soft Bioelectronics Based on Light-Transmitting Polydopamine-Doped Polypyrrole Nanofibrils’, *Chemistry of Materials*, vol. 30, no. 16, pp. 5561–5572, Aug. 2018, doi: 10.1021/acs.chemmater.8b01446.

[4] A. Gargava, C. Arya, and S. R. Raghavan, ‘Smart Hydrogel-Based Valves Inspired by the Stomata in Plants’, *ACS Appl Mater Interfaces*, vol. 8, no. 28, pp. 18430–18438, Jul. 2016, doi: 10.1021/acsami.6b04625.

[5] J. Nie *et al.*, ‘Vessel-on-a-chip with Hydrogel-based Microfluidics’, *Small*, vol. 14, no. 45, Nov. 2018, doi: 10.1002/smll.201802368.

[6] U. S. K. Madduma-Bandarage and S. v. Madihally, ‘Synthetic hydrogels: Synthesis, novel trends, and applications’, *Journal of Applied Polymer Science*, vol. 138, no. 19. John Wiley and Sons Inc, May 15, 2021. doi: 10.1002/app.50376.

[7] D. A. Butterfield and W. O. Opii, ‘Mitochondrial Dysfunction in Nervous System Injury’, in *Encyclopedia of Neuroscience*, L. R. Squire, Ed. Oxford: Academic Press, 2009, pp. 887–894. doi: https://doi.org/10.1016/B978-008045046-9.00506-4.

[8] R. A. Cripps, B. B. Lee, P. Wing, E. Weerts, J. MacKay, and D. Brown, ‘A global map for traumatic spinal cord injury epidemiology: Towards a living data repository for injury prevention’, *Spinal Cord*, vol. 49, no. 4. pp. 493–501, Apr. 2011. doi: 10.1038/sc.2010.146.

[9] A. Singh, L. Tetreault, S. Kalsi-Ryan, A. Nouri, and M. G. Fehlings, ‘Global Prevalence and incidence of traumatic spinal cord injury’, *Clinical Epidemiology*, vol. 6. Dove Medical Press Ltd, pp. 309–331, Sep. 23, 2014. doi: 10.2147/CLEP.S68889.

[10] H. S. Chhabra, R. Sharawat, and G. Vishwakarma, ‘In-hospital mortality in people with complete acute traumatic spinal cord injury at a tertiary care center in India—a retrospective analysis’, *Spinal Cord*, 2021, doi: 10.1038/s41393-021-00657-x.

[11] Universitat Zurich, ‘Antibodies against Nogo-A to enhance plasticity, regeneration and functional recovery after acute spinal cord injury, a multicenter European clinical proof of concept trial’. Horizon Europe 2020, 2021.

[12] X. Wang, J. He, Y. Wang, and F. Z. Cui, ‘Hyaluronic acid-based scaffold for central neural tissue engineering’, *Interface Focus*, vol. 2, no. 3. Royal Society, pp. 278–291, 2012. doi: 10.1098/rsfs.2012.0016.

[13] C. S. Ahuja *et al.*, ‘Traumatic spinal cord injury - Repair and regeneration’, *Clin Neurosurg*, vol. 80, no. 3, pp. S22–S90, Mar. 2017, doi: 10.1093/neuros/nyw080.

[14] B. G. Ballios, M. Douglas Baumann, M. J. Cooke, and M. S. Shoichet, ‘Central Nervous System’, in *Principles of Regenerative Medicine*, Elsevier Inc., 2011, pp. 1023–1046. doi: 10.1016/B978-0-12-381422-7.10055-0.

[15] N. Hlavac, M. Kasper, and C. E. Schmidt, ‘Progress toward finding the perfect match: hydrogels for treatment of central nervous system injury’, *Materials Today Advances*, vol. 6. Elsevier Ltd, Jun. 01, 2020. doi: 10.1016/j.mtadv.2019.100039.

[16] C. E. Turner, ‘Paxillin and focal adhesion signalling’, *Nat Cell Biol*, vol. 2, no. 12, pp. E231–E236, 2000, doi: 10.1038/35046659.

[17] K. H. Vining and D. J. Mooney, ‘Mechanical forces direct stem cell behaviour in development and regeneration’, *Nature Reviews Molecular Cell Biology*, vol. 18, no. 12. Nature Publishing Group, pp. 728–742, Dec. 01, 2017. doi: 10.1038/nrm.2017.108.

[18] N. Annabi *et al.*, ‘Controlling the Porosity and Microarchitecture of Hydrogels for Tissue Engineering’.

[19] M. Zhang, C. G. Wiener, P. I. Sepulveda-Medina, J. F. Douglas, and B. D. Vogt, ‘Influence of Sodium Salts on the Swelling and Rheology of Hydrophobically Cross-linked Hydrogels Determined by QCM-D’, *Langmuir*, vol. 35, no. 50, pp. 16612–16623, Dec. 2019, doi: 10.1021/acs.langmuir.9b03063.

[20] M. Jaspers, A. E. Rowan, and P. H. J. Kouwer, ‘Tuning Hydrogel Mechanics Using the Hofmeister Effect’, *Adv Funct Mater*, vol. 25, no. 41, pp. 6503–6510, Nov. 2015, doi: 10.1002/adfm.201502241.

[21] P. H. J. Kouwer *et al.*, ‘Responsive biomimetic networks from polyisocyanopeptide hydrogels’, *Nature*, vol. 493, no. 7434, pp. 651–655, Jan. 2013, doi: 10.1038/nature11839.

[22] Q. Chai, Y. Jiao, and X. Yu, ‘Hydrogels for biomedical applications: Their characteristics and the mechanisms behind them’, *Gels*, vol. 3, no. 1. MDPI AG, Mar. 01, 2017. doi: 10.3390/gels3010006.

[23] I. M. El-Sherbiny and M. H. Yacoub, ‘Hydrogel scaffolds for tissue engineering: Progress and challenges’, *Glob Cardiol Sci Pract*, vol. 2013, no. 3, p. 38, Sep. 2013, doi: 10.5339/gcsp.2013.38.

[24] A. S. Hoffman, ‘Hydrogels for biomedical applications’, *Advanced Drug Delivery Reviews*, vol. 64, no. SUPPL. pp. 18–23, Dec. 2012. doi: 10.1016/j.addr.2012.09.010.

[25] R. Parhi, ‘Cross-linked hydrogel for pharmaceutical applications: A review’, *Advanced Pharmaceutical Bulletin*, vol. 7, no. 4. Tabriz University of Medical Sciences, pp. 515–530, 2017. doi: 10.15171/apb.2017.064.

[26] B. v. Slaughter, S. S. Khurshid, O. Z. Fisher, A. Khademhosseini, and N. A. Peppas, ‘Hydrogels in regenerative medicine’, *Advanced Materials*, vol. 21, no. 32–33. pp. 3307–3329, Sep. 04, 2009. doi: 10.1002/adma.200802106.

[27] O. WICHTERLE and D. LÍM, ‘Hydrophilic Gels for Biological Use’, *Nature*, vol. 185, no. 4706, pp. 117–118, Jan. 1960, doi: 10.1038/185117a0.

[28] Z. Jia, I. Sukker, M. Müller, and H. Schönherr, ‘Selective Discrimination of Key Enzymes of Pathogenic and Nonpathogenic Bacteria on Autonomously Reporting Shape-Encoded Hydrogel Patterns’, *ACS Appl Mater Interfaces*, vol. 10, no. 6, pp. 5175–5184, Feb. 2018, doi: 10.1021/acsami.7b15147.

[29] F. Abasalizadeh *et al.*, ‘Alginate-based hydrogels as drug delivery vehicles in cancer treatment and their applications in wound dressing and 3D bioprinting’, *Journal of Biological Engineering*, vol. 14, no. 1. BioMed Central Ltd, Mar. 13, 2020. doi: 10.1186/s13036-020-0227-7.

[30] D. Lin, L. Lei, S. Shi, and X. Li, 'Stimulus-Responsive Hydrogel for Ophthalmic Drug Delivery', *Macromolecular Bioscience*, vol. 19, no. 6. Wiley-VCH Verlag, Jun. 01, 2019. doi: 10.1002/mabi.201900001.

[31] M. H. Nabavi *et al.*, 'A collagen-based hydrogel containing tacrolimus for bone tissue engineering', *Drug Deliv Transl Res*, vol. 10, no. 1, pp. 108–121, Feb. 2020, doi: 10.1007/s13346-019-00666-7.

[32] T. Su *et al.*, 'Mussel-inspired agarose hydrogel scaffolds for skin tissue engineering', *Bioact Mater*, vol. 6, no. 3, pp. 579–588, Mar. 2021, doi: 10.1016/j.bioactmat.2020.09.004.

[33] C. Xie, X. Wang, H. He, Y. Ding, and X. Lu, 'Mussel-Inspired Hydrogels for Self-Adhesive Bioelectronics', *Advanced Functional Materials*, vol. 30, no. 25. Wiley-VCH Verlag, Jun. 01, 2020. doi: 10.1002/adfm.201909954.

[34] J. Chen, Q. Peng, T. Thundat, and H. Zeng, 'Stretchable, Injectable, and Self-Healing Conductive Hydrogel Enabled by Multiple Hydrogen Bonding toward Wearable Electronics', *Chemistry of Materials*, vol. 31, no. 12, pp. 4553–4563, Jun. 2019, doi: 10.1021/acs.chemmater.9b01239.

[35] A. Tuladhar, N. Mitrousis, T. Führmann, and M. S. Shoichet, 'Central Nervous System', in *Translational Regenerative Medicine*, Elsevier Inc., 2015, pp. 415–435. doi: 10.1016/B978-0-12-410396-2.00030-X.

[36] K. Kitamura *et al.*, 'Recombinant Human Hepatocyte Growth Factor Promotes Functional Recovery After Spinal Cord Injury', in *Neuroprotection and Regeneration of the Spinal Cord*, K. Uchida, M. Nakamura, H. Ozawa, S. Katoh, and Y. Toyama, Eds. Tokyo: Springer Japan, 2014, pp. 147–167. doi: 10.1007/978-4-431-54502-6_14.

[37] K. Kitamura *et al.*, 'Human hepatocyte growth factor promotes functional recovery in primates after spinal cord injury', *PLoS One*, vol. 6, no. 11, Nov. 2011, doi: 10.1371/journal.pone.0027706.

[38] K. Kitamura *et al.*, 'Hepatocyte growth factor promotes endogenous repair and functional recovery after spinal cord injury', *J Neurosci Res*, vol. 85, no. 11, pp. 2332–2342, Aug. 2007, doi: 10.1002/jnr.21372.

[39] 'Clinical Trials.gov', *2022. https://clinicaltrials.gov/. Accessed September 24, 2022.*

[40] N. Nagoshi *et al.*, ‘Phase I/II Study of Intrathecal Administration of Recombinant Human Hepatocyte Growth Factor in Patients with Acute Spinal Cord Injury: A Double-Blind, Randomized Clinical Trial of Safety and Efficacy’, *J Neurotrauma*, vol. 37, no. 15, pp. 1752–1758, Aug. 2020, doi: 10.1089/neu.2019.6854.

[41] R. Mohammed, K. Opara, R. Lall, U. Ojha, and J. Xiang, ‘Evaluating the effectiveness of anti-Nogo treatment in spinal cord injuries’, *Neural Development*, vol. 15, no. 1. BioMed Central Ltd., Jan. 09, 2020. doi: 10.1186/s13064-020-0138-9.

[42] K. Kucher *et al.*, ‘First-in-man intrathecal application of neurite growth-promoting anti-nogo- a antibodies in acute spinal cord injury’, *Neurorehabil Neural Repair*, vol. 32, no. 6–7, pp. 578–589, May 2018, doi: 10.1177/1545968318776371.

[43] R. G. Fessler *et al.*, ‘A phase 1/2a dose-escalation study of oligodendrocyte progenitor cells in individuals with subacute cervical spinal cord injury’, *J Neurosurg Spine*, pp. 1–9, Jul. 2022, doi: 10.3171/2022.5.spine22167.

[44] J. D. Guest *et al.*, ‘Internal decompression of the acutely contused spinal cord: Differential effects of irrigation only versus biodegradable scaffold implantation’, *Biomaterials*, vol. 185, pp. 284–300, Dec. 2018, doi: 10.1016/j.biomaterials.2018.09.025.

[45] K. D. Kim, K. S. Lee, D. Coric, J. S. Harrop, N. Theodore, and R. M. Toselli, ‘Acute Implantation of a Bioresorbable Polymer Scaffold in Patients With Complete Thoracic Spinal Cord Injury: 24-Month Follow-up From the INSPIRE Study’, *Neurosurgery*, vol. 90, no. 6, pp. 668–675, Jun. 2022, doi: 10.1227/neu.0000000000001932.

[46] A. Borzacchiello, L. Russo, B. M. Malle, K. Schwach-Abdellaoui, and L. Ambrosio, ‘Hyaluronic acid based hydrogels for regenerative medicine applications’, *Biomed Res Int*, vol. 2015, 2015, doi: 10.1155/2015/871218.

[47] D. Zhou *et al.*, ‘Dopamine-Modified Hyaluronic Acid Hydrogel Adhesives with Fast-Forming and High Tissue Adhesion’, *ACS Appl Mater Interfaces*, vol. 12, no. 16, pp. 18225–18234, Apr. 2020, doi: 10.1021/acsami.9b22120.

[48] W. M. Tian *et al.*, ‘Hyaluronic acid hydrogel as Nogo-66 receptor antibody delivery system for the repairing of injured rat brain: In vitro’, *Journal of Controlled Release*, vol. 102, no. 1, pp. 13–22, Jan. 2005, doi: 10.1016/j.jconrel.2004.09.025.

[49] E. Papakonstantinou, M. Roth, and G. Karakiulakis, ‘Hyaluronic acid: A key molecule in skin aging’, *Dermato-Endocrinology*, vol. 4, no. 3. Landes Bioscience, 2012. doi: 10.4161/derm.21923.

[50] R. C. Gupta, R. Lall, A. Srivastava, and A. Sinha, ‘Hyaluronic acid: Molecular mechanisms and therapeutic trajectory’, *Front Vet Sci*, vol. 6, no. JUN, 2019, doi: 10.3389/fvets.2019.00192.

[51] C. M. Lin *et al.*, ‘Hyaluronic acid inhibits the glial scar formation after brain damage with tissue loss in rats’, *Surg Neurol*, vol. 72, no. SUPPL. 2, Dec. 2009, doi: 10.1016/j.wneu.2009.09.004.

[52] Z. Z. Khaing, B. D. Milman, J. E. Vanscoy, S. K. Seidlits, R. J. Grill, and C. E. Schmidt, ‘High molecular weight hyaluronic acid limits astrocyte activation and scar formation after spinal cord injury’, in *Journal of Neural Engineering*, Aug. 2011, vol. 8, no. 4. doi: 10.1088/1741-2560/8/4/046033.

[53] C. A. McKay *et al.*, ‘An injectable, calcium responsive composite hydrogel for the treatment of acute spinal cord injury’, *ACS Appl Mater Interfaces*, vol. 6, no. 3, pp. 1424–1438, Feb. 2014, doi: 10.1021/am4027423.

[54] S. v. Kushchayev *et al.*, ‘Hyaluronic acid scaffold has a neuroprotective effect in hemisection spinal cord injury’, *J Neurosurg Spine*, vol. 25, no. 1, pp. 114–124, Jul. 2016, doi: 10.3171/2015.9.SPINE15628.

[55] D. Tarus *et al.*, ‘Design of Hyaluronic Acid Hydrogels to Promote Neurite Outgrowth in Three Dimensions’, *ACS Appl Mater Interfaces*, vol. 8, no. 38, pp. 25051–25059, Sep. 2016, doi: 10.1021/acsami.6b06446.

[56] K. Zaviskova *et al.*, ‘Injectable hydroxyphenyl derivative of hyaluronic acid hydrogel modified with RGD as scaffold for spinal cord injury repair’, *J Biomed Mater Res A*, vol. 106, no. 4, pp. 1129–1140, Apr. 2018, doi: 10.1002/jbm.a.36311.

[57] L. A. Flanagan, L. M. Rebaza, S. Derzic, P. H. Schwartz, and E. S. Monuki, ‘Regulation of human neural precursor cells by laminin and integrins’, *J Neurosci Res*, vol. 83, no. 5, pp. 845–856, Apr. 2006, doi: 10.1002/jnr.20778.

[58] S. Plantman *et al.*, ‘Integrin-laminin interactions controlling neurite outgrowth from adult DRG neurons in vitro’, *Molecular and Cellular Neuroscience*, vol. 39, no. 1, pp. 50–62, Sep. 2008, doi: 10.1016/j.mcn.2008.05.015.

[59] S. Hou *et al.*, 'The repair of brain lesion by implantation of hyaluronic acid hydrogels modified with laminin', *J Neurosci Methods*, vol. 148, no. 1, pp. 60–70, Oct. 2005, doi: 10.1016/j.jneumeth.2005.04.016.

[60] C. P. Addington, J. M. Heffernan, C. S. Millar-Haskell, E. W. Tucker, R. W. Sirianni, and S. E. Stabenfeldt, 'Enhancing neural stem cell response to SDF-1α gradients through hyaluronic acid-laminin hydrogels', *Biomaterials*, vol. 72, pp. 11–19, Dec. 2015, doi: 10.1016/j.biomaterials.2015.08.041.

[61] S. A. Geissler *et al.*, 'Biomimetic hydrogels direct spinal progenitor cell differentiation and promote functional recovery after spinal cord injury', *J Neural Eng*, vol. 15, no. 2, Feb. 2018, doi: 10.1088/1741-2552/aaa55c.

[62] K. Saha *et al.*, 'Substrate modulus directs neural stem cell behavior', *Biophys J*, vol. 95, no. 9, pp. 4426–4438, Nov. 2008, doi: 10.1529/biophysj.108.132217.

[63] E. Moeendarbary *et al.*, 'The soft mechanical signature of glial scars in the central nervous system', *Nat Commun*, vol. 8, Mar. 2017, doi: 10.1038/ncomms14787.

[64] P. C. Georges, W. J. Miller, D. F. Meaney, E. S. Sawyer, and P. A. Janmey, 'Matrices with compliance comparable to that of brain tissue select neuronal over glial growth in mixed cortical cultures', *Biophys J*, vol. 90, no. 8, pp. 3012–3018, 2006, doi: 10.1529/biophysj.105.073114.

[65] L. Fan *et al.*, 'Directing Induced Pluripotent Stem Cell Derived Neural Stem Cell Fate with a Three-Dimensional Biomimetic Hydrogel for Spinal Cord Injury Repair', *ACS Appl Mater Interfaces*, vol. 10, no. 21, pp. 17742–17755, May 2018, doi: 10.1021/acsami.8b05293.

[66] K. W. Kolewe, S. R. Peyton, and J. D. Schiffman, 'Fewer Bacteria Adhere to Softer Hydrogels', *ACS Appl Mater Interfaces*, vol. 7, no. 35, pp. 19562–19569, Sep. 2015, doi: 10.1021/acsami.5b04269.

[67] M. Paidikondala, S. Wang, J. Hilborn, S. Larsson, and O. P. Varghese, 'Impact of Hydrogel Cross-Linking Chemistry on the in Vitro and in Vivo Bioactivity of Recombinant Human Bone Morphogenetic Protein-2', *ACS Appl Bio Mater*, vol. 2, no. 5, pp. 2006–2012, May 2019, doi: 10.1021/acsabm.9b00060.

[68] P. Maturavongsadit, X. Bi, K. Metavarayuth, J. A. Luckanagul, and Q. Wang, 'Influence of cross-linkers on the in vitro chondrogenesis of mesenchymal stem cells in hyaluronic acid hydrogels',

ACS Appl Mater Interfaces, vol. 9, no. 4, pp. 3318–3329, Feb. 2017, doi: 10.1021/acsami.6b12437.

[69] M. T. Poldervaart *et al.*, '3D bioprinting of methacrylated hyaluronic acid (MeHA) hydrogel with intrinsic osteogenicity', *PLoS One*, vol. 12, no. 6, Jun. 2017, doi: 10.1371/journal.pone.0177628.

[70] J. Shin *et al.*, 'Tissue Adhesive Catechol-Modified Hyaluronic Acid Hydrogel for Effective, Minimally Invasive Cell Therapy', *Adv Funct Mater*, vol. 25, no. 25, pp. 3814–3824, Jul. 2015, doi: 10.1002/adfm.201500006.

[71] J. Kim, C. Lee, and J. H. Ryu, 'Adhesive catechol-conjugated hyaluronic acid for biomedical applications: A mini review', *Applied Sciences (Switzerland)*, vol. 11, no. 1. MDPI AG, pp. 1–14, Jan. 01, 2021. doi: 10.3390/app11010021.

[72] S. Hong *et al.*, 'Hyaluronic acid catechol: A biopolymer exhibiting a pH-dependent adhesive or cohesive property for human neural stem cell engineering', *Adv Funct Mater*, vol. 23, no. 14, pp. 1774–1780, Apr. 2013, doi: 10.1002/adfm.201202365.

[73] J. Lee, K. Chang, S. Kim, V. Gite, H. Chung, and D. Sohn, 'Phase controllable hyaluronic acid hydrogel with iron(III) ion-catechol induced dual cross-linking by utilizing the gap of gelation kinetics', *Macromolecules*, vol. 49, no. 19, pp. 7450–7459, Oct. 2016, doi: 10.1021/acs.macromol.6b01198.

[74] D. G. Barrett, D. E. Fullenkamp, L. He, N. Holten-Andersen, K. Y. C. Lee, and P. B. Messersmith, 'PH-based regulation of hydrogel mechanical properties through mussel-inspired chemistry and processing', *Adv Funct Mater*, vol. 23, no. 9, pp. 1111–1119, Mar. 2013, doi: 10.1002/adfm.201201922.

[75] M. Shin, K. H. Song, J. C. Burrell, D. K. Cullen, and J. A. Burdick, 'Injectable and Conductive Granular Hydrogels for 3D Printing and Electroactive Tissue Support', *Advanced Science*, vol. 6, no. 20, Oct. 2019, doi: 10.1002/advs.201901229.

[76] K. Zhang *et al.*, 'Injectable, anti-inflammatory and conductive hydrogels based on graphene oxide and diacerein-terminated four-armed polyethylene glycol for spinal cord injury repair', *Mater Des*, vol. 196, Nov. 2020, doi: 10.1016/j.matdes.2020.109092.

[77] R. Boni, A. Ali, A. Shavandi, and A. N. Clarkson, ‘Current and novel polymeric biomaterials for neural tissue engineering’, *Journal of Biomedical Science*, vol. 25, no. 1. BioMed Central Ltd., Dec. 20, 2018. doi: 10.1186/s12929-018-0491-8.

[78] S. Peressotti, G. E. Koehl, J. A. Goding, and R. A. Green, ‘Self-Assembling Hydrogel Structures for Neural Tissue Repair’, *ACS Biomaterials Science and Engineering*, vol. 7, no. 9. American Chemical Society, pp. 4136–4163, Sep. 13, 2021. doi: 10.1021/acsbiomaterials.1c00030.

[79] L. Zhou *et al.*, ‘Soft Conducting Polymer Hydrogels Cross-Linked and Doped by Tannic Acid for Spinal Cord Injury Repair’, *ACS Nano*, vol. 12, no. 11, pp. 10957–10967, Nov. 2018, doi: 10.1021/acsnano.8b04609.

[80] R. Zhu, Z. Sun, C. Li, S. Ramakrishna, K. Chiu, and L. He, ‘Electrical stimulation affects neural stem cell fate and function in vitro’, *Experimental Neurology*, vol. 319. Academic Press Inc., Sep. 01, 2019. doi: 10.1016/j.expneurol.2019.112963.

[81] C. E. Schmidt, A. Kotwal, and C. E. Schmidt, ‘Electrical stimulation alters protein adsorption and nerve cell interactions with electrically conducting biomaterials’, 2001.

[82] V. Kumar, T. Yokozeki, T. Goto, and T. Takahashi, ‘Mechanical and electrical properties of PANI-based conductive thermosetting composites’, *Journal of Reinforced Plastics and Composites*, vol. 34, no. 16, pp. 1298–1305, Aug. 2015, doi: 10.1177/0731684415588551.

[83] Y. Luo *et al.*, ‘An injectable, self-healing, electroconductive extracellular matrix-based hydrogel for enhancing tissue repair after traumatic spinal cord injury’, *Bioact Mater*, vol. 7, pp. 98–111, Jan. 2022, doi: 10.1016/j.bioactmat.2021.05.039.

[84] M. Silva *et al.*, ‘Biomedical films of graphene nanoribbons and nanoflakes with natural polymers’, *RSC Adv*, vol. 7, no. 44, pp. 27578–27594, 2017, doi: 10.1039/c7ra04173j.

[85] E. B. Malarkey, K. A. Fisher, E. Bekyarova, W. Liu, R. C. Haddon, and V. Parpura, ‘Conductive single-walled carbon nanotube substrates modulate neuronal growth’, *Nano Lett*, vol. 9, no. 1, pp. 264–268, Jan. 2009, doi: 10.1021/nl802855c.

[86] J. Shin *et al.*, ‘Three-Dimensional Electroconductive Hyaluronic Acid Hydrogels Incorporated with Carbon Nanotubes and Polypyrrole by Catechol-Mediated Dispersion Enhance Neurogenesis of Human Neural Stem Cells’, *Biomacromolecules*, vol. 18, no. 10, pp. 3060–3072, Oct. 2017, doi: 10.1021/acs.biomac.7b00568.

[87] H. Sun *et al.*, 'Carbon nanotube-incorporated collagen hydrogels improve cell alignment and the performance of cardiac constructs', *Int J Nanomedicine*, vol. 12, pp. 3109–3120, Apr. 2017, doi: 10.2147/IJN.S128030.

[88] P. Kumar, P. Huo, R. Zhang, and B. Liu, 'Antibacterial properties of graphene-based nanomaterials', *Nanomaterials*, vol. 9, no. 5. MDPI AG, May 01, 2019. doi: 10.3390/nano9050737.

[89] Q. Song *et al.*, 'Anti-inflammatory effects of three-dimensional graphene foams cultured with microglial cells', *Biomaterials*, vol. 35, no. 25, pp. 6930–6940, 2014, doi: 10.1016/j.biomaterials.2014.05.002.

[90] M. Silva, N. M. Alves, and M. C. Paiva, 'Graphene-polymer nanocomposites for biomedical applications', *Polymers for Advanced Technologies*, vol. 29, no. 2. John Wiley and Sons Ltd, pp. 687–700, Feb. 01, 2018. doi: 10.1002/pat.4164.

[91] F. Song *et al.*, 'Enzymatically cross-linked hyaluronic acid/graphene oxide nanocomposite hydrogel with pH-responsive release', *J Biomater Sci Polym Ed*, vol. 26, no. 6, pp. 339–352, Apr. 2015, doi: 10.1080/09205063.2015.1007413.

[92] K. Pradhan *et al.*, 'Neuro-Regenerative Choline-Functionalized Injectable Graphene Oxide Hydrogel Repairs Focal Brain Injury', *ACS Chem Neurosci*, vol. 10, no. 3, pp. 1535–1543, Mar. 2019, doi: 10.1021/acschemneuro.8b00514.

[93] A. Servant *et al.*, 'Graphene-based electroresponsive scaffolds as polymeric implants for on-demand drug delivery', *Adv Healthc Mater*, vol. 3, no. 8, pp. 1334–1343, 2014, doi: 10.1002/adhm.201400016.

[94] Y. Liang *et al.*, 'Adhesive Hemostatic Conducting Injectable Composite Hydrogels with Sustained Drug Release and Photothermal Antibacterial Activity to Promote Full-Thickness Skin Regeneration During Wound Healing', *Small*, vol. 15, no. 12, Mar. 2019, doi: 10.1002/smll.201900046.

[95] S. Das, F. Irin, L. Ma, S. K. Bhattacharia, R. C. Hedden, and M. J. Green, 'Rheology and morphology of pristine graphene/polyacrylamide gels', *ACS Appl Mater Interfaces*, vol. 5, no. 17, pp. 8633–8640, Sep. 2013, doi: 10.1021/am402185r.

[96] M. Silva *et al.*, 'Poly(Lactic acid)/graphite nanoplatelet nanocomposite filaments for ligament scaffolds', *Nanomaterials*, vol. 11, no. 11, Nov. 2021, doi: 10.3390/nano11112796.

[97] M. M. Silva, D. Ribeiro, E. Cunha, M. Fernanda Proença, R. J. Young, and M. C. Paiva, 'A simple method for anchoring silver and copper nanoparticles on single wall carbon nanotubes', *Nanomaterials*, vol. 9, no. 10, Oct. 2019, doi: 10.3390/nano9101416.

[98] J. Yi, G. Choe, J. Park, and J. Y. Lee, 'Graphene oxide-incorporated hydrogels for biomedical applications', *Polymer Journal*, vol. 52, no. 8. Springer Nature, pp. 823–837, Aug. 01, 2020. doi: 10.1038/s41428-020-0350-9.

[99] G. Jensen, J. L. Holloway, and S. E. Stabenfeldt, 'Hyaluronic Acid Biomaterials for Central Nervous System Regenerative Medicine', *Cells*, vol. 9, no. 9. NLM (Medline), Sep. 17, 2020. doi: 10.3390/cells9092113.

[100] M. Zarei-Kheirabadi *et al.*, 'Human embryonic stem cell-derived neural stem cells encapsulated in hyaluronic acid promotes regeneration in a contusion spinal cord injured rat', *Int J Biol Macromol*, vol. 148, pp. 1118–1129, Apr. 2020, doi: 10.1016/j.ijbiomac.2020.01.219.

[101] S. K. Seidlits *et al.*, 'Peptide-modified, hyaluronic acid-based hydrogels as a 3D culture platform for neural stem/progenitor cell engineering', *J Biomed Mater Res A*, vol. 107, no. 4, pp. 704–718, Apr. 2019, doi: 10.1002/jbm.a.36603.

[102] I. Elliott Donaghue, C. H. Tator, and M. S. Shoichet, 'Local Delivery of Neurotrophin-3 and Anti-NogoA Promotes Repair after Spinal Cord Injury', *Tissue Eng Part A*, vol. 22, no. 9–10, pp. 733–741, May 2016, doi: 10.1089/ten.tea.2015.0471.

[103] Z. He *et al.*, 'An anti-inflammatory peptide and brain-derived neurotrophic factor-modified hyaluronan-methylcellulose hydrogel promotes nerve regeneration in rats with spinal cord injury', *Int J Nanomedicine*, vol. 14, pp. 721–732, 2019, doi: 10.2147/IJN.S187854.

[104] J. Lu *et al.*, 'Enhanced angiogenesis by the hyaluronic acid hydrogels immobilized with a VEGF mimetic peptide in a traumatic brain injury model in rats', *Regen Biomater*, vol. 6, no. 6, pp. 325–334, Dec. 2019, doi: 10.1093/rb/rbz027.

[105] S. Hou *et al.*, 'The enhancement of cell adherence and inducement of neurite outgrowth of dorsal root ganglia co-cultured with hyaluronic acid hydrogels modified with Nogo-66 receptor antagonist in vitro', *Neuroscience*, vol. 137, no. 2, pp. 519–529, 2006, doi: 10.1016/j.neuroscience.2005.09.029.

[106] Y. T. Wei *et al.*, 'Hyaluronic acid hydrogel modified with nogo-66 receptor antibody and poly-L-lysine to promote axon regrowth after spinal cord injury', *J Biomed Mater Res B Appl Biomater*, vol. 95, no. 1, pp. 110–117, Oct. 2010, doi: 10.1002/jbm.b.31689.

[107] C. J. J. L. M *et al.*, 'β-Helical Polymers from Isocyanopeptides', *Science (1979)*, vol. 293, no. 5530, pp. 676–680, Jul. 2001, doi: 10.1126/science.1062224.

[108] J. Vandaele, B. Louis, K. Liu, R. Camacho, P. H. J. Kouwer, and S. Rocha, 'Structural characterization of fibrous synthetic hydrogels using fluorescence microscopy', *Soft Matter*, vol. 16, no. 17, pp. 4210–4219, May 2020, doi: 10.1039/c9sm01828j.

[109] C. Storm, J. J. Pastore, F. C. MacKintosh, T. C. Lubensky, and P. A. Janmey, 'Nonlinear elasticity in biological gels', *Nature*, vol. 435, no. 7039, pp. 191–194, 2005, doi: 10.1038/nature03521.

[110] S. Haupert, D. Mitton, S. Guérard, F. Peyrin, and P. Laugier, 'Quantification of nonlinear elasticity for the evaluation of submillimeter crack length in cortical bone', *J Mech Behav Biomed Mater*, vol. 48, Aug. 2015, doi: 10.1016/j.jmbbm.2015.04.013.

[111] K. Liu, M. Wiendels, H. Yuan, C. Ruan, and P. H. J. Kouwer, 'Cell-matrix reciprocity in 3D culture models with nonlinear elasticity', *Bioactive Materials*, vol. 9. KeAi Communications Co., pp. 316–331, Mar. 01, 2022. doi: 10.1016/j.bioactmat.2021.08.002.

[112] J. P. Winer, S. Oake, and P. A. Janmey, 'Non-linear elasticity of extracellular matrices enables contractile cells to communicate local position and orientation', *PLoS One*, vol. 4, no. 7, Jul. 2009, doi: 10.1371/journal.pone.0006382.

[113] R. K. Das, V. Gocheva, R. Hammink, O. F. Zouani, and A. E. Rowan, 'Stress-stiffening-mediated stem-cell commitment switch in soft responsive hydrogels', *Nat Mater*, vol. 15, no. 3, pp. 318–325, 2016, doi: 10.1038/nmat4483.

[114] K. Liu, S. M. Mihaila, A. Rowan, E. Oosterwijk, and P. H. J. Kouwer, 'Synthetic Extracellular Matrices with Nonlinear Elasticity Regulate Cellular Organization', *Biomacromolecules*, vol. 20, no. 2, pp. 826–834, Feb. 2019, doi: 10.1021/acs.biomac.8b01445.

[115] J. Zimoch *et al.*, 'Polyisocyanopeptide hydrogels: A novel thermo-responsive hydrogel supporting pre-vascularization and the development of organotypic structures', *Acta Biomater*, vol. 70, pp. 129–139, Apr. 2018, doi: 10.1016/j.actbio.2018.01.042.

[116] K. Liu *et al.*, 'Rapid stem cell spreading induced by high affinity α5β1 integrin-selective bicyclic RGD peptide in biomimetic hydrogels', doi: 10.1101/2022.02.01.478177.

[117] J. Weiden *et al.*, 'Injectable biomimetic hydrogels as tools for efficient T Cell expansion and delivery', *Front Immunol*, vol. 9, no. NOV, Nov. 2018, doi: 10.3389/fimmu.2018.02798.

[118] P. de Almeida *et al.*, 'Cytoskeletal stiffening in synthetic hydrogels', *Nat Commun*, vol. 10, no. 1, Dec. 2019, doi: 10.1038/s41467-019-08569-4.

[119] J. Guo, C. Xing, H. Yuan, R. Chai, and Y. Zhan, 'Oligo (p-Phenylene Vinylene)/Polyisocyanopeptide Biomimetic Composite Hydrogel-Based Three-Dimensional Cell Culture System for Anticancer and Antibacterial Therapeutics', *ACS Appl Bio Mater*, vol. 2, no. 6, pp. 2520–2527, Jun. 2019, doi: 10.1021/acsabm.9b00217.

[120] N. Celikkin *et al.*, '3D printing of thermoresponsive polyisocyanide (PIC) hydrogels as bioink and fugitive material for tissue engineering', *Polymers (Basel)*, vol. 10, no. 5, May 2018, doi: 10.3390/polym10050555.

[121] R. C. op 't Veld *et al.*, 'Monitoring 111In-labelled polyisocyanopeptide (PIC) hydrogel wound dressings in full-thickness wounds', *Biomater Sci*, vol. 7, no. 7, pp. 3041–3050, 2019, doi: 10.1039/C9BM00661C.

[122] R. C. op 't Veld *et al.*, 'Thermosensitive biomimetic polyisocyanopeptide hydrogels may facilitate wound repair', *Biomaterials*, vol. 181, pp. 392–401, 2018, doi: https://doi.org/10.1016/j.biomaterials.2018.07.038.

[123] B. Wang *et al.*, 'A tunable and injectable local drug delivery system for personalized periodontal application', *Journal of Controlled Release*, vol. 324, pp. 134–145, Aug. 2020, doi: 10.1016/j.jconrel.2020.05.004.

[124] B. Wang *et al.*, 'Antimicrobial and anti-inflammatory thermo-reversible hydrogel for periodontal delivery', *Acta Biomater*, vol. 116, pp. 259–267, Oct. 2020, doi: 10.1016/j.actbio.2020.09.018.

[125] D. C. Schoenmakers, A. E. Rowan, and P. H. J. Kouwer, 'Crosslinking of fibrous hydrogels', *Nat Commun*, vol. 9, no. 1, Dec. 2018, doi: 10.1038/s41467-018-04508-x.

[126] F. Hofmeister, 'Zur Lehre von der Wirkung der Salze', *Archiv für experimentelle Pathologie und Pharmakologie*, vol. 24, no. 4, pp. 247–260, 1888, doi: 10.1007/BF01918191.

[127] Y. Zhang, S. Furyk, D. E. Bergbreiter, and P. S. Cremer, ‘Specific Ion Effects on the Water Solubility of Macromolecules: PNIPAM and the Hofmeister Series’, *J Am Chem Soc*, vol. 127, no. 41, pp. 14505–14510, Oct. 2005, doi: 10.1021/ja0546424.

[128] J. P. Magnusson, A. Khan, G. Pasparakis, A. O. Saeed, W. Wang, and C. Alexander, ‘Ion-Sensitive “Isothermal” Responsive Polymers Prepared in Water’, *J Am Chem Soc*, vol. 130, no. 33, pp. 10852–10853, Aug. 2008, doi: 10.1021/ja802609r.

[129] H. Mira and J. Morante, ‘Neurogenesis From Embryo to Adult – Lessons From Flies and Mice’, *Frontiers in Cell and Developmental Biology*, vol. 8. Frontiers Media S.A., Jun. 30, 2020. doi: 10.3389/fcell.2020.00533.

[130] G. G. Kovacs, ‘Cellular reactions of the central nervous system’, in *Handbook of Clinical Neurology*, vol. 145, Elsevier B.V., 2018, pp. 13–23. doi: 10.1016/B978-0-12-802395-2.00003-1.

[131] J. M. Goaillard, E. Moubarak, M. Tapia, and F. Tell, ‘Diversity of Axonal and Dendritic Contributions to Neuronal Output’, *Frontiers in Cellular Neuroscience*, vol. 13. Frontiers Media S.A., Jan. 22, 2020. doi: 10.3389/fncel.2019.00570.

[132] S. Jäkel and L. Dimou, ‘Glial cells and their function in the adult brain: A journey through the history of their ablation’, *Frontiers in Cellular Neuroscience*, vol. 11. Frontiers Research Foundation, Feb. 13, 2017. doi: 10.3389/fncel.2017.00024.

[133] N. Lannes, E. Eppler, S. Etemad, P. Yotovski, and L. Filgueira, ‘Microglia at center stage: a comprehensive review about the versatile and unique residential macrophages of the central nervous system’, 2017. [Online]. Available: www.impactjournals.com/oncotarget/

[134] A. D. Greenhalgh, S. David, and F. C. Bennett, ‘Immune cell regulation of glia during CNS injury and disease’, *Nature Reviews Neuroscience*, vol. 21, no. 3. Nature Research, pp. 139–152, Mar. 01, 2020. doi: 10.1038/s41583-020-0263-9.

[135] F. L. Xuan, K. Chithanathan, K. Lilleväli, X. Yuan, and L. Tian, ‘Differences of Microglia in the Brain and the Spinal Cord’, *Front Cell Neurosci*, vol. 13, Nov. 2019, doi: 10.3389/fncel.2019.00504.

[136] H. Tsujioka and T. Yamashita, ‘Neural circuit repair after central nervous system injury’, *Int Immunol*, vol. 33, no. 6, pp. 301–309, Jun. 2021, doi: 10.1093/intimm/dxaa077.

[137] E. E. Benarroch, ‘Extracellular matrix in the CNS’, *Neurology*, vol. 85, no. 16, pp. 1417–1427, Oct. 2015, doi: 10.1212/WNL.0000000000002044.

[138] A. E. Haggerty, M. M. Marlow, and M. Oudega, ‘Extracellular matrix components as therapeutics for spinal cord injury’, *Neuroscience Letters*, vol. 652. Elsevier Ireland Ltd, pp. 50–55, Jun. 23, 2017. doi: 10.1016/j.neulet.2016.09.053.

[139] J. W. Fawcett, T. Oohashi, and T. Pizzorusso, ‘The roles of perineuronal nets and the perinodal extracellular matrix in neuronal function’, *Nature Reviews Neuroscience*, vol. 20, no. 8. Nature Publishing Group, pp. 451–465, Aug. 01, 2019. doi: 10.1038/s41583-019-0196-3.

[140] A. C. Reichelt, D. J. Hare, T. J. Bussey, and L. M. Saksida, ‘Perineuronal Nets: Plasticity, Protection, and Therapeutic Potential’, *Trends in Neurosciences*, vol. 42, no. 7. Elsevier Ltd, pp. 458–470, Jul. 01, 2019. doi: 10.1016/j.tins.2019.04.003.

[141] M. E. Schwab, ‘Functions of Nogo proteins and their receptors in the nervous system’, *Nature Reviews Neuroscience*, vol. 11, no. 12. pp. 799–811, Dec. 2010. doi: 10.1038/nrn2936.

[142] Z. Sun *et al.*, ‘A novel Nogo-66 receptor antagonist peptide promotes neurite regeneration in vitro’, *Molecular and Cellular Neuroscience*, vol. 71, pp. 80–91, Mar. 2016, doi: 10.1016/j.mcn.2015.12.011.

[143] C. L. Mcdonald, C. Bandtlow, and M. Reindl, ‘Targeting the Nogo Receptor Complex in Diseases of the Central Nervous System’, 2011.

[144] A. Kempf *et al.*, ‘The Sphingolipid Receptor S1PR2 Is a Receptor for Nogo-A Repressing Synaptic Plasticity’, *PLoS Biol*, vol. 12, no. 1, Jan. 2014, doi: 10.1371/journal.pbio.1001763.

[145] C. S. Ahuja *et al.*, ‘Traumatic spinal cord injury’, *Nature Reviews Disease Primers*, vol. 3. Nature Publishing Group, Apr. 27, 2017. doi: 10.1038/nrdp.2017.18.

[146] T. M. O’Shea, J. E. Burda, and M. v. Sofroniew, ‘Cell biology of spinal cord injury and repair’, *Journal of Clinical Investigation*, vol. 127, no. 9. American Society for Clinical Investigation, pp. 3259–3270, Sep. 01, 2017. doi: 10.1172/JCI90608.

[147] P. Snetkov, K. Zakharova, S. Morozkina, R. Olekhnovich, and M. Uspenskaya, ‘Hyaluronic acid: The influence of molecular weight on structural, physical, physico-chemical, and degradable properties of biopolymer’, *Polymers*, vol. 12, no. 8. MDPI AG, Aug. 01, 2020. doi: 10.3390/polym12081800.

[148] N. Schweigert, A. J. B. Zehnder, and R. I. L. Eggen, ‘Chemical properties of catechols and their molecular modes of toxic action in cells, from microorganisms to mammals’, *Environ Microbiol*, vol. 3, no. 2, pp. 81–91, 2001, doi: 10.1046/j.1462-2920.2001.00176.x.

[149] M. Muhammad, C. Willems, J. Rodríguez-fernández, G. Gallego- Ferrer, and T. Groth, ‘Synthesis and characterization of oxidized polysaccharides for in situ forming hydrogels’, *Biomolecules*, vol. 10, no. 8, pp. 1–18, Aug. 2020, doi: 10.3390/biom10081185.

[150] B. Howell, S. P. Lad, W. M. Grill, and J. C. Glorioso, ‘Evaluation of intradural stimulation efficiency and selectivity in a computational model of spinal cord stimulation’, *PLoS One*, vol. 9, no. 12, Dec. 2014, doi: 10.1371/journal.pone.0114938.

[151] M. Suneetha, K. M. Rao, and S. S. Han, ‘Mussel-inspired cell/tissue-adhesive, hemostatic hydrogels for tissue engineering applications’, *ACS Omega*, vol. 4, no. 7, pp. 12647–12656, Jul. 2019, doi: 10.1021/acsomega.9b01302.

[152] J. Uggeri *et al.*, ‘Calcein-AM is a detector of intracellular oxidative activity’, *Histochem Cell Biol*, vol. 122, no. 5, pp. 499–505, 2000, doi: 10.1007/s00418-004-0712-y.

[153] W. Cao *et al.*, ‘The preparation and biocompatible evaluation of injectable dual crosslinking hyaluronic acid hydrogels as cytoprotective agents’, *J Mater Chem B*, vol. 7, no. 28, pp. 4413–4423, 2019, doi: 10.1039/C9TB00839J.

[154] J. Fu, C. Wiraja, H. B. Muhammad, C. Xu, and D.-A. Wang, ‘Improvement of endothelial progenitor outgrowth cell (EPOC)-mediated vascularization in gelatin-based hydrogels through pore size manipulation’, *Acta Biomater*, vol. 58, pp. 225–237, 2017, doi: https://doi.org/10.1016/j.actbio.2017.06.012.

[155] Y. Han, M. Lian, Q. Wu, Z. Qiao, B. Sun, and K. Dai, ‘Effect of Pore Size on Cell Behavior Using Melt Electrowritten Scaffolds’, *Front Bioeng Biotechnol*, vol. 9, Jul. 2021, doi: 10.3389/fbioe.2021.629270.

[156] Y. Liu *et al.*, ‘Stiffness-mediated mesenchymal stem cell fate decision in 3D-bioprinted hydrogels’, *Burns Trauma*, vol. 8, 2021, doi: 10.1093/BURNST/TKAA029.

[157] M. Guvendiren and J. A. Burdick, ‘The control of stem cell morphology and differentiation by hydrogel surface wrinkles’, *Biomaterials*, vol. 31, no. 25, pp. 6511–6518, 2010, doi: https://doi.org/10.1016/j.biomaterials.2010.05.037.

[158] H. J. Kim, U. J. Kim, G. Vunjak-Novakovic, B. H. Min, and D. L. Kaplan, 'Influence of macroporous protein scaffolds on bone tissue engineering from bone marrow stem cells', *Biomaterials*, vol. 26, no. 21, pp. 4442–4452, Jul. 2005, doi: 10.1016/j.biomaterials.2004.11.013.

[159] D. J. Griffon, M. R. Sedighi, D. v. Schaeffer, J. A. Eurell, and A. L. Johnson, 'Chitosan scaffolds: Interconnective pore size and cartilage engineering', *Acta Biomater*, vol. 2, no. 3, pp. 313–320, 2006, doi: 10.1016/j.actbio.2005.12.007.

[160] I. N. Savina, G. C. Ingavle, A. B. Cundy, and S. v. Mikhalovsky, 'A simple method for the production of large volume 3D macroporous hydrogels for advanced biotechnological, medical and environmental applications', *Sci Rep*, vol. 6, Feb. 2016, doi: 10.1038/srep21154.

[161] B. Chen *et al.*, 'Repair of spinal cord injury by implantation of bFGF-incorporated HEMA-MOETACL hydrogel in rats', *Sci Rep*, vol. 5, 2015, doi: 10.1038/srep09017.

[162] M. K. Lee, M. H. Rich, K. Baek, J. Lee, and H. Kong, 'Bioinspired tuning of hydrogel permeability-rigidity dependency for 3D cell culture', *Sci Rep*, vol. 5, 2015, doi: 10.1038/srep08948.

[163] T. G. Kim, H. J. Chung, and T. G. Park, 'Macroporous and nanofibrous hyaluronic acid/collagen hybrid scaffold fabricated by concurrent electrospinning and deposition/leaching of salt particles', *Acta Biomater*, vol. 4, no. 6, pp. 1611–1619, 2008, doi: 10.1016/j.actbio.2008.06.008.

[164] T. Caykara, S. Küçüktepe, and E. Turan, 'Swelling characteristics of thermosensitive poly[(2-diethylaminoethyl methacrylate)-co-(N,N-dimethylacrylamide)] porous hydrogels', *Polym Int*, vol. 56, no. 4, pp. 532–537, Apr. 2007, doi: 10.1002/pi.2166.

[165] V. M. Gun'ko, I. N. Savina, and S. v. Mikhalovsky, 'Cryogels: Morphological, structural and adsorption characterisation', *Advances in Colloid and Interface Science*, vol. 187–188. Elsevier B.V., pp. 1–46, 2013. doi: 10.1016/j.cis.2012.11.001.

[166] Y. H. Tsou, J. Khoneisser, P. C. Huang, and X. Xu, 'Hydrogel as a bioactive material to regulate stem cell fate', *Bioactive Materials*, vol. 1, no. 1. KeAi Communications Co., pp. 39–55, Sep. 01, 2016. doi: 10.1016/j.bioactmat.2016.05.001.

[167] T. Hozumi, T. Kageyama, S. Ohta, J. Fukuda, and T. Ito, 'Injectable Hydrogel with Slow Degradability Composed of Gelatin and Hyaluronic Acid Cross-Linked by Schiff's Base Formation', *Biomacromolecules*, vol. 19, no. 2, pp. 288–297, Feb. 2018, doi: 10.1021/acs.biomac.7b01133.

[168] B. Podhorská *et al.*, 'Revealing the true morphological structure of macroporous soft hydrogels for tissue engineering', *Applied Sciences (Switzerland)*, vol. 10, no. 19. MDPI AG, Oct. 01, 2020. doi: 10.3390/APP10196672.

[169] M. E. Harmon, M. Tang, and C. W. Frank, 'A microfluidic actuator based on thermoresponsive hydrogels', *Polymer (Guildf)*, vol. 44, no. 16, pp. 4547–4556, Jul. 2003, doi: 10.1016/S0032-3861(03)00463-4.

[170] J. Wang *et al.*, 'Self-Actuated, Thermo-Responsive Hydrogel Valves for Lab on a Chip', Springer Science + Business Media, Inc. Manufactured in The Netherlands, 2005.

SUPPLEMENTARY INFORMATION

Herein, additional data and information about the conducted studies is presented.

APPENDIX TO CHAPTER 3

A. Electrical Conductivity

Table 3.A. Electrical conductivity of DHA hydrogels without and with graphene. In particular, two graphene formulations were tested: PG and FG. Different w/w % of these materials were assessed. For each condition, three hydrogels were formulated, and their electrical conductivity was measured by applying 1 V to the hydrogels and measuring the current that passed through them. The dimensions of the hydrogels were measured with a calliper. Their electrical conductivity was then calculated through the Ohm's Law.

Graphene Content (w/w) %		Electrical Current (mA)	Length (mm)	Width (mm)	Height (mm)	Electrical Conductivity (uS/mm)	Average (uS/mm)
No Graphene	0	0.004	9.08	9.33	3.25	1.20	1.17
		0.005	10.20	9.12	3.74	1.50	
		0.003	8.78	7.48	4.39	0.80	
PG	1	0.006	8.76	9.42	2.86	1.95	1.52
		0.005	9.24	9.75	2.78	1.70	
		0.003	8.68	9.56	3.02	0.90	
	5	0.007	8.85	9.30	2.94	2.27	1.61
		0.004	8.70	10.71	2.29	1.42	
		0.003	9.01	8.87	2.65	1.15	
	50	0.005	8.62	7.43	3.71	1.56	2.53
		0.011	9.27	9.10	3.73	3.00	
		0.014	9.01	9.21	4.52	3.03	
FG	1	0.003	8.95	10.31	2.64	0.99	1.18
		0.004	8.66	10.58	2.73	1.20	
		0.005	9.09	9.41	3.54	1.36	
		0.004	8.93	9.45	2.79	1.35	

5	0.006	9.35	9.77	2.91	1.97	1.66
	0.005	9.55	10.70	2.68	1.67	
50	0.014	9.13	9.84	3.27	3.97	4.25
	0.020	9.79	9.95	3.53	5.57	
	0.008	10.30	8.12	3.16	3.21	

B. Adhesion Strength

Table 3.B. Adhesion strength of DHA hydrogels to porcine skin. For each condition, experiments in triplicate were performed.

FG (w/w) %	Maximum Force (N)	Thickness (mm)	Width (mm)	Adhesion (Pa)	Average (Pa)	SD
0	0.05	3.69	13.61	995.60	10099	4736
	0.7	4.74	15.56	9490.96		
	0.2	4.24	13.84	3408.22		
5	1.1	4.68	15.51	15154.27	4632	4378
	0.3	3.86	13.48	5765.59		
	0.3	3.50	9.14	9377.93		

C. Cell Viability

Below, microscopic images of DHA hydrogels with seeded neuronal cells obtained during the Live/Dead assay are presented. These images are respective to the third day after the cell seeding and they are different from the images presented in the fourth chapter, as these images include the transmittance of the sample. Therefore, FG sheets are visible in black, and it is possible to visualize live cells around this material.

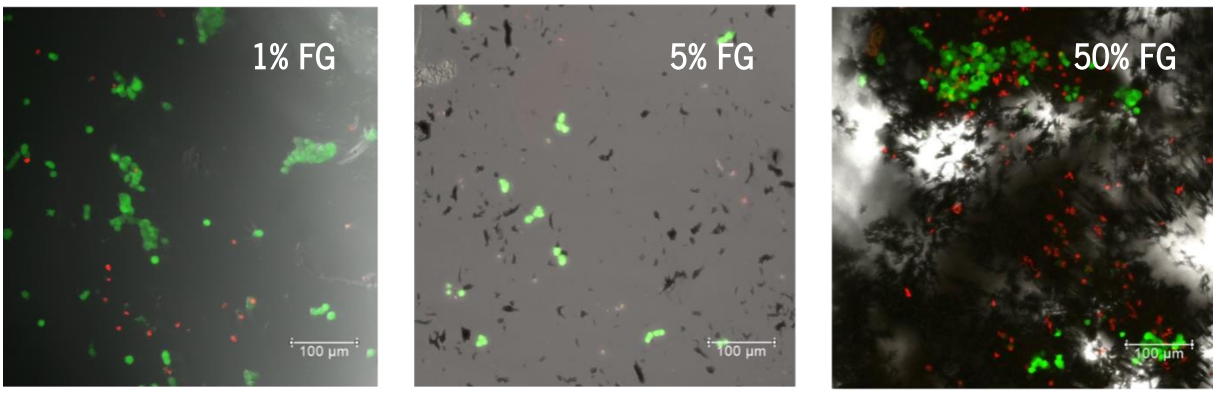

FIGURE 3.C

Cell viability analysis with the Live/Dead assay after 3 of the seeding of neuronal cells on the DHA hydrogel. Live cells (green) were stained with Calcein AM, while dead cells (red) were stained with PI. The scale bar is 100 µm.

D. Cell Morphology and Adhesion

Herein are represented SEM images of the DHA hydrogels with different w/w % of FG after 1, 3 and 7 days of the seeding of neuronal cells. On the fourth chapter, SEM images are already presented, but their amplification is higher (1000x). Below SEM images with an amplification of 500x are provided.

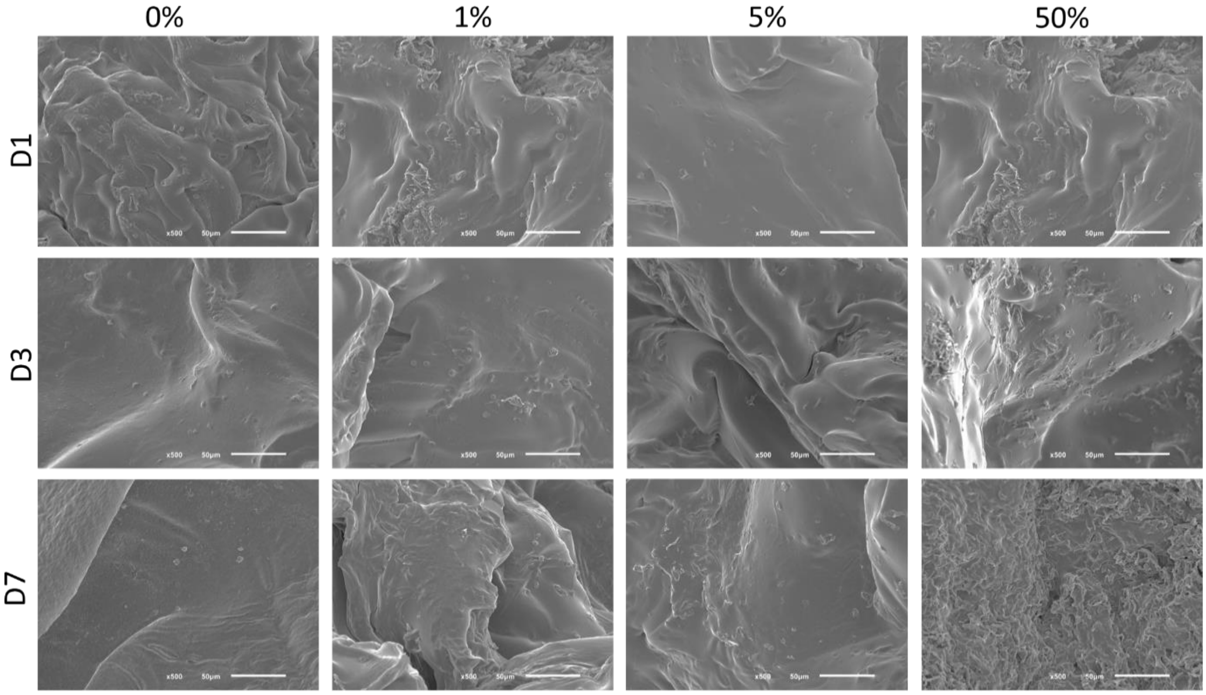

FIGURE 3.D

SEM images of neuronal cells adhered on the DHA hydrogel surfaces with an amplification of 500. The scale bar is 50 µm.

APPENDIX TO CHAPTER 4

A. Pore Network Properties of the Different Hydrogels

Table 4.A.1. Structural properties of the PIC hydrogels with no added salts and at two different temperatures: 35 and 50 °C.

		Pore Diameter (μm)			Connectivity (a.u.)			Pore Ratio (%)		
		Median	Mean	SD	Median	Mean	SD	Median	Mean	SD
35 °C	0.5 mg ml^{-1} Short-PIC	1.514	1.559	0.8221	5.000	5.800	3.010	55.675	55.17	1.314
	1.0 mg ml^{-1} Short-PIC	0.9313	0.9318	0.4335	5.000	5.384	2.920	48.475	48.449	0.235
	0.5 mg ml^{-1} Long-PIC	1.333	1.507	0.9787	5.000	5.851	3.303	54.845	55.257	2.959
	1.0 mg ml^{-1} Long-PIC	1.055	1.200	0.7211	5.000	5.878	3.105	53.695	54.455	6.968
50 °C	0.5 mg ml^{-1} Short-PIC	1.681	1.717	0.9064	5.000	5.952	3.149	58.545	58.594	1.301
	1.0 mg ml^{-1} Short-PIC	1.002	1.025	0.5319	5.000	5.560	3.090	50.020	50.010	0.365
	0.5 mg ml^{-1} Long-PIC	1.926	2.018	1.103	6.000	6.556	3.536	63.490	63.634	6.377
	1.0 mg ml^{-1} Long-PIC	1.258	1.345	0.7494	5.000	5.939	3.307	57.935	57.874	2.892

Table 4.A.2. Structural properties of the short-polymer PIC hydrogels with added salts.

Short-PIC			Pore Diameter (µm)			Connectivity (a.u.)			Pore Ratio (%)		
			Median	Mean	SD	Median	Mean	SD	Median	Mean	SD
NaI	0.5 mg ml^{-1}	[0.5M]	0.9792	1.099	0.7378	5.000	5.962	4.005	54.745	54.565	1.023
		[1M]	0.7799	0.8940	0.6352	5.000	5.828	4.087	53.380	52.705	1.835
		[2M]	0.9313	0.9856	0.5935	5.000	5.677	3.457	52.670	52.648	1.552
	1.0 mg ml^{-1}	[0.5M]	0.8158	0.8370	0.4597	5.000	5.293	3.198	47.040	47.176	1.007
		[1M]	0.8039	0.8189	0.4733	5.000	5.161	3.251	46.605	47.187	1.764
		[2M]	0.7447	0.7683	0.4786	5.000	5.169	3.407	46.405	46.550	1.954
$NaClO_4$	0.5 mg ml^{-1}	[0.5M]	1.404	1.513	0.9148	5.000	5.686	3.333	56.155	55.263	2.653
		[1M]	1.365	1.494	0.9359	5.000	5.882	3.413	56.545	56.677	2.296
		[2M]	1.272	1.318	0.6608	6.000	6.295	3.553	58.050	57.810	2.760
	1.0 mg ml^{-1}	[0.5M]	0.9313	0.9590	0.4927	5.000	5.279	3.095	48.055	47.864	0.652
		[1M]	1.098	1.153	0.6273	5.000	5.441	3.147	50.145	50.112	2.271
NaCl	0.5 mg ml^{-1}	[0.5M]	1.813	1.857	1.005	6.000	6.539	3.414	63.870	63.579	5.521
		[1M]	2.834	2.980	1.608	7.000	7.821	4.640	74.745	75.538	4.298
	1.0 mg ml^{-1}	[0.5M]	1.081	1.110	0.5651	5.000	5.453	3.014	50.420	50.624	0.872
		[1M]	1.231	1.244	0.5689	5.000	5.786	3.031	51.675	51.710	0.600

Table 4.A.3. Structural properties of the long-polymer PIC hydrogels with added salts.

Long-PIC			Pore Diameter (µm)			Connectivity (a.u.)			Pore Ratio (%)		
			Median	Mean	SD	Median	Mean	SD	Median	Mean	SD
NaI	0.5 mg ml^{-1}	[0.5M]	0.9638	1.179	0.8974	6.000	6.788	4.734	63.540	63.802	13.771
		[1M]	0.9833	1.223	0.9362	6.000	7.005	4.923	65.415	65.064	13.602
		[2M]	0.7576	1.001	0.8649	6.000	6.991	5.246	66.060	65.128	13.494
	1.0 mg ml^{-1}	[0.5M]	0.8701	0.9291	0.5821	5.000	6.112	3.935	55.420	55.445	1.011
		[1M]	0.9213	1.019	0.6840	5.000	6.018	3.836	56.805	56.202	2.225
		[2M]	0.9555	1.078	0.7215	5.000	6.025	3.926	57.300	57.296	2.064
$NaClO_4$	0.5 mg ml^{-1}	[0.5M]	1.871	1.953	1.115	6.000	6.580	3.719	65.020	63.983	2.926
		[1M]	1.832	1.882	1.042	6.000	6.776	3.893	64.620	64.336	1.405
		[2M]	2.197	2.213	1.357	6.000	7.066	4.411	66.750	67.002	1.474
	1.0 mg ml^{-1}	[0.5M]	1.292	1.297	0.6264	6.000	6.256	3.478	56.485	56.332	0.954
		[1M]	1.214	1.238	0.6738	5.000	6.001	3.555	55.735	55.701	0.734
		[2M]	1.216	1.257	0.6707	6.000	6.313	3.492	57.190	57.567	1.239
NaCl	0.5 mg ml^{-1}	[0.5M]	1.342	1.581	1.054	6.000	6.808	3.841	64.555	64.863	12.607
		[1M]	1.452	1.737	1.154	6.000	6.752	3.543	64.780	65.781	11.048
	1.0 mg ml^{-1}	[0.5M]	1.139	1.310	0.8628	5.000	5.991	3.414	56.490	57.925	6.761
		[1M]	1.978	2.019	0.8899	7.000	7.391	3.794	64.235	65.340	5.005

B. Structural Characterization of the Long-PIC Hydrogel

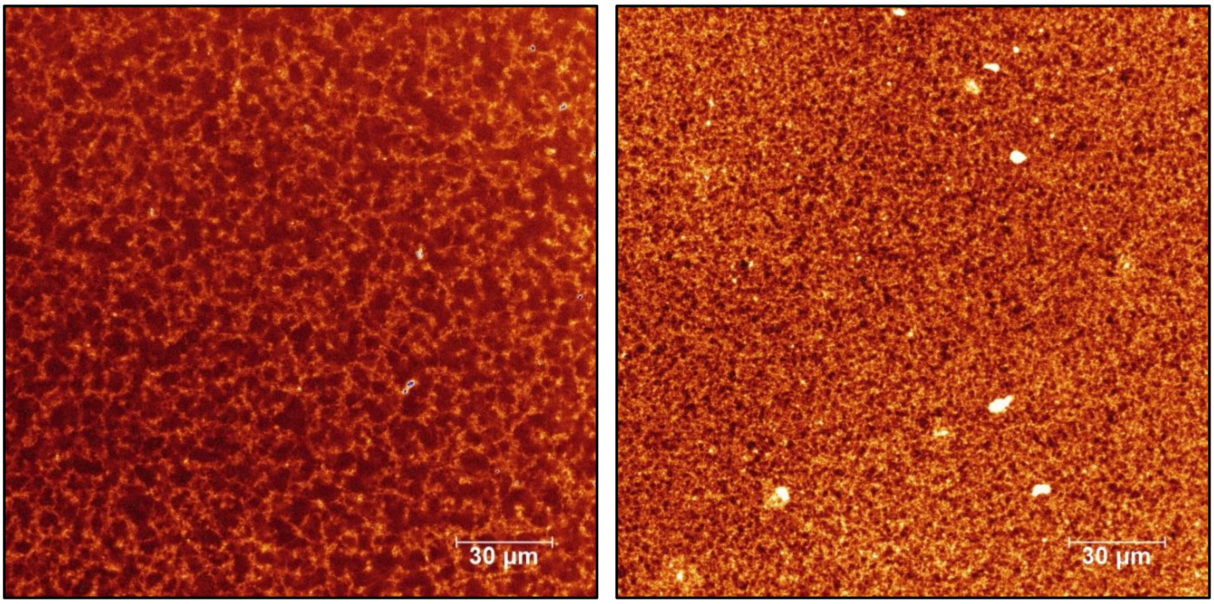

FIGURE 4.B.1

Representative fluorescence images of TAMRA-labelled and long-polymer PIC hydrogels, with a polymer concentration of 0.5 mg ml^{-1} (left) and 1.0 mg ml^{-1} (right). Both images were recorded at 35 °C with the same settings.

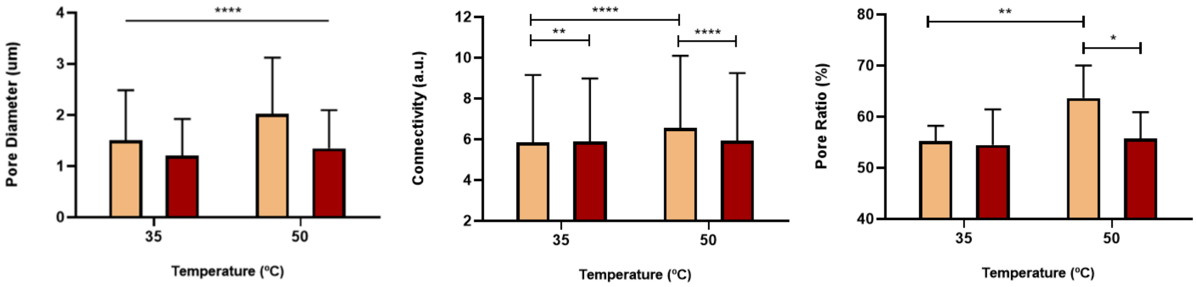

FIGURE 4.B.2

The average pore diameter, pore connectivity and pore ratio in the overall network of long-PIC hydrogels with two different polymer concentrations (0.5 and 1.0 mg ml^{-1}) at two different temperatures (35 and 50 °C). The orange (○) bars represent the 0.5 mg ml^{-1} PIC hydrogel, whereas the red (○) bars are respective of 1.0 mg ml^{-1} of polymer concentration. Data are displayed as mean ± SD. The significantly different groups are indicated in the graphs, with * being $p < 0.03$, ** $p < 0.002$, *** $p < 0.0002$, and **** being $p < 0.0001$. All experiments were performed in duplicate, with 5 different areas measured in each sample.

Table 4.B. The influence of polymer concentration and temperature expressed by the increment or decrement percentage of the structural parameters of the long-polymer PIC hydrogel. The signal of each value is referred to the difference between the group on the line (reference) versus the group on the column.

	Pore Diameter	
	0.5 mg ml^{-1} at 50 °C	1.0 mg ml^{-1} at 35 °C
0.5 mg ml^{-1} at 35 °C	+33.9 %	-20.3 %
1.0 mg ml^{-1} at 50 °C	+50.1 %	-10.8 %
	Pore Connectivity	
	0.5 mg ml^{-1} at 50 °C	1.0 mg ml^{-1} at 35 °C
0.5 mg ml^{-1} at 35 °C	+12.0 %	+0.5 %
1.0 mg ml^{-1} at 50 °C	+10.4 %	-1.0 %
	Pore Ratio	
	0.5 mg ml^{-1} at 50 °C	1.0 mg ml^{-1} at 35 °C
0.5 mg ml^{-1} at 35 °C	+15.2 %	-1.5 %
1.0 mg ml^{-1} at 50 °C	+14.3 %	-2.2 %

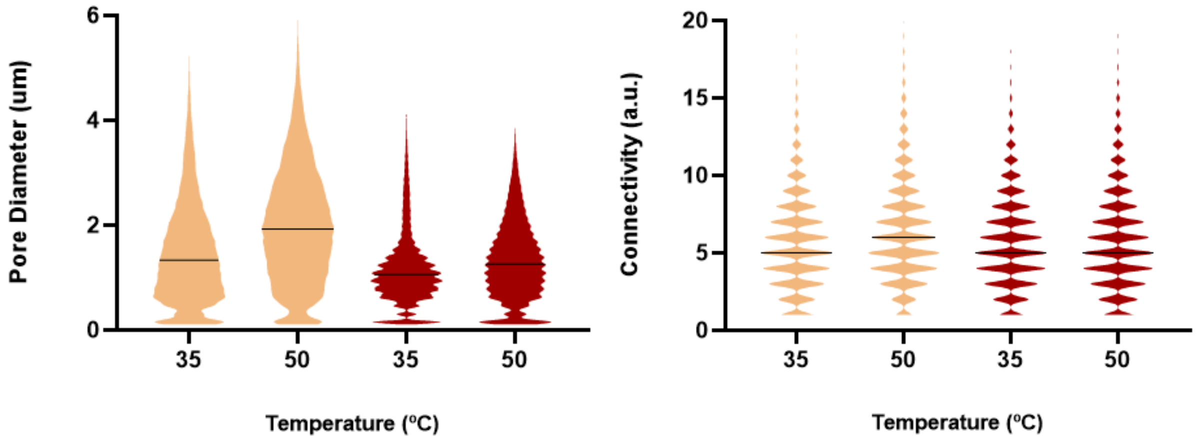

FIGURE 4.B.3

The diameter and connectivity distributions of all the pores in the long-polymer PIC hydrogel with two different polymer concentrations (0.5 and 1.0 mg ml^{-1}) and at different temperatures (35 and 50 °C). The orange (○) bars represent the 0.5 mg ml^{-1} PIC hydrogel, whereas the red (○) bars are respective of 1.0 mg ml^{-1} of polymer concentration. The black straight line represents the median of the distribution. All experiments were performed in duplicate, with 5 different areas measured in each sample.

C. The Influence of the Salts on the Microstructure of Long-Polymer PIC Hydrogels

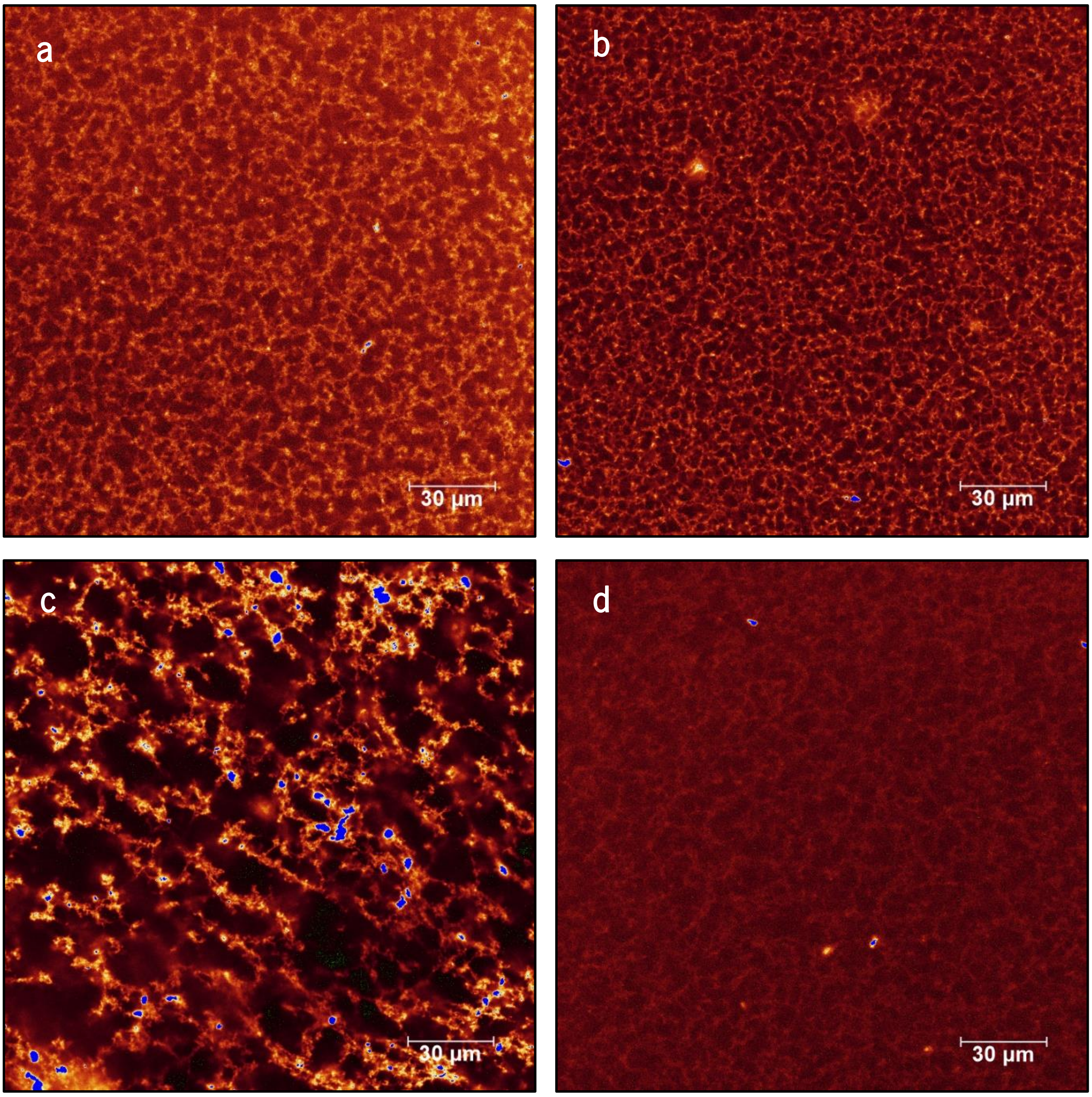

FIGURE 4.C.1

Representative fluorescence images of TAMRA-labelled and long-polymer PIC hydrogels, with a polymer concentration of 0.5 mg ml^{-1}. (a) represents the PIC hydrogel without any salt added. In (b) the PIC hydrogel was formulated with [1M] of NaCl, (c) with [1M] of $NaClO_4$ and (d) with [1M] of NaI. (a), (b) and (d) were recorded at 35 °C. (c) was recorded at 50 °C due to the high increasement of the gelation temperature induced by this salt. The same settings were employed in the microscope for the four measurements.

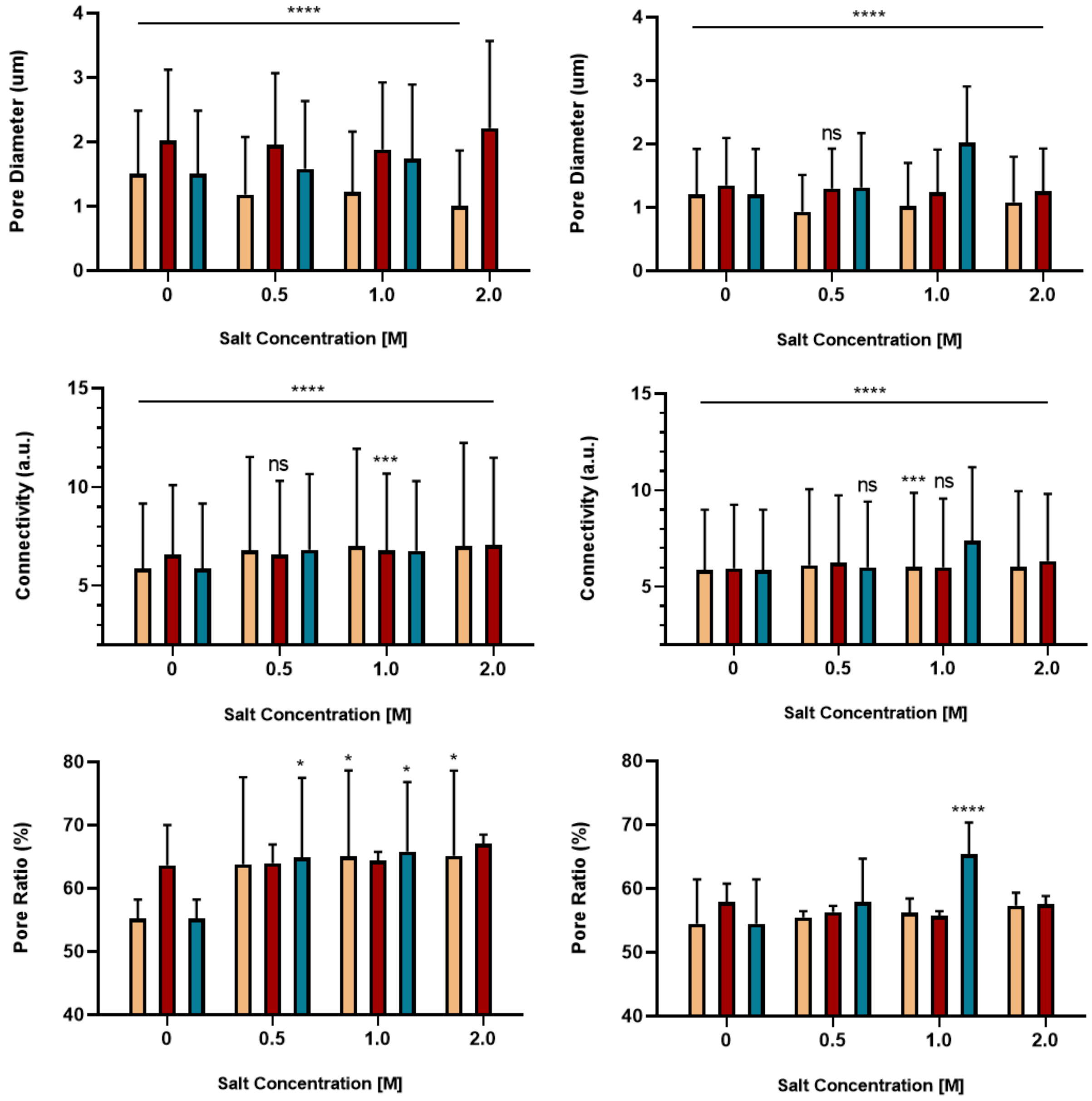

FIGURE 4.C.2

The average pore diameter, pore connectivity and pore ratio in the overall network of long-PIC hydrogels with different salt concentrations. Data are displayed as mean ± SD. The first column refers to the data obtained for a polymer concentration of 0.5, while the second column refers to a concentration of 1.0 mg ml^{-1}. The orange (○) bars are respective to NaI and the red (○) bars are respective to $NaClO_4$, whereas the PIC hydrogel with NaCl is represented by the blue (○) bars. The significantly different groups are indicated in the graphs, with * being $p < 0.03$, ** $p < 0.002$, *** $p < 0.0002$, and **** being $p < 0.0001$. Every statistical comparison is related to the respective control group (which have no added salts). All experiments were performed in duplicate, with 5 different areas measured in each sample.

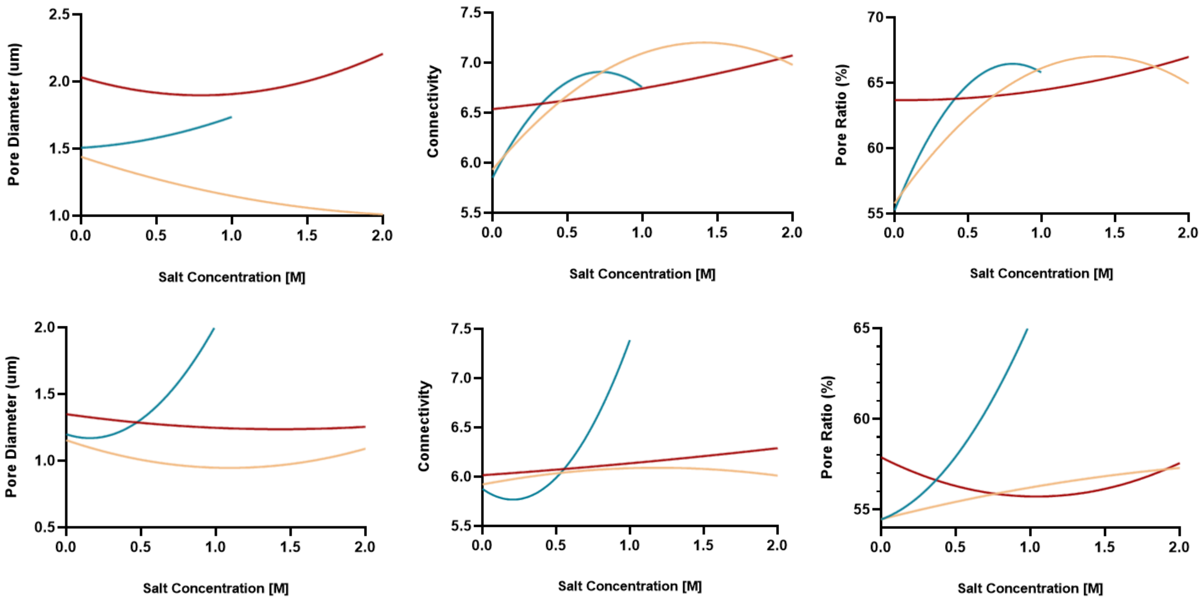

FIGURE 4.C.3

Quadratic regressions of the averaged pore diameter, pore connectivity and pore ratio of the long-polymer PIC hydrogel per salt concentration. The graphics on the top are representative of a polymer concentration of 0.5 mg ml^{-1}, whereas the bottom three graphics represent data of hydrogels with 1.0 mg ml^{-1} of polymer. The orange (○) curves are respective to NaI and the red (○) curves are respective to NaClO$_4$, whereas the PIC hydrogel with NaCl is represented by the blue (○) curves.

Table 4.C.1. The influence of NaI, NaClO$_4$ and NaCl in the analysed structural parameters of the long-PIC hydrogel, expressed in percentage related to the original values of the hydrogels with no added salts.

0.5 mg ml^{-1}

	NaI			NaClO$_4$			NaCl		
Salt Concentration	0.5	1.0	2.0	0.5	1.0	2.0	0.5	1.0	2.0
Pore Diameter	-21.8 %	-18.9 %	-33.6 %	-3.2 %	-6.8 %	+9.6 %	+4.9 %	+15.3 %	-
Pore Connectivity	+16.0 %	+19.7 %	+19.5 %	+0.4 %	+3.4 %	+7.8 %	+16.4 %	+15.4 %	-
Porosity	+15.5 %	+17.7 %	+17.9 %	0.6 %	+1.1 %	+5.3 %	+17.4 %	+19.0 %	-

1.0 mg ml^{-1}

	NaI			NaClO$_4$			NaCl		
Salt Concentration	0.5	1.0	2.0	0.5	1.0	2.0	0.5	1.0	2.0
Pore Diameter	-22.6 %	-15.1 %	-10.2 %	-3.6 %	-7.9 %	-6.6 %	+9.2 %	+68.2 %	-

Pore Connectivity	+4.0 %	+2.4 %	+2.5 %	+5.3 %	+1.1 %	+6.3 %	+1.9 %	+25.7 %	-
Porosity	+1.8 %	+3.2 %	+5.2 %	-2.7 %	-3.8 %	-0.5 %	+6.4 %	+20.0 %	-

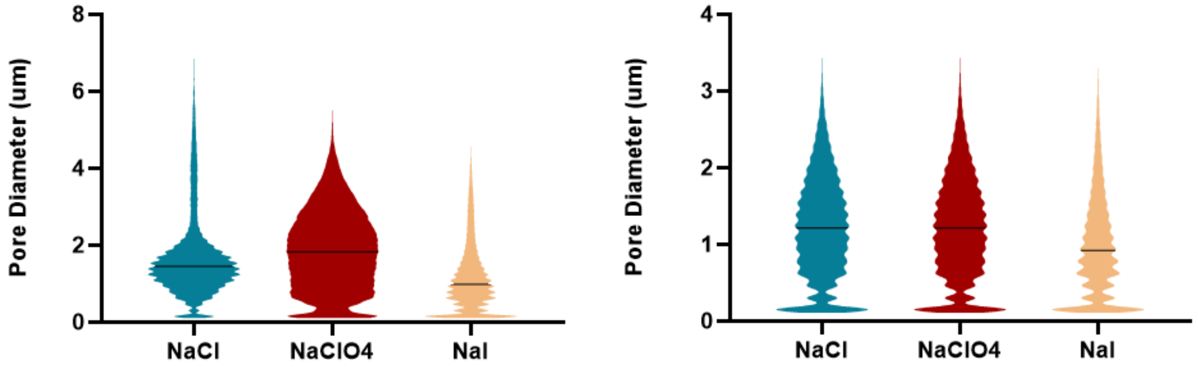

FIGURE 4.C.4

The diameter distribution of all the pores in the long-polymer PIC hydrogel with 0.5 mg ml^{-1} (left) and 1.0 mg ml^{-1} (right) of polyisocyanopeptides and with 1 M of three different salts. The black straight line represents the median of the distribution. All experiments were performed in duplicate, with 5 different areas measured in each sample.

Table 4.C.2. Quadratic regressions of the averaged pore diameter, pore connectivity and pore ratio of PIC hydrogels. The variable *c* is referred to the salt concentration.

Pore Diameter (µm)	NaI	NaClO$_4$	NaCl
0.5 mg ml^{-1} Short-PIC	$1.546c^2 - 1.047c + 0.3836$	$1.695c^2 - 0.2842c + 0.04885$	$1.559c^2 - 0.2265c + 1.648$
1.0 mg ml^{-1} Short-PIC	$0.9239c^2 - 0.1602c + 0.04172$	$1.025c^2 - 0.3918c + 0.5201$	$0.9318c^2 + 0.3993c - 0.08738$
0.5 mg ml^{-1} Long-PIC	$1.440c^2 - 0.3688c + 0.07712$	$2.033c^2 - 0.3383c\ 0.2128$	$1.507c^2 + 0.0664c + 0.1640$
1.0 mg ml^{-1} Long-PIC	$1.155c^2 - 0.3819c + 0.1749$	$1.35c^2 - 0.1578c + 0.05513$	$1.2c^2 - 0.3773c + 1.196$
Connectivity (a.u.)	**NaI**	**NaClO$_4$**	**NaCl**
0.5 mg ml^{-1} Short-PIC	$5.848c^2 + 0.1322c - 0.1108$	$5.910c^2 - 0.3893c + 0.2931$	$5.800c^2 + 0.9330c + 1.088$
1.0 mg ml^{-1} Short-PIC	$5.397c^2 - 0.3127c + 0.09865$	$5.56c^2 - 1.005c + 0.8864$	$5.384c^2 - 0.1233c + 0.525$
0.5 mg ml^{-1} Long-PIC	$5.931c^2 + 1.802c - 0.6388$	$6.538c^2 + 0.1445c + 0.06164$	$5.851c^2 + 2.928c - 2.027$
1.0 mg ml^{-1} Long-PIC	$5.922c^2 + 0.2855c - 0.1203$	$6.016c^2 + 0.1045c + 0.01627$	$5.878c^2 - 1.062c + 2.576$

Pore Ratio (%)	**NaI**	**NaClO$_4$**	**NaCl**
0.5 mg ml^{-1} Short-PIC	$55.37c^2 - 3.129c + 0.8664$	$58.16c^2 - 4.601c + 2.249$	$55.17c^2 + 13.27c + 7.1$
1.0 mg ml^{-1} Short-PIC	$48.33c^2 - 1.903c + 0.5175$	$50.01c^2 - 8.686c + 8.788$	$48.45c^2 + 5.439c - 2.178$
0.5 mg ml^{-1} Long-PIC	$55.79c^2 + 16.09c - 5.753$	$63.69c^2 - 0.1383c + 0.8935$	$55.26c^2 + 27.90c - 17.38$
1.0 mg ml^{-1} Long-PIC	$54.46c^2 + 2.094c - 0.3392$	$57.88c^2 - 4.164c + 2.002$	$54.46c^1 + 2.995c + 7.89$

Table 4.C.3. *R* squared values relative to the quadratic regressions presented in Table C.2.

	Pore Diameter			**Connectivity**			**Pore Ratio**		
	NaI	NaClO$_4$	NaCl	NaI	NaClO$_4$	NaCl	NaI	NaClO$_4$	NaCl
0.5 mg ml^{-1} Short-PIC	0.08993	0.02640	0.1971	0.0006215	0.004416	0.04402	0.3536	0.1546	0.8212
1.0 mg ml^{-1} Short-PIC	0.01448	0.01974	0.05996	0.0007429	0.001497	0.003287	0.1889	0.3851	0.8391
0.5 mg ml^{-1} Long-PIC	0.02563	0.01016	0.007605	0.006286	0.002438	0.01403	0.1112	0.1278	0.2067
1.0 mg ml^{-1} Long-PIC	0.01254	0.003371	0.1369	0.0002262	0.0008586	0.03166	0.07555	0.2356	0.3654

D. The Hofmeister Effect on Covalently Crosslinked PIC Hydrogels

Table 4.D. Structural properties of the covalently crosslinked-PIC hydrogels. Only one polymer length and concentration were assessed: 0.5 mg ml^{-1} of short-PIC.

	Pore Diameter (µm)			Connectivity (a.u.)			Pore Ratio (%)		
	Median	Mean	SD	Median	Mean	SD	Median	Mean	SD
No Salt (35 °C)	1.279	1.3463	0.81873	5.000	6.0416	3.7769	56.485	56.531	1,339
No Salt (50 °C)	1.650	1.6545	0.84889	5.000	5.9233	3.1539	56.460	56.747	1.016
NaI	0.6095	0.76033	0.64703	5.000	6.6311	5.2465	63.150	62.257	16.410
NaClO$_4$	1.549	1.6093	0.95465	5.000	6.1128	3.8088	58.230	57.995	1.572
NaCl	1.730	1.7670	0.83575	6.000	6.8150	3.5962	63.440	63.802	9.783